Review

Atomic Models of Dense Plasmas, Applications, and Current Challenges

Robin Piron [1,2]

[1] CEA, DAM, DIF, F-91297 Arpajon, France; robin.piron@cea.fr
[2] Laboratoire Matière en Conditions Extrêmes, Université Paris-Saclay, CEA, F-91680 Bruyères-le-Châtel, France

Abstract: Modeling plasmas in terms of atoms or ions is theoretically appealing for several reasons. When it is relevant, the notion of atom or ion in a plasma provides us with an interpretation scheme of the plasma's internal functioning. From the standpoint of quantitative estimation of plasma properties, atomic models of plasma allow one to extend many theoretical tools of atomic physics to plasmas. This notably includes the statistical approaches to the detailed accounting for excited states, or the collisional-radiative modeling of non-equilibrium plasmas, which is based on the notion of atomic processes. This paper is focused on the theoretical challenges raised by the atomic modeling of dense, non-ideal plasmas. It is intended to give a synthetic and pedagogical view on the evolution of ideas in the field, with an accent on the theoretical consistency issues, rather than an exhaustive review of models and experimental benchmarks. First we make a brief, non-exhaustive review of atomic models of plasmas, from ideal plasmas to strongly-coupled and pressure-ionized plasmas. We discuss the limitations of these models and pinpoint some open problems in the field of atomic modeling of plasmas. We then address the peculiarities of atomic processes in dense plasmas and point out some specific issues relative to the calculation of their cross-sections. In particular, we discuss the modeling of fluctuations, the accounting for channel mixing and collective phenomena in the photoabsorption, or the impact of pressure ionization on collisional processes.

Keywords: dense plasmas; nonideal plasmas; atomic model; radiative properties; collisional processes

1. Introduction

Plasma physics, in its generality, deals with the physics of partially or fully ionized matter, not having a periodic structure (i.e., ionized fluids). Fundamentally, a plasma is just a collection of a large number of electrons and nuclei interacting through Coulomb potentials, both repulsive and attractive. The notions of atom, ion, free-electron, and ionization are interpreting schemes that may emerge from particular models and should not be seen as objects whose existence is pre-supposed.

In the following, we focus on the case of homogeneous plasmas in thermodynamic equilibrium. In this context, homogeneous means that the thermodynamic averages of the particle densities have no spatial variation. Any spatial inhomogeneity or *structure* (electronic structure or fluid structure) that is considered is then a matter of *correlations* among the particle positions.

Due to the existence of long-range attractive potentials in the system, a first-principle modeling of plasmas based on classical mechanics only is virtually impossible because of the classical Coulomb catastrophe. It requires either an *ad hoc* modification of the potential at short distances (regularization, cut-off, smearing of charges, etc.) or a well-chosen hypothesis that allows one to circumvent this problem. In a sense, whatever the thermodynamic conditions, the quantum behavior of the electrons is always essential in founding the stability of plasmas [1–5].

Among the various models that may be used to describe plasmas, models that define a notion of atom or ion are particularly appealing. We mean here an idealized system

that describes the plasma using effective 1-electron states (orbitals) stemming from a spherically symmetric 1-electron Hamiltonian. With such a model, one can greatly reduce the complexity of the description of the microstates of the plasma, using the notion of atomic excited states.

A description of the atomic excited states in the plasma is essential to the modeling of spectral quantities, such as radiative properties, which can reveal the fluctuations around the average atomic state. More generally, many phenomena are described using approaches based on the notion of atomic processes. One may cite, for instance, the collisional-radiative modeling of plasmas out of local thermodynamic equilibrium [6,7], or the approaches to line-broadening mechanisms (see [8–12], and [13] for a review).

Being spherically symmetric, the effective 1-electron Hamiltonian commutes with angular momentum operators, which enables the separation of the angular part of the 1-electron states (spherical harmonic or spinors). Many-electron states can then be built from the orbitals using a well-established mathematical apparatus, with the Wigner–Eckart theorem as a cornerstone of matrix-element evaluation. Methods of angular-momentum coupling were thoroughly studied, both as regards the formalism [14–18] and the numerical methods [19,20].

Due to the tremendous number of populated atomic states at high temperatures, statistical grouping of energy levels is particularly useful for hot-plasma modeling. Analytic results from atomic physics are available for the statistical properties of configurations [21] and transition arrays between configurations [22–24] (UTA, SOSA). This enables powerful detailed configuration accounting (DCA) approaches. In order to handle the calculation of spectra for ions with a highly complex electronic structure, coarser statistical approaches were developed, such as the Gaussian approximation [25] and the super transition arrays (STA) formalism [26,27]. On the other hand, in order to refine the UTA approach, finer approaches were also developed, such as the mixed-UTA [28] and the partially resolved transition arrays (PRTA) [29].

In the present article, we briefly review a selection of atomic models of plasmas, from ideal plasmas (Section 2) to non-ideal (Section 3) and pressure-ionized plasmas (Section 4). We discuss the limitations of these models and pinpoint some open problems in the field of atomic modeling of plasmas. We then address the peculiarities of atomic processes in dense plasmas and point out some specific issues relative to the calculation of their cross-sections. Radiative processes and photoabsorption are first considered (Section 5). In particular, we discuss the modeling of fluctuations, accounting for channel mixing and collective phenomena in the photoabsorption. Finally, the impact of pressure ionization on collisional processes is briefly discussed (Section 6).

2. Atomic Modeling of Ideal Plasmas

The simplest hypothesis allowing one to circumvent the classical catastrophe is to neglect all interactions in the plasma (ideal-gas approximation). Applying this approximation directly to the system of nuclei and electrons yields an ideal-gas model valid for a fully ionized plasma at zero coupling.

Usually, in plasma physics, the ideal-gas approximation is only partially applied. One first defines a quasi-particle composed of a nucleus and a set of bound electrons that interact with the nucleus and among themselves. This is the definition of an *ion* in this model. All electrons of the plasma that are not bound to a nucleus are viewed as "free" electrons. One then makes the ideal-gas hypothesis on the system of ions and free electrons. This is the picture of an *ideal plasma*.

In this type of model, one usually resorts to a quantum model for the electronic structure of the ion, which of course does not lead to the Coulomb catastrophe. On the other hand, the ideal-gas approximation allows one to circumvent the Coulomb catastrophe for the whole plasma of ions and free electrons.

In this context, the ion is seen as a charged, isolated system having a finite spatial extension. It is an *isolated* ion since its electronic structure is obtained disregarding all

the other particle of the plasma: other ions and free electrons. To describe this electronic structure requires one to address an N-body problem with $N \sim Z + 1$ at most, where Z is the atomic number of the nucleus.

2.1. Saha–Boltzmann Model and Isolated Ion: A Variational Detailed Model of Ideal Plasma

The approach in which one accounts for the various electronic states of the ions as different species is known as *detailed* modeling (sometimes also called the "chemical approach"). For an ideal plasma in thermal equilibrium, this approach yields the Saha–Boltzmann model of plasma [30,31].

The modeling of the isolated-ion electronic structure can be treated independently from the modeling of the whole plasma. A typical quantum Hamiltonian of the isolated ion having Q bound electrons is the Q-electron operator:

$$\hat{H}^Q_{\text{isol.ion}} = \sum_{j=1}^{Q} \frac{\tilde{\mathbf{P}}_j^2}{2m_{\text{e}}} - \sum_{j=1}^{Q} \frac{Z\text{e}^2}{|\tilde{\mathbf{R}}_j|} + \sum_{j=1}^{Q} \sum_{\substack{k=1 \\ k \neq j}}^{Q} \frac{\text{e}^2}{|\tilde{\mathbf{R}}_j - \tilde{\mathbf{R}}_k|} \tag{1}$$

where $\tilde{\mathbf{P}}_j$ is the 1-electron momentum operator acting on the j electron, $\tilde{\mathbf{R}}_j$ is the 1-electron position operator acting on the j electron, and $\text{e}^2 = q_{\text{e}}^2/(4\pi\epsilon_0)$, with q_{e} being the elementary charge.

The problem of finding the stationnary states of this isolated-ion Hamiltonian has a variational formulation (Ritz theorem). However, to tackle this problem, one resorts to approximate methods. Such methods often start with a model based on effective 1-electron states φ_ξ (i.e., orbitals), which are solutions of a 1-electron Schrödinger equation associated with an effective spherically symmetric potential $v_{\text{eff}}(r)$.

$$\tilde{H}_{\text{eff}}|\varphi_\xi\rangle = \left(\tilde{H}_0 + v_{\text{eff}}(\tilde{\mathbf{R}})\right)|\varphi_\xi\rangle = \varepsilon_\xi|\varphi_\xi\rangle \tag{2}$$

$$-\frac{\hbar^2}{2m_{\text{e}}}\nabla_{\mathbf{r}}^2\varphi_\xi(\mathbf{r}) + v_{\text{eff}}(r)\varphi_\xi(\mathbf{r}) = \varepsilon_\xi\varphi_\xi(\mathbf{r}) \tag{3}$$

with $\tilde{H}_0 = \tilde{\mathbf{P}}^2/(2m_{\text{e}})$ being the 1-electron free-particle Hamiltonian.

Various models exist, which mostly differ in their way of obtaining the effective potential $v_{\text{eff}}(r)$ (Hartree–Fock–Slater [32], optimized effective potential [33], parametric potential [34]...). In the Hartree–Fock model [35], a nonlocal exchange term is added to Equation (3). However, the problem is often restricted to an effective 1-electron problem having spherical symmetry (the restricted Hartree–Fock approach; see, for instance, [36]).

One then refines this approximate description using perturbation theory, performing the diagonalization of the many-electron perturbation operators in a many-electron basis built from the orbitals (see, for instance, [36–38]). Depending on the approach used, such an approximate model may have a variational formulation or not.

The approximate many-electron states are naturally grouped into degenerate energy levels, which in practice depend on the coupling scheme that is chosen. Accounting for each level as a species is called a detailed level accounting (DLA) approach. One may also perform detailed configuration accounting (DCA), grouping the levels according to their parent configuration [39]. One may even group the configurations into broader statistical objects: superconfigurations [26]. Each degree of statistical grouping goes along with a set of ion species α to consider, each having as main properties a mean energy E_α and a degeneracy g_α. Usually the reference of energies is taken such as $E_\alpha = 0$ for the bare nucleus and the free electrons.

The classical Hamiltonian for the ion-free-electron ideal plasma is the following:

$$\mathcal{H}_{\text{id}}(\{p_{\alpha,j}\}) = \sum_{\alpha=1}^{M,\text{e}} \sum_{j=1}^{N_\alpha} \left(\frac{p_{\alpha,j}^2}{2m_\alpha} + E_\alpha\right) \tag{4}$$

where the first sum runs over the M ion species plus the free-electron species labelled by "e". In this Hamiltonian, interactions among the particles of the plasma are neglected. The ion-free-electron system is considered in the canonical ensemble and the free energy per ion of the classical ideal-gas mixture is:

$$\dot{F}_{id}(\{n_\alpha\}, T) = -\sum_{\alpha=1}^{M,e} \frac{n_\alpha}{n_i \beta}\left(\log\left(\frac{g_\alpha e^{-\beta E_\alpha}}{n_\alpha \Lambda_\alpha^3}\right) + 1\right) \tag{5}$$

where n_α is the number of particle of species α per unit volume (in particular, n_e is the free-electron density), $n_i = \sum_{\alpha=1}^{M} n_\alpha$, and $\Lambda_\alpha = h/\sqrt{2\pi m_\alpha k_B T}$ is the classical thermal length. We will denote by a dot the quantities per ion, in order to avoid confusion with total quantities or quantities per unit volume.

The equations of the Saha equilibrium model are obtained through a minimization of the free energy of the system with respect to the species populations, while also requiring the neutrality of the plasma and a fixed number of ions. Thus, transfers of population among the various ion species are allowed, and the populations are ultimately set by the condition of thermodynamic equilibrium. Only the populations, and not the quantities related to the shell structure of the ions, stem from the model.

$$\dot{F}_{eq}(n_i, T) = \underset{\{n_\alpha\}}{\text{Min}}\ \dot{F}(\{n_\alpha\}, T)\ \text{ s. t. } \sum_\alpha n_\alpha = n_i$$
$$\text{s. t. } \sum_\alpha n_\alpha Z_\alpha^* = n_e \tag{6}$$

The latter minimization yields the following condition on the chemical potentials:

$$\text{for all } \alpha \neq e,\ \mu_{id,\alpha}(n_\alpha, T) + \mu_{id,e}(n_e, T)Z_\alpha^* = \lambda_i \text{ independent of } \alpha \tag{7}$$

with the classical-ideal-gas chemical potentials being:

$$\mu_{id,\alpha}(n_\alpha, T) = \frac{\partial}{\partial n_\alpha}\left(n_i \dot{F}(\{n_\alpha\}, T)\right) = \frac{1}{\beta}\log\left(\frac{g_\alpha e^{-\beta E_\alpha}}{n_\alpha \Lambda_\alpha^3}\right) \tag{8}$$

For a plasma of a pure substance, one usually assumes the thermal lengths Λ_α of all ion species to be equal: $\Lambda_\alpha \approx \Lambda_i$. From Equation (7) and the two contrains, one obtains the populations:

$$\frac{n_\alpha}{n_i} = \frac{g_\alpha e^{-\beta(E_\alpha - \mu_{id,e} Z_\alpha^*)}}{\sum_{\gamma=1}^{M} g_\gamma e^{-\beta(E_\gamma - \mu_{id,e} Z_\gamma^*)}} \tag{9}$$
$$\sum_\alpha n_\alpha Z_\alpha^* = n_e \tag{10}$$

From these populations follows notably the mean ionization of the plasma $Z^* = n_e/n_i$, as a value set by the thermodynamic equilibrium condition. Obtaining the ionization state of the plasma as a result of its equilibrium state is among the *purposes* of plasma modeling.

The plasma being treated in the ideal-gas approximation, the pair distribution functions among the particle of the plasma are identically $g_{\alpha,\gamma} = 1$, and the mean interparticle distance is $\Gamma(4/3)R_{\alpha,\gamma}$ with $R_{\alpha,\gamma} = (3/(4\pi\sqrt{n_\alpha n_\gamma}))^{1/3}$ (see [40]).

The thermodynamic quantities stemming from this model (internal energy, pressure...) can be obtained from the free energy, using the appropriate derivatives. They simply correspond to those of the ideal-gas mixture, taken with the equilibrium values of the species populations. Moreover they obviously fulfill the virial theorem (in its non-relativistic version):

$$P_{thermo} = n_i^2 \frac{\partial \dot{F}_{eq}(n_i, T)}{\partial n_i} = P_{virial} = \frac{n_i}{3}\left(2\dot{U}_{eq}(n_i, T) - \dot{U}_{inter,eq}(n_i, T)\right) \tag{11}$$

where $\dot{U}_{\mathrm{eq}}$ denotes the internal energy per ion, and $\dot{U}_{\mathrm{inter,eq}}$ denotes the interaction energy per ion, which is zero for the ideal-gas mixture. This is an important feature as regards the consistency of the equation of state.

An issue with the present model is that, in principle, when accounting for the excited states in a complete manner, the partition function (denominator in the right-hand side of Equation (9)) diverges because of the infinite number of bound states. Let us consider, for instance, the hydrogen-like atomic states. We have:

$$\sum_{\gamma \text{ H-like}} g_\gamma e^{-\beta(E_\gamma - \mu_{\mathrm{id,e}} Z_\gamma^*)} = e^{\beta\mu_{\mathrm{id,e}}(Z-1)} \sum_{n=1}^{\infty} 2n^2 e^{\frac{\beta Z^2}{2n^2}\alpha^2 m_e c^2} \tag{12}$$

$$\lim_{n \to \infty} \left(2n^2 e^{\frac{\beta Z^2}{2n^2}\alpha^2 m_e c^2} \right) = 2n^2 + \beta Z^2 \alpha^2 m_e c^2 + O\left(\frac{1}{n^2}\right) \tag{13}$$

The two first terms of the right-hand side of Equation (13) lead to the divergence of the sum.

The solution to this puzzle is to be found in the distortion of the continuum wave functions and in the non-ideal corrections to the Saha equilibrium. These somehow restrict the set of states to be accounted for in the calculation. We postpone the discussion of this point to Section 3.5 and consider that the sum is in practice truncated at some value of the principal quantum number.

Finally, let us mention the straightforward extension of the Saha model that consists of replacing the classical-ideal-gas free energy for the free electrons with that of the Fermi ideal gas.

$$\dot{F}(\{n_\alpha\}, T) = -\sum_{\alpha=1}^{M} \frac{n_\alpha}{n_i \beta} \left(\log\left(\frac{g_\alpha e^{-\beta E_\alpha}}{n_\alpha \Lambda_\alpha^3} \right) + 1 \right) + \frac{f_e^{\mathrm{F}}(n_e, T)}{n_i} \tag{14}$$

$$f_e^{\mathrm{F}}(n_e, T) = n_e \mu_e^{\mathrm{F}}(n_e, T) - \frac{2}{3} u_e^{\mathrm{F}}(n_e, T) \tag{15}$$

$$u_e^{\mathrm{F}}(n_e, T) = \frac{4}{\beta\sqrt{\pi}\Lambda_e^3} I_{3/2}\left(\beta\mu_e^{\mathrm{F}}(n_e)\right) \tag{16}$$

$$n_e = \frac{4}{\sqrt{\pi}\Lambda_e^3} I_{1/2}\left(\beta\mu_e^{\mathrm{F}}(n_e, T)\right) \tag{17}$$

where the sum in Equation (14) only runs over the M ion species. $f_e^{\mathrm{F}}(n_e, T)$ and $u_e^{\mathrm{F}}(n_e, T)$ are the free and internal energies per unit volume of a Fermi gas of density n_e and temperature T, respectively. $\mu_e^{\mathrm{F}}(n_e, T)$ is the corresponding canonical chemical potential.

2.2. Average-Atom Model of Isolated Ion from a Variational Perspective

The case of an ideal plasma of isolated ions can also be addressed through an *average-atom* approach. In this kind of approach, instead of accounting for the many-electron states in a detailed fashion, one only aims to describe the average many-electron state of the plasma, associating fractional occupation numbers with the orbitals. The finite-temperature density-functional theory [41–43] offers a sound theoretical basis for such models. In order to model an average isolated ion, we just have to restrict interactions to the ion nucleus and bound electrons and to consider that any continuum electron participate in a uniform, noninteracting electron density n_e.

The free energy per ion of such a system can be written as follows:

$$\dot{F}\left\{\{p_\xi\}, \underline{v}_{\mathrm{trial}}, n_e; n_i, T\right\} = \dot{F}_{\mathrm{id,i}}(n_i, T) + \dot{F}_{\mathrm{id,e}}(n_e; n_i, T) + \Delta F_1\left\{\{p_\xi\}, \underline{v}_{\mathrm{trial}}\right\} \tag{18}$$

where the functional dependencies are underlined. Here, the $\dot{F}_{\mathrm{id,i}}$ term corresponds to the contribution of the nuclei ideal-gas and $\dot{F}_{\mathrm{id,e}}$ corresponds to the contribution of the free-electron ideal gas:

$$\dot{F}_{\mathrm{id,i}} = \frac{1}{\beta}\left(\ln\left(n_{\mathrm{i}}\Lambda_{\mathrm{i}}^3\right) - 1\right) \ ; \ \dot{F}_{\mathrm{id,e}} = \frac{n_{\mathrm{e}}}{n_{\mathrm{i}}\beta}\left(\ln\left(n_{\mathrm{e}}\Lambda_{\mathrm{e}}^3\right) - 1\right) \tag{19}$$

where Λ_{i} and Λ_{e} are the nucleus and electron thermal lengths, respectively. As in the Saha model, the classical ideal-gas free energy of the electrons may also be replaced by the Fermi ideal-gas free energy:

$$\dot{F}_{\mathrm{id,e}} = \frac{f_{\mathrm{e}}^{\mathrm{F}}(n_{\mathrm{e}}, T)}{n_{\mathrm{i}}} \tag{20}$$

The ΔF_1 term corresponds to the free-energy of the average ion electronic structure, that is: the interacting system of bound electrons and the nucleus. We treat this system using the Kohn–Sham method [42], that is, we split ΔF_1 into the three contributions:

$$\Delta F_1\{\{p_\xi\}, \underline{v}_{\mathrm{trial}}; T\} = \Delta F_1^0 + \Delta F_1^{\mathrm{el}} + \Delta F_1^{\mathrm{xc}} \tag{21}$$

where ΔF_1^0 is the kinetic-entropic contribution to the free energy of a system of independent bound electrons, feeling an external potential $\underline{v}_{\mathrm{trial}}(r)$ and having 1-electron-orbital occupation numbers $\{p_\xi\}$ that together yield the density $n(r)$ of the interacting bound electrons. ΔF_1^{el} is the direct electrostatic contribution, and ΔF_1^{xc} is the contribution of exchange and correlation to the free energy of the electronic structure.

According to its definition, the expression of ΔF_1^0 is:

$$\Delta F_1^0\{\{p_\xi\}, \underline{v}_{\mathrm{trial}}; T\} = \sum_{\xi \text{ bound}} \left(p_\xi \langle \varphi_\xi | \tilde{H}_0 | \varphi_\xi \rangle - T s_\xi\right) \tag{22}$$

$$= \sum_{\xi \text{ bound}} \left(p_\xi \varepsilon_\xi - \int d^3 r\{n(r) v_{\mathrm{trial}}(r)\} - T s_\xi\right) \tag{23}$$

where the sum over the ξ-indices only runs over the bound 1-electron states (bound orbitals). p_ξ is the mean occupation number of the 1-electron state ξ, and the corresponding contribution to the entropy of the effective non-interacting system is:

$$s_\xi = s(p_\xi) = -k_{\mathrm{B}}\left(p_\xi \ln\left(p_\xi\right) + (1 - p_\xi)\ln\left(1 - p_\xi\right)\right) \tag{24}$$

ε_ξ and $\varphi_\xi(\mathbf{r})$ are shorthand notations for $\varepsilon_\xi\{\underline{v}_{\mathrm{trial}}\}$ and $\varphi_\xi\{\underline{v}_{\mathrm{trial}}; \mathbf{r}\}$, respectively. These are the eigenvalues and wave functions of the 1-electron states obtained in the trial potential $v_{\mathrm{trial}}(r)$. In the non-relativistic case, they are obtained by solving the 1-electron Schrödinger equation:

$$-\frac{\hbar^2}{2m_{\mathrm{e}}}\nabla_{\mathbf{r}}^2 \varphi_\xi(\mathbf{r}) + v_{\mathrm{trial}}(r)\varphi_\xi(\mathbf{r}) = \varepsilon_\xi \varphi_\xi(\mathbf{r}) \tag{25}$$

We take the convention of normalizing the φ_ξ to unity. The trial potential $v_{\mathrm{trial}}(r)$ and occupation numbers $\{p_\xi\}$ are such that the density of the system of independent bound electrons is $n(r)$. In this context, $n(r)$ is a shorthand notation for $n\{\{p_\xi\}, \underline{v}_{\mathrm{trial}}; r\}$:

$$n\{\underline{v}_{\mathrm{trial}}, \{p_\xi\}; r\} = \sum_{\xi \text{ bound}} p_\xi |\varphi_\xi(\mathbf{r})|^2 \tag{26}$$

The direct electrostatic contribution ΔF_1^{el} can be written as a functional of $n(r)$:

$$\Delta F_1^{\mathrm{el}}\{\{p_\xi\}, \underline{v}_{\mathrm{trial}}\} = \tilde{\Delta F}_1^{\mathrm{el}}\{\underline{n}\} = \mathrm{e}^2 \int d^3 r\left\{\frac{-Zn(r)}{r}\right\} + \frac{\mathrm{e}^2}{2}\int d^3 r d^3 r'\left\{\frac{n(r)n(r')}{|\mathbf{r} - \mathbf{r}'|}\right\} \tag{27}$$

The exchange-correlation contribution can be approximated by:

$$\Delta F_1^{\mathrm{xc}}\big\{\{p_\xi\},\underline{v}_{\mathrm{trial}};T\big\} = \tilde{\Delta F}_1^{\mathrm{xc}}\{\underline{n};T\} = \int d^3r\{f_{\mathrm{xc}}(n(r),T)\} \tag{28}$$

where f_{xc} is the exchange-correlation free energy per unit volume of a homogeneous electron gas (local density approximation).

We stress that in this model, as in the Saha model, there is a strong distinction between bound and free electrons since any electron that belongs to the continuum is considered as non-interacting, whereas bound electrons participate in $n(r)$ and interact both with the other bound electrons of the same ion and with its nucleus, as is seen from the expressions of ΔF_1^{el} and ΔF_1^{xc}.

In order to obtain the equations of the model, we minimize the free energy per ion, requiring the additional constraint of overall neutrality:

$$\dot{F}_{\mathrm{eq}}(n_{\mathrm{i}},T) = \underset{p_\xi,v_{\mathrm{trial}},n_{\mathrm{e}}}{\mathrm{Min}}\ \dot{F}\big\{\{p_\xi\},\underline{v}_{\mathrm{trial}},n_{\mathrm{e}};n_{\mathrm{i}},T\big\}\ \ \mathrm{s.\ t.}\ \ Z - \sum_{\xi\ \mathrm{bound}} p_\xi = \frac{n_{\mathrm{e}}}{n_{\mathrm{i}}} \tag{29}$$

Performing this constrained minimization, we obtain the equations of the average-atom model of isolated-ion (AAII):

$$v_{\mathrm{trial}}(r) = v_{\mathrm{el}}(r) + \mu_{\mathrm{xc}}(n(r),T) \tag{30}$$

$$p_\xi = p_{\mathrm{F}}(\mu,T,\varepsilon_\xi) = \frac{1}{e^{\beta(\varepsilon_\xi-\mu)}+1} \tag{31}$$

$$\mu = \begin{cases} \mu_{\mathrm{id,e}}(n_{\mathrm{e}},T) & \text{(classical ideal gas)} \\ \mu_{\mathrm{id,e}}^{\mathrm{F}}(n_{\mathrm{e}},T) & \text{(Fermi ideal gas)} \end{cases} \tag{32}$$

$$Z - \sum_{\xi\ \mathrm{bound}} p_\xi = \frac{n_{\mathrm{e}}}{n_{\mathrm{i}}} \tag{33}$$

where $\mu_{\mathrm{xc}}(n,T) = \partial f_{\mathrm{xc}}(n,T)/\partial n$, and where $v_{\mathrm{el}}(r)$ is a shorthand notation for $v_{\mathrm{el}}\{\underline{n};r\}$, defined as follows:

$$v_{\mathrm{el}}\{\underline{n};r\} = \frac{\delta\tilde{\Delta F}_1^{\mathrm{el}}}{\delta n(r)} = -\frac{Ze^2}{r} + e^2\int d^3r'\left\{\frac{n(r')}{|\mathbf{r}-\mathbf{r}'|}\right\} \tag{34}$$

As a consequence of addressing the average electronic configuration of an ion, the electronic structure has to be determined self-consistently with the occupation numbers. The calculation of the electronic structure cannot be separated from the statistical modeling, as it is in the Saha model. This may appear as a major drawback of this model but, on the other hand, the average-atom approach is intrinsically complete. It has no issue of practical limitation in the number of excited multi-electron states that may be accounted for.

However, the average atom model has the same issue of divergence of the partition function as the Saha model. If one considers, for instance, the sum of the occupation numbers, in the non-degenerate limit of the Fermi–Dirac distribution:

$$\sum_{\xi\ \mathrm{bound}} p_\xi^{\mathrm{F}} = 2\sum_{n=1}^{\infty}\sum_{\ell=0}^{n-1}(2\ell+1)e^{-\beta(\varepsilon_{n,\ell}-\mu)} \tag{35}$$

Assuming that the exchange-correlation potential μ_{xc} does not compensate the self interaction in v_{el}, we have:

$$\lim_{r\to\infty} v_{\mathrm{trial}}(r) = -\frac{Z^*e^2}{r}\ ;\ \lim_{n\to\infty}\varepsilon_{n,\ell} = -\frac{Z^{*2}}{2n^2}\alpha^2 m_{\mathrm{e}}c^2\ ;\ \lim_{n\to\infty}\sum_{\ell=0}^{n-1}2(2\ell+1)e^{-\beta\varepsilon_{n,\ell}} = 2n^2 + \beta Z^{*2}\alpha^2 m_{\mathrm{e}}c^2 + O\left(\frac{1}{n^2}\right) \tag{36}$$

Again, we postpone a longer discussion of this point to Section 3.5 and will assume that the principal quantum number is limited somehow.

From the free energy at equilibrium, we can derive all the thermodynamic quantities of interest, in particular, the pressure:

$$P = n_i^2 \frac{\partial \dot{F}_{eq}}{\partial n_i} = \begin{cases} n_i k_B T + n_e k_B T & \text{(classical ideal gas)} \\ n_i k_B T - f_e^F(n_e, T) + n_e \mu_e^F(n_e, T) & \text{(Fermi ideal gas)} \end{cases} \quad (37)$$

This corresponds to the pressure of the ideal-gas mixture of ions and free-electrons. It may be shown easily (the method is described in [44]) that the virial theorem is fulfilled in this model.

To conclude about this derivation, let us note that instead of considering as variables the arbitrary occupation numbers p_ξ and trial potential $v_{trial}(r)$, one can consider the electron density $n(r)$ as the variable, formally inverting the relation between $v_{trial}(r)$ and $n(r)$. In this case, one defines $v_{trial}\{\underline{n}, n_e; r\}$ as the external potential yielding the density $n(r)$ for a system of independent particle at equilibrium, that is, with $p_\xi = p_F(\mu, T, \varepsilon_\xi)$. This corresponds more closely to the usual standpoint of density functional theory, and we will use this one in the following derivations.

Figure 1 presents a comparison between the mean ionization: $Z^* \equiv n_e/n_i$ obtained from the Saha equilibrium model, using a detailed configuration accounting for the ion electron states, and the present average-atom model of isolated ion, for the case of silicon, with an arbitrary limitation of the principal quantum number to $n \leq 8$. Though the results differ slightly, they are rather close. The qualitative behavior of decreasing mean ionization when the density increases is similar, clearly exhibiting the lack of pressure ionization in these models.
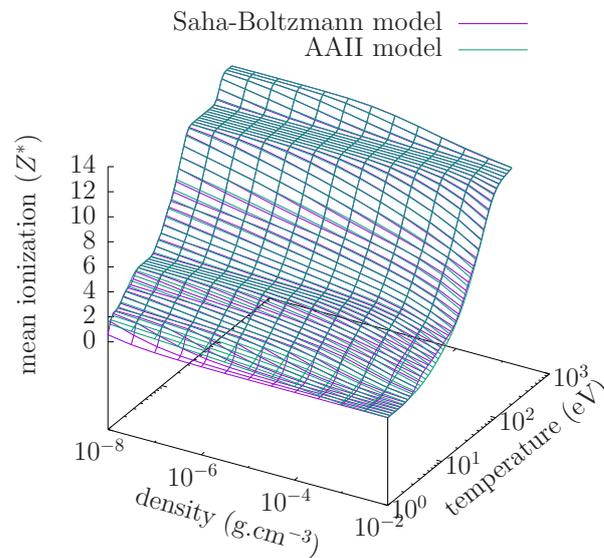

Figure 1. Mean ionization Z^* of silicon stemming from the Saha equilibrium model, with detailed configuration accounting for the ion electron states, and from the average-atom model of isolated ion (AAII).

3. Nonideality Corrections to Isolated Ions

3.1. General Considerations, Notion of Ionization-Potential Depression

Nonideal plasmas specifically correspond to those plasmas for which the interactions of the ions with the surrounding ions and free electrons cannot be disregarded. In first approximation, one may assume that the internal structure of the ions remains untouched and simply refine the ideal-gas approximation for the system of point-like ions and free electrons (ion-free-electron plasma) by accounting for the interaction energy. The classical Hamiltonian for this interacting ion-free-electron plasma is the following:

$$\mathcal{H}(\{\mathbf{p}_{\alpha,j}, \mathbf{r}_{\alpha,j}\}) = \mathcal{H}_{\mathrm{id}}(\{\mathbf{p}_{\alpha,j}\}) + W_{\mathrm{IFE}}(\{\mathbf{r}_{\alpha,j}\}) \tag{38}$$

$$W_{\mathrm{IFE}}(\{\mathbf{r}_{\alpha,j}\}) = \frac{\mathrm{e}^2}{2} \sum_{\alpha=1}^{M,\mathrm{e}} \sum_{j=1}^{N_\alpha} \sum_{\substack{\gamma=1 \\ (\gamma,k) \neq (\alpha,j)}}^{M,\mathrm{e}} \sum_{k=1}^{N_\gamma} \frac{Z_\alpha^* Z_\gamma^*}{|\mathbf{r}_{\alpha,j} - \mathbf{r}_{\gamma,k}|} \tag{39}$$

where the charge of a free electron is $Z_{\mathrm{e}}^* = -1$.

Since the ions are assumed to be point-like in this approach, interactions can only be sensitive to the ion charge rather than to the detail of its electronic structure. All species α sharing a same ion charge Z_α^* behave the same. Consequently, effective changes only occur in energy differences among different charge states, yielding the notion of ionization-potential depression (IPD) or continuum lowering.

Two ways of accounting for this interaction energy are often described in the literature. These two mostly lead to the same results and rather pertain to different standpoints on the problem than to strictly distinct approaches.

A first approach is to evaluate the average potentials v_α^* per unit charge, acting on the various point-like particles of the plasma, due to the interactions with all of the other particles of the plasma. Typically, if we set $v_\alpha(\mathbf{r})$ to be the average potential around a particle of species α, we have:

$$v_\alpha^* = \lim_{r \to 0} \left(v_\alpha(\mathbf{r}) - \frac{Z_\alpha \mathrm{e}^2}{r} \right) \tag{40}$$

For each ion, one then adds the corresponding v_α^* potential to the binding energy E_α found from the Hamiltonian $\hat{H}_{\mathrm{isol.ion}}^Q$ pertaining to the electronic structure. This may be interpreted as adding a constant perturbing potential to the Hamiltonian. This interpretation is, for instance, used in [45]. The nucleus and each bound electron of the ion are subject to the same perturbing potential. This is consistent with the point-like ion hypothesis made in Equation (39). Of course, this hypothesis ceases to be relevant if $v_\alpha(\mathbf{r})$ varies appreciably over the scale of the electronic structure of the ion. In the context of detailed modeling, this approach results in substituting for the energies E_α in Equation (9):

$$E_\alpha^* = E_\alpha + Z_\alpha^* v_\alpha^* \tag{41}$$

The correction to the ionization potential is thus:

$$\Delta I_\alpha = Z_\gamma^* v_\gamma^* - Z_\alpha^* v_\alpha^* \text{ with } Z_\gamma^* = Z_\alpha^* + 1 \tag{42}$$
$$\approx v_\gamma^* \tag{43}$$

In the average-atom model, each of the independent electrons (of charge -1) is subject to the same perturbing potential v^*. The energies of the orbitals, in Equation (31), then become:

$$\varepsilon_\alpha^* = \varepsilon_\alpha - v^* \tag{44}$$

with v^* calculated for the average ion charge Z^*.

However, this does not correspond to a unified treatment of both the atomic structure of the ions and the interactions among the particles of the plasma. Such a transposition of the interaction potentials in the plasma, stemming from a particular model, to the effective potentials pertaining to the ions' electronic structure is rather heuristic than formally justified. Moreover, this standpoint on the treatment of interactions in the plasma can lead to some confusion as it may appear as accounting for the effect of interactions on the ion electronic structure, which it does not really do. This procedure shifts the energy reference of each charge state without modifying the spectrum or the orbitals of the electronic structure *per se*.

A slightly different standpoint, maybe less heuristic, on the accounting for the interaction energy is to add an approximate interaction contribution to the free energy of the ideal plasma. In statistical mechanics, such a contribution is called an excess free energy.

In the detailed approach, Equation (5) becomes:

$$\dot{F}(\{n_\alpha\}, T) = \dot{F}_{\mathrm{id}}(\{n_\alpha\}, T) + \dot{F}_{\mathrm{ex}}(\{n_\alpha\}, T) \tag{45}$$

This results in adding excess chemical potentials $\mu_{\mathrm{ex},\alpha}$ in the chemical-equilibrium equation Equation (7). This standpoint is, for instance, adopted in [46].

$$\text{for all } \alpha \neq \mathrm{e}, \ \mu_{\mathrm{id},\alpha}(n_\alpha, T) + \mu_{\mathrm{ex},\alpha}(\{n_\alpha\}, T) + \big(\mu_{\mathrm{id},\mathrm{e}}(n_\mathrm{e}, T) + \mu_{\mathrm{ex},\mathrm{e}}(\{n_\alpha\}, T)\big) Z_\alpha^* = \lambda_\mathrm{i} \tag{46}$$

In this framework, the effective correction to the ionization potential appears when one calculates, for instance, the ratio of populations for levels belonging to neighbouring charge states. It results from the corrections to the chemical potentials of the neighbouring charge states, and free electrons:

$$\Delta I_\alpha = \mu_{\mathrm{ex},\gamma} - \mu_{\mathrm{ex},\alpha} + \mu_{\mathrm{ex},\mathrm{e}} \text{ with } Z_\gamma = Z_\alpha + 1 \tag{47}$$

In the average-atom case, one simply adds the excess free energy $\dot{F}_{\mathrm{ex}}(n_\mathrm{e}, n_\mathrm{i}, Z^*, T)$ corresponding to the plasma of free electrons and a sole species of ions having the average charge Z^*, which depends on n_e. Equation (18) becomes:

$$\dot{F}\{\{p_\xi\}, \underline{v}_{\mathrm{trial}}, n_\mathrm{e}; n_\mathrm{i}, T\} = \dot{F}_{\mathrm{id},\mathrm{i}}(n_\mathrm{i}, T) + \dot{F}_{\mathrm{id},\mathrm{e}}(n_\mathrm{e}; n_\mathrm{i}, T) + \dot{F}_{\mathrm{ex}}(n_\mathrm{e}, n_\mathrm{i}, Z^* = n_\mathrm{e}/n_\mathrm{i}, T) + \Delta F_1\{\{p_\xi\}, \underline{v}_{\mathrm{trial}}\} \tag{48}$$

and Equation (32) becomes

$$\mu = \mu_{\mathrm{id},\mathrm{e}}(n_\mathrm{e}, T) + \frac{\partial}{\partial n_\mathrm{e}} \dot{F}_{\mathrm{ex}}(n_\mathrm{e}, n_\mathrm{i}, Z^* = n_\mathrm{e}/n_\mathrm{i}, T) \tag{49}$$

where one must account for the dependency of Z^* on n_e when calculating the derivative.

The underlying hypothesis common to these approaches is that the ion is point-like when compared to the typical interparticle distance d in the ion-free-electron plasma.

$$r_{\mathrm{outer}} << d \tag{50}$$

In a detailed model, r_{outer} is the largest mean radius of any populated orbital of any significantly populated multi-electron state. In an average-atom model, r_{outer} is the mean radius of the outer significantly populated orbital. The relevant interparticle distance d depends on the model used for the ion-free-electron plasma.

The point-like-ion hypothesis is the key argument in separating the modeling of interactions in the plasma from the modeling of the ion electronic structure. However, it excludes the case where some populated orbitals of an ion are perturbed by the effect of its surrounding particles, that is, the case of pressure-ionized plasmas.

3.2. Mean-Field Approach

Calculating the interaction energy in the ion-free-electron plasma requires one to address its spatial correlations functions. In classical mechanics, this may be achieved using the Percus picture, which relates the two-particle correlation functions in a homogeneous system to 1-particle densities in inhomogeneous fictitious systems [47]. In brief, the α, γ pair distribution function of the homogeneous fluid is related to the average density $n_{\alpha,\gamma}(r)$ of particles of species γ, around a particle of species α placed at the origin:

$$n_{\alpha,\gamma}(r) = n_\gamma g_{\alpha,\gamma}(r) \tag{51}$$

One is then left with the problem of calculating the particle densities $n_{\alpha,\gamma}(r)$ in a set of fictitious systems, each rendered inhomogeneous by a particle of species α placed at the

origin. The mean field (or Hartree) approach to this problem yields the nonlinear Debye–Hückel model (NLDH model) of the ion-free-electron plasma, which can also be called the Poisson–Boltzmann model of ion-free-electron plasma. The equations of this model may be summarized as follows:

$$\nabla^2 v_\alpha(r) = -4\pi e^2 \sum_{\gamma=1}^{M,e} Z_\gamma^* n_{\alpha,\gamma}(r) \tag{52}$$

$$\lim_{r\to 0} v_\alpha(r) = \frac{Z_\alpha^* e^2}{r} \tag{53}$$

$$\lim_{r\to\infty} v_\alpha(r) = 0 \tag{54}$$

$$n_{\alpha,\gamma}(r) = n_\gamma e^{-\beta Z_\gamma^* v_\alpha(r)} \tag{55}$$

$$\sum_{\gamma=1}^{M,e} n_\gamma Z_\gamma^* = 0 \tag{56}$$

Here, $v_\alpha(r)$ corresponds to the self-consistent-field potential around the central particle of species α, in the related Percus fictitious system. Equation (52) is the Poisson equation for $v_\alpha(r)$, Equations (53) and (54) are the associated boundary conditions, Equation (55) follows from the 1-particle Boltzmann distribution, and Equation (56) expresses the neutrality of the system.

In itself, the NLDH model of ion-free-electron plasma is of no use since it leads to the Coulomb collapse. However, in the context of non-ideality corrections, the accounting for interactions in the ion-free-electron plasma is often performed using two more-approximate models based on classical mechanics: the Debye–Hückel model and the ion-sphere model. Each of these models is based on a different hypothesis, both of them allowing one to circumvent the Coulomb catastrophe.

3.3. Debye–Hückel Model

The Debye–Hückel model [48] (DH) is based on a linearization with respect to the mean-field potential in Equation (55).

$$n_{\alpha,\gamma}(r) = n_\gamma(1 - \beta Z_\gamma v_\alpha(r)) \tag{57}$$

This linerization both allows one to have an analytical solution and to circumvent the Coulomb catastrophe. It is valid in the weak-coupling limit, but is in fact strongly unphysical in the vicinity of the nucleus at any conditions. This yields an unphysical singularity at the origin in the Debye–Hückel correlation functions, which can be seen as a consequence of circumventing the Coulomb catastrophe.

The analytical solution of Equations (51)–(53), (56) and (57) is

$$v_\alpha^{\mathrm{DH}}(r) = Z_\alpha^* e^2 \frac{e^{-r/\lambda_{\mathrm{D}}}}{r} \tag{58}$$

$$g_{\alpha,\gamma}^{\mathrm{DH}}(r) = 1 - \beta Z_\alpha^* Z_\gamma^* e^2 \frac{e^{-r/\lambda_{\mathrm{D}}}}{r} \tag{59}$$

where $\lambda_{\mathrm{D}} = \left(4\pi\beta e^2 \sum_{\alpha=1}^{M,e} n_\alpha Z_\alpha^2\right)^{-1/2}$ is the Debye length.

The mean-field potential applied on the central particle of species α, due to the other particles, is the divergence-free mean-field potential at the origin:

$$v_\alpha^{*\mathrm{DH}} = v_\alpha^{\mathrm{DH}}(r) - \frac{Z_\alpha e^2}{r} = -\frac{Z_\alpha e^2}{\lambda_{\mathrm{D}}} \tag{60}$$

The excess free energy can be calculated either by using an integration over the inverse temperature (see [49]), or by using the Debye–Kirkwood charging method [50] (see, for instance, [51] for an application to the DH model with arbitrary potential).

$$\dot{F}_{\text{ex}}^{\text{DH}} = -\frac{1}{12\pi\beta n_{\text{i}}\lambda_{\text{D}}^3} \tag{61}$$

From this free energy, the excess contribution to the pressure and internal energy are readily obtained, and it can be shown that the model fulfills the virial theorem of Equation (11). Thus, adding the excess free-energy $F_{\text{ex}}^{\text{DH}}$ to the Saha model, as in Equation (45), preserves the virial theorem.

The free energy can also be used to calculate the chemical potentials

$$\mu_{\text{ex},\alpha}^{\text{DH}} = -\frac{1}{2}\frac{Z_\alpha^{*2}e^2}{\lambda_{\text{D}}} \tag{62}$$

which yields the following correction to the ionization potentials (see, for instance, [46]):

$$\Delta I_\alpha^{\text{DH}} = -\frac{(Z_\alpha^*+1)e^2}{\lambda_{\text{D}}} \tag{63}$$

The latter correction is equivalent to applying the correction $v_\alpha^{*\text{DH}}$ using the upper charge state, as in [45].

In the average-atom context, the excess free energy of Equation (48) is:

$$\dot{F}_{\text{ex}}^{\text{DH}} = -\frac{1}{12\pi\beta n_{\text{i}}}\left(4\pi e^2\beta\left(n_{\text{e}}+n_{\text{i}}\frac{n_{\text{e}}^2}{n_{\text{i}}^2}\right)\right)^{3/2} \tag{64}$$

Accounting for this interaction correction leads to shifting the 1-electron eigenvalues as follows:

$$\varepsilon_\xi^* = \varepsilon_\xi + \frac{(Z^*+1/2)e^2}{\lambda_{\text{D}}} \tag{65}$$

3.4. Ion-Sphere Model from a Classical-Plasma Perspective

In order to apply the notion of IPD to strongly coupled plasma, one often resorts to the "ion-sphere" (IS) model (see e.g., [45]). In this model, one considers a point-like ion placed at the center of a sphere filled only with a uniform density of free electrons, with which it interacts (see Figure 2). The uniform density of free electrons corresponds to the mean free-electron density of the plasma $n_{\text{e}} = \sum_\alpha n_\alpha Z_\alpha^*$, while the radius of the sphere is such that the ion sphere is neutral:

$$R_{Z_\alpha^*} = \left(\frac{3Z_\alpha^*}{4\pi n_{\text{e}}}\right)^{1/3} \tag{66}$$

In the case of an average ion, $n_{\text{e}} = n_{\text{i}}Z^*$, the ion charge Z_α^* is replaced by Z^* and the sphere radius is just the Wigner–Seitz radius $R_{\text{WS}} = (3/(4\pi n_{\text{i}}))^{1/3}$.

From this model, one may evaluate the interaction energy of the central ion with the surrounding electrons in the sphere. This yields the correction $v_\alpha^{*\text{IS}}$ to the energy of the α species.

$$v_\alpha^{\text{IS}}(r) = \frac{Z_\alpha^*e^2}{r} + \frac{1}{2}\frac{Z_\alpha^*e^2}{R_{Z_\alpha^*}}\frac{r^2}{R_{Z_\alpha^*}^2} - \frac{3}{2}\frac{Z_\alpha^*e^2}{R_{Z_\alpha^*}} \quad ; \quad v_\alpha^{*\text{IS}} = -\frac{3}{2}\frac{Z_\alpha^*e^2}{R_{Z_\alpha^*}} \tag{67}$$

One may also evaluate the total interaction energy of the ion sphere, which corresponds to the energy added if one adds an ion to the system and thus gives the correction to the chemical potential.

$$\mu_{\text{ex},\alpha}^{\text{IS}} = -\frac{9}{10}\frac{Z_\alpha^{*2}e^2}{R_{Z_\alpha^*}} \tag{68}$$

This leads to the following correction to the ionization potentials:

$$\Delta I_\alpha^{\text{IS}} = -\frac{9}{10}\left(\frac{Z_\gamma^{*2}e^2}{R_{Z_\gamma^*}} - \frac{Z_\alpha^{*2}e^2}{R_{Z_\alpha^*}}\right) \text{ with } Z_\gamma = Z_\alpha + 1 \tag{69}$$

$$\approx -\frac{3}{2}\frac{Z_\alpha^*e^2}{R_{Z_\alpha^*}} \text{ to first order} \tag{70}$$

which is equivalent to first order to applying the correction $v_\alpha^{*\text{IS}}$, as in [45].
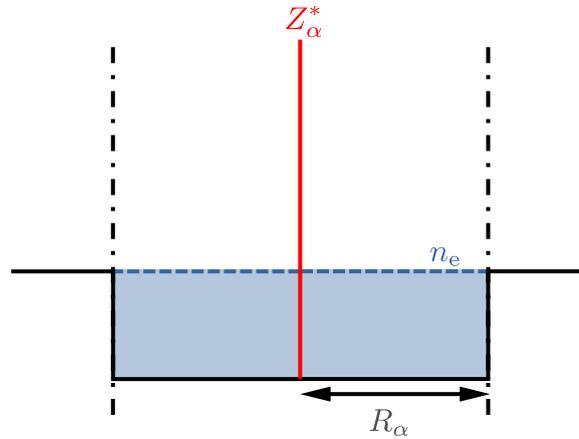
Figure 2. Schematic picture of the ion-sphere model. The electron density of the uniform background corresponds to the free-electron density of the plasma. The radius of the sphere R_α is such as to neutralize the central ion charge Z_α^*.

On the interpretation of this model, two different physical pictures may be put forward. In the first, the plasma is seen as a highly structured set of neutral spheres, somehow resembling a solid-state situation. This interpretation is given, for instance, in [45]. Another interpretation is that the medium surrounding the ion may be split in two regions: a spherical statistical cavity in which other ions do not enter, and a uniform neutral plasma beyond the cavity (physical picture illustrated on Figure 2). This more resembles a liquid-state situation, and we will elaborate on the latter picture hereafter.

In the ion-sphere model, the founding hypothesis that allows one to circumvent the Coulomb catastrophe is to neglect the polarization of the free electrons, which is driven by the attractive long range potential. Free electrons then constitute a uniform background neutralizing the ions. If multiple ion species are considered, the system corresponds to the multi-component classical plasma (MCP) system. The Hamiltonian of such a system is

$$\mathcal{H}_{\text{MCP}}(\{\mathbf{p}_{\alpha,j}, \mathbf{r}_{\alpha,j}\}) = \mathcal{H}_{\text{id}}(\{\mathbf{p}_{\alpha,j}\}) + W_{\text{MCP}}(\{\mathbf{r}_{\alpha,j}\}) \tag{71}$$

$$W_{\text{MCP}}(\{\mathbf{r}_{\alpha,j}\}) = \frac{e^2}{2}\sum_{\alpha=1}^{M}\sum_{j=1}^{N_\alpha}\sum_{\substack{\gamma=1 \\ (\gamma,k)\neq(\alpha,j)}}^{M}\sum_{k=1}^{N_\gamma}\frac{Z_\alpha^*Z_\gamma^*}{|\mathbf{r}_{\alpha,j}-\mathbf{r}_{\gamma,k}|} - e^2\sum_{\alpha=1}^{M}\sum_{j=1}^{N_\alpha}\int_V d^3r\left\{\frac{n_e Z_\alpha^*}{|\mathbf{r}_{\alpha,j}-\mathbf{r}|}\right\} + \frac{e^2}{2}\int_V d^3r\, d^3r'\left\{\frac{n_e^2}{|\mathbf{r}'-\mathbf{r}|}\right\} \tag{72}$$

where the sums only run over the M ions species. If only one ion species is considered, the system corresponds to the one-component plasma (OCP).

Rigorously speaking, such a rigid electron background hypothesis is applicable only in the case of electron–electron and ion–electron couplings much weaker than the ion–ion coupling. Such conditions are found only when free electrons are strongly degenerate. Yet, this model is often used in practice to address the qualitative behavior of moderately or strongly coupled plasmas, as the only classical model available.

The OCP/MCP system may be addressed in the thermodynamic limit of the canonical ensemble either using methods of simulation [52,53] or statistical physics models (e.g., hypernetted chain [54,55], Percus–Yevick [56,57], etc.). Among the statistical-physics models, the mean-field approach yields the nonlinear Debye–Hückel model (or Poisson–Boltzmann model) of the OCP/MCP, whose equations are:

$$n_\gamma h_{\alpha,\gamma}(r) = n_\gamma (g_{\alpha,\gamma}(r) - 1) = n_{\alpha,\gamma}(r) - n_\gamma \tag{73}$$

$$\nabla^2 v_\alpha(r) = -4\pi \mathrm{e}^2 \sum_{\gamma=1}^{M,\mathrm{e}} Z_\gamma^* (n_{\alpha,\gamma}(r) - n_\gamma) \tag{74}$$

$$\lim_{r \to 0} v_\alpha(r) = \frac{Z_\alpha^* \mathrm{e}^2}{r} \tag{75}$$

$$\lim_{r \to \infty} v_\alpha(r) = 0 \tag{76}$$

$$n_{\alpha,\gamma}(r) = n_\gamma e^{-\beta Z_\gamma^* v_\alpha(r)} \tag{77}$$

$$\sum_{\gamma=1}^{M} n_\gamma Z_\gamma^* = n_\mathrm{e} \tag{78}$$

In the weak coupling limit $\Gamma_{\alpha,\gamma} \to 0$, one can perform the Debye–Hückel linearization, replacing Equation (77) with Equation (57). This leads to the DH model of the OCP/MCP, that is, a DH model in which polarization of free electrons is neglected.

In the strong-coupling limit $\Gamma_{\alpha,\gamma} \to \infty$ of this model, the pair distribution functions $g_{\alpha,\gamma}(r)$ take the form of Heaviside functions, yielding spherical, statistical cavities around each ion:

$$g_{\alpha,\gamma}(r) \to \theta(r - R_{\alpha,\gamma}) \tag{79}$$

In the OCP case, there is only one ion–ion pair distribution function to consider, and the mean density of ion charge $\varrho(r)$ around an ion directly becomes that of the ion-sphere with radius R_WS.

$$\varrho(r) = n_\mathrm{i} Z^* q_\mathrm{e} \theta(r - R_\mathrm{WS}) = n_\mathrm{e} q_\mathrm{e} \theta(r - R_\mathrm{WS}) \tag{80}$$

Figure 3 shows how the OCP pair distribution function obtained from the NLDH model changes from the DH shape to the IS shape when Γ is increased. Consistently, Figure 4 displays the values of the divergence-free mean-field potential at the origin v^* and of the excess chemical potential μ_ex as functions of Γ. One clearly sees how these two quantities go from the DH behavior (in the sense of the OCP) to the IS limiting values.

In the MCP case, the mean density of ion charge $\varrho_\alpha(r)$ around a given ion of species α results from the sum of the multiple pair distribution functions $g_{\alpha,\gamma}$. In the $\Gamma_{\alpha,\gamma} \to \infty$ limit, it ultimately tends to the ion sphere form:

$$\varrho_\alpha(r) = \sum_\gamma n_\gamma Z_\gamma^* q_\mathrm{e} \theta(r - R_\alpha) \approx n_\mathrm{e} q_\mathrm{e} (1 - \theta(r - R_{Z_\alpha^*})) \tag{81}$$

As an example, we present in Figure 5 the case of a 6-component classical plasma corresponding to the charge-state distribution obtained from the DCA model [58] for an iron plasma at solid density and 40-eV temperature. Ion coupling in this case is moderate to strong, going from $\Gamma_{4+,4+} = 1.4$ to $\Gamma_{9+,9+} = 7.6$.

Let us mention that the hypothesis of a Heaviside-shaped cavity with a radius varying so as to ensure neutrality for each charge state is precisely the hypothesis made in the model described in [58], and the present discussion gives the physical picture underlying this hypothesis.

The problem of bridging the gap between the DH model of ion-free-electron plasma and the IS model of the OCP is notably addressed by Stewart and Pyatt in [45], using an approach inspired from the Thomas–Fermi model (see next section) and the Poisson–Boltzmann model of the OCP. However, in this paper, the model is used to describe the electron cloud around an ion rather than the electronic structure of the ion itself. They obtain the following formula, which smoothly switches from the DH to the IS result, according to the ratio between the Debye length and the ion-sphere radius:

$$\Delta I_\alpha^{\mathrm{SP}} = -\frac{1}{\beta}\left(\frac{n_{\mathrm{e}}}{n_{\mathrm{i}}}+1\right)^{-1}\left(\left[\left(\frac{R_{Z_\alpha^*}}{\lambda_{\mathrm{D}}^*}\right)^3+1\right]^{2/3}-1.\right) \tag{82}$$

with $\lambda_{\mathrm{D}}^* = \left(4\pi\beta\mathrm{e}^2 n_{\mathrm{e}}(n_{\mathrm{e}}/n_{\mathrm{i}}+1)\right)^{-1/2}$.
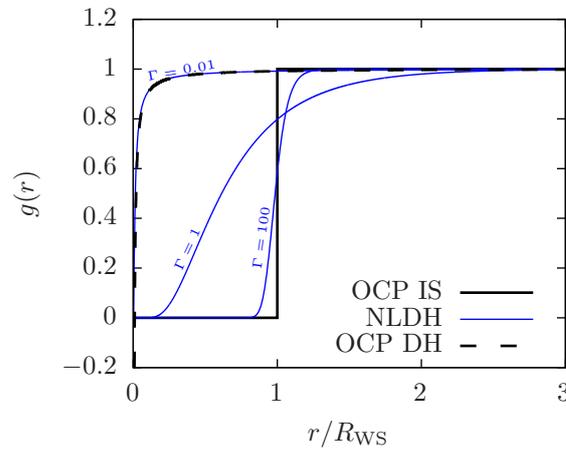
Figure 3. Pair distribution function $g(r)$ from the NLDH model of the OCP for various values of Γ. Comparison with $g(r)$ obtained from the Debye–Hückel model of the OCP at $\Gamma = 0.01$, and with the ion-sphere assumption for $g(r)$.
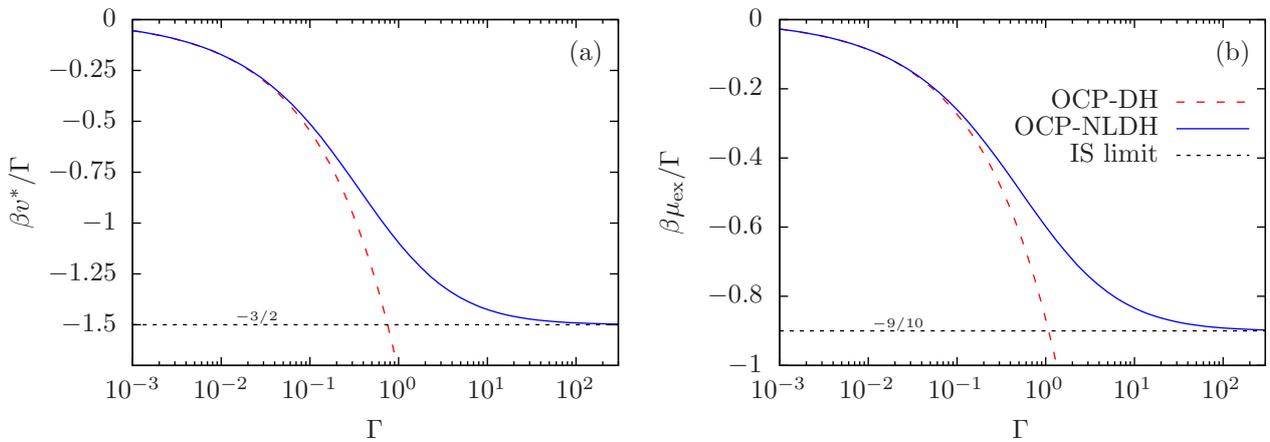

Figure 4. Divergence-free average potential at the origin (**a**) and chemical potential (**b**) as functions of the coupling paramter, for the nonlinear Debye–Hückel model of the one-component plasma (OCP-NLDH). The linear Debye–Hückel limit (OCP-DH) as well as the ion-sphere (IS) limit are also shown.
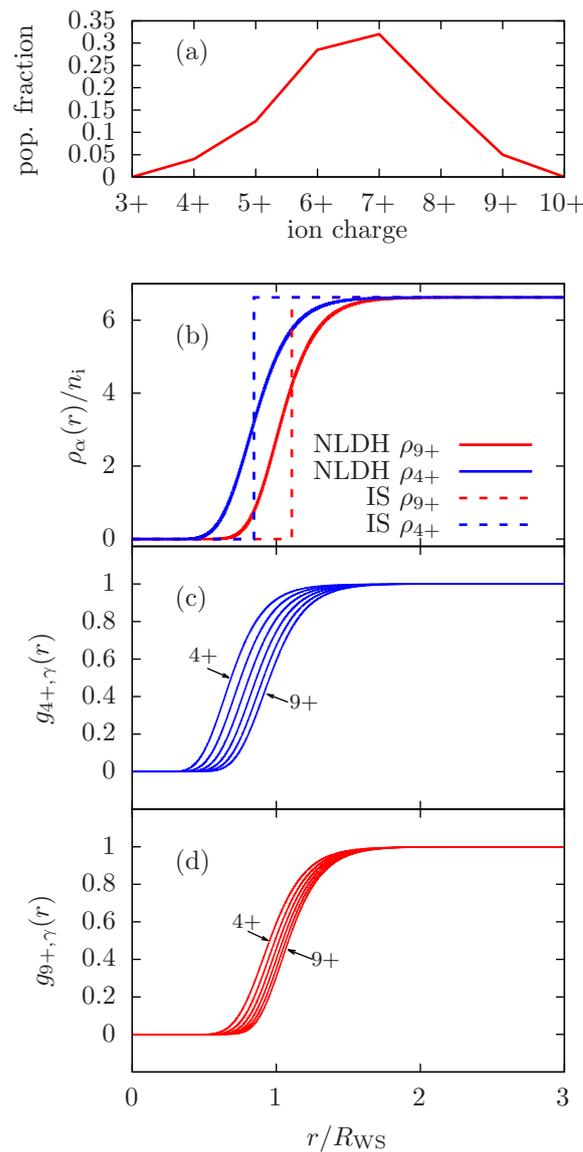
Figure 5. Example of a 6-component classical plasma, typical of the charge-state distribution of an iron plasma at solid density (7.8 g·cm^{-3}) and 40-eV temperature, after [58] (**a**). Ion–ion coupling of significantly populated ions spans from $\Gamma_{4+,4+} = 1.4$ to $\Gamma_{9+,9+} = 7.6$. Plots of the average ion charge density $\varrho_\alpha(r)$ around an ion of of species α (**b**) and of the related pair distribution functions $g_{\alpha,\gamma}(r)$ (**c**,**d**) obtained using the NLDH model of the MCP, for the two charge states $\alpha = 4+$ and $9+$. Comparison with the IS approximation of $\varrho_\alpha(r)$ is shown in (**b**).

Finally, whereas the DH model of ion-free-electron plasma may be seen as rigorously valid in the limit of weak coupling, the ion-sphere model may only be related to the mean-field approach of the OCP/MCP model. In the case of strong coupling, the effect of correlations, beyond the reach of the mean-field approximation, becomes important. Models that account for these effects, such as the hypernetted-chain model (HNC) [59,60], exhibit a different behavior of the pair distribution functions at high Γ, as well as a different limit for the chemical potential. Figure 6 illustrates these differences between the NLDH and HNC model of the OCP, as regards both the pair distribution function and the excess chemical potential.
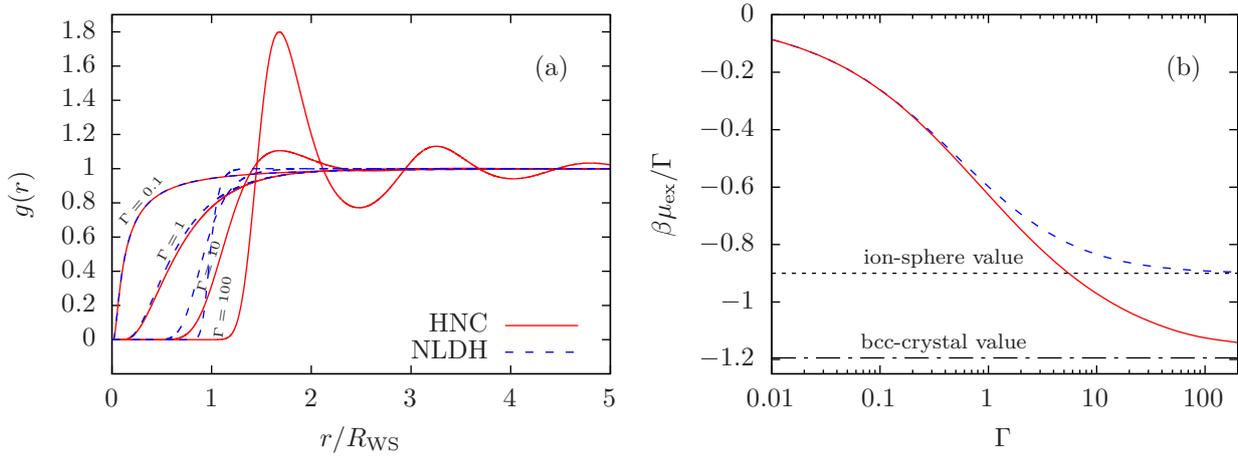
Figure 6. Comparison between the NLDH and HNC models of the OCP. Pair distribution functions for various values of Γ (**a**) and excess chemical potential as a function of Γ (**b**).

One may then put forward the other interpretation of the ion-sphere model: a highly ordered, periodical set of neutral spheres, which may consistute a good approximation of the lattice situation. Indeed, it is known that the OCP system crystallizes at Γ close to 175, yielding a Wigner crystal having a body-centered-cubic lattice (bcc, see [61–63]). For the bcc crystal of an OCP, at zero temperature, we have [63]:

$$\beta U_0 = -0.895929\,\Gamma \tag{83}$$

$$\beta\mu = \frac{4}{3}\beta U_0 \tag{84}$$

where U_0 is the internal energy per ion.

As may be seen on Figure 6, a statistical model accounting for correlations beyond the mean-field approximation, such as HNC, yields results much closer to those of the OCP bcc lattice than does the IS model. In fact, the close proximity in a large range of Γ between thermodynamic quantities stemming from the fluid phase and those from the bcc crystal is among the challenges in the precise determination of the OCP phase transition.

3.5. Divergence of Partition Functions, Suppression of Bound States, Screening and Limitations of the Nonideality Corrections

The isolated-ion models of Section 2 both exhibit divergences of their partition functions. One may relate this divergence issue to the Coulombic behavior of the atomic potential at large distances, typical of isolated-ion models.

First, let us remark that in the $n \to \infty$ limit, the 1-electron spectrum of the average-atom model of isolated ion forms a quasi-continuum having a density of states ϱ_{qc}, which diverges for $\varepsilon \to 0^-$:

$$\varrho_{\text{qc}}(\varepsilon) = \frac{Z^{*2}}{\varepsilon^2} \tag{85}$$

The partition function of high-lying levels $\varepsilon > \varepsilon_{\text{qc}}$ may be seen as the diverging integral:

$$\int_{\varepsilon_{\text{qc}}}^{0} d\varepsilon \left\{ \varrho_{\text{qc}}(\varepsilon) p^{\text{F}}(\mu, T, \varepsilon) \right\} \tag{86}$$

However, limiting the partition function to the negative-energy part of spectrum, one disregards the distortion of the density of states induced by the atomic potential in the positive-energy part.

Let us consider two 1-electron Hamiltonians: the Hamiltonian of free electrons $\tilde{H}_0$ and the Hamiltionian of electrons feeling the external effective potential $\tilde{H}_{\text{eff}}$. Eigenstates of

each of those Hamiltonians constitute a complete orthonormal basis of the *same* 1-electron-state space $\mathcal{E}$. The total number of states within each of these bases is thus the same. If those two bases share a common continuous label, for instance ε, then the density of states with respect to this label may change, but its integral over the label remains the same. This principle is the foundation of Levinson's theorem [64,65]. From this principle, one may expect the divergence of the density of states induced by a Coulomb-tail potential at $\varepsilon \to 0^-$ to be compensated elsewhere; more precisely, in the continuum.

A spherically symmetric potential does not couple the subspaces associated with the various orbital quantum number ℓ. Consequently, it is possible to show that the total number of states is conserved for each value of ℓ (see, for instance, [65,66]). Moreover, for a spherically symmetric potential, the distortion of the density of states with respect to that of free particles is related to the *scattering phase shift*.

Let us consider a the radial wave functions defined as follows:

$$\varphi_{\varepsilon,\ell,m}(\mathbf{r}) = \frac{P_{\varepsilon,\ell}(r)}{r} Y_{\ell,m_\ell}(\hat{r}) \tag{87}$$

$$\int_0^\infty dr \{ P_{\varepsilon,\ell}(r) P_{\varepsilon',\ell}(r) \} = \delta(\varepsilon - \varepsilon') \text{ (normalization convention)} \tag{88}$$

In the case of a free particle (zero external potential, Hamiltonian $\tilde{H}_0$), the Schrödinger radial equation is the Bessel equation and the radial wave functions are the spherical Bessel function regular at $r = 0$:

$$P_{\varepsilon,\ell}(r) = A_\varepsilon k r j_\ell(kr) \text{ with } k = \sqrt{2m_e\varepsilon} \tag{89}$$

where j_ℓ is the spherical Bessel function regular at 0, y_ℓ denoting the irregular one in the following [67]. We define the phase shift $\Delta_{\varepsilon,\ell}(R)$ of a continuum radial wave function $P_{\varepsilon,\ell}(r)$ with respect to the regular Bessel function as follows. Setting the potential to zero for $r \geq R$, $\Delta_{\varepsilon,\ell}(R)$ is such that

$$P_{\varepsilon,\ell}(r \geq R) = A_\varepsilon k r (\cos(\Delta_{\varepsilon,\ell}(R)) j_\ell(kr) - \sin(\Delta_{\varepsilon,\ell}(R)) y_\ell(kr)) \tag{90}$$

For a finite-range potential, the Schrödinger equation tends to the Bessel equation far from the origin, and the phase shift has a finite asymptotic value, which is the scattering phase shift.

$$\lim_{r\to\infty} \Delta_{\varepsilon,\ell}(r) = \Delta_{\varepsilon,\ell} \tag{91}$$

The latter scattering phase shift is related to the change of the density of state as follows (see, for instance, [68]):

$$\Delta\varrho_\ell(\varepsilon) = 2(2\ell + 1)\frac{1}{\pi}\frac{\partial \Delta_{\varepsilon,\ell}}{\partial \varepsilon} \tag{92}$$

Applying the conservation of the total number of states for a given ℓ, and remembering that there is no bound state for a free electron (no classically allowed region for $\varepsilon < 0$), one immediately obtains:

$$\int_{-\infty}^0 d\varepsilon \left\{ \sum_{n=1}^{n_{\max,\ell}} 2(2\ell + 1)\delta(\varepsilon - \varepsilon_{n,\ell}) \right\} = -\int_0^\infty d\varepsilon \{ \Delta\varrho_\ell(\varepsilon) \} \tag{93}$$

$$n_{\max,\ell} = \lim_{\varepsilon\to 0} \frac{\Delta_{\varepsilon,\ell}}{\pi} \tag{94}$$

which corresponds to Levinson's theorem. For a finite-range potential, the number of discrete orbitals is thus finite [69].

For a Coulomb-tail potential, the solution of the Schrödinger equation tends to a combination of regular and irregular Coulomb wave functions:

$$\lim_{r \to \infty} P_{\varepsilon,\ell}(r) = A_k \left(\cos(\Delta_{\varepsilon,\ell}^C) F_\ell^C \left(-\frac{Z^*}{k}; kr \right) + \sin(\Delta_{\varepsilon,\ell}^C) G_\ell^C \left(-\frac{Z^*}{k}; kr \right) \right) \tag{95}$$

where F_ℓ^C, G_ℓ^C are the Coulomb wave functions regular and singular at 0, respectively [67], and where $\Delta_{k,\ell}^C$ is a constant phase shift with respect to the Coulomb wave functions. This yields:

$$\lim_{r \to \infty} \Delta_{\varepsilon,\ell}(r) \sim \frac{Z^*}{k} \log(2kr) \tag{96}$$

This singularity of the scattering phase shift is fully consistent with the infinite number of bound states for a Coulomb-tail potential.

The detailed analysis of the compensation between bound and continuum parts of the partition function was studied thoroughly in the framework of the virial expansion by Beth and Uhlenbeck [70], Larkin [71], Ebeling [72–74] and Rogers [75,76]. Accounting for the density of state modification in the continuum yields the Planck–Larkin suppression of the diverging terms in Equations (13) and (36). As a conclusion, the divergence of the partition functions related to the infinite number of bound states is mostly a problem related to a lack of proper accounting for the continuum.

However, non-ideal effects such as the screening by free electrons and the perturbation by surrounding ions may also limit *physically* the range of the effective atomic potential and consequently the number of bound states. In fact, in the context of the virial expansion, the Debye–Hückel correction appears at the second order, together with the Planck–Larkin regularization (see, for instance, [71]).

For the most weakly bound states (both in the sense of many-electron states or in the sense of 1-electron orbitals), the non-ideality correction to the energy may be of the same order as the energy itself, or even greater. The question then is: how to treat these states that potentially end up in the continuum?

In [77], Herzfeld employs the heuristic argument of the mean radius of an hydrogenic orbital being of the same order of the interparticle distance, in order to truncate the set of bound states accounted for in the Saha equilibrium for hydrogen. Qualitatively, this corresponds to limiting the spatial extension of existing states to the size of an ion sphere. In [78,79], Urey and Fermi independently elaborate on this idea, introducing, in the free energy, an excluded-volume term associated with the volume occupied by the various hydrogenic states. Minimizing the free energy, Fermi obtains that the population of a state drops when the total volume is smaller than the excluded volume of this state times the population of the most populated state.

In [71], Larkin relates the truncation to an assumed Debye–Hückel decay of the 1-electron effective potential. Qualitatively, this corresponds to limiting the spatial extension of existing states to the Debye length. However, without a unified treatment for both the electronic structure and the screening in the whole plasma, the argument for using the Debye–Hückel potential in the ion electronic structure is heuristic.

In [45], Stewart and Pyatt recommend suppressing any level for which the ionization-potential correction is greater than the level energy.

One may put forward that, if one sees the non-ideality correction as a lowering of the continuum, then the intersection of this lowered continuum boundary with the isolated-ion potential sets a restriction on the range of the potential, yielding the truncation of the bound state spectrum. This qualitative standpoint is fully consistent with that of suppressing the states whose energy lies above the lowered continuum.

However, correct accounting for the effect of the potential on the continuum remains a crucial issue. In this context, even if there is no singularity of the density of state to

compensate, a compensation still occurs between *finite* quantities, through the appearance of resonances.

For any small perturbation of the potential that leads to the passing of a bound state above the continuum limit, Levinson's theorem informs us that the phase shift at zero energy jumps accordingly. Since this small perturbation cannot lead to a modification of the phase-shift at energies that are large compared to the perturbation, a rapid variation of the phase shift necessarily occurs just above zero energy. This rapid variation corresponds to a sharp peak in the continuum density of states, called a resonance. In the end, the density of state, defined over the whole spectrum with Dirac δ in the negative energy part, just evolves continuously when one of the Dirac δ crosses the zero energy. This way, any observable remains continuous.

As an elementary illustration of the effect of a finite-range potential, Figure 7 presents the 1-electron eigenvalues and the total $\Delta\varrho(\varepsilon) = \sum_\ell \Delta\varrho_\ell(\varepsilon)$ contribution to the density of states for a screened Coulomb potential, with charge $Z = 26$, as a function of the screening length. For infinite screening length, one recovers the usual Coulomb eigenvalues, with the accidental ℓ-degeneracy. As the screening length is decreased, one can see how the accidental degeneracy is removed and how the eigenvalues are gradually shifted towards the continuum until the removal of the orbital from the discrete spectrum. Once the orbital is removed from the discrete spectrum, one can see how it is compensated for by a resonance in the continuum, which gradually spreads out as screening length is further decreased.
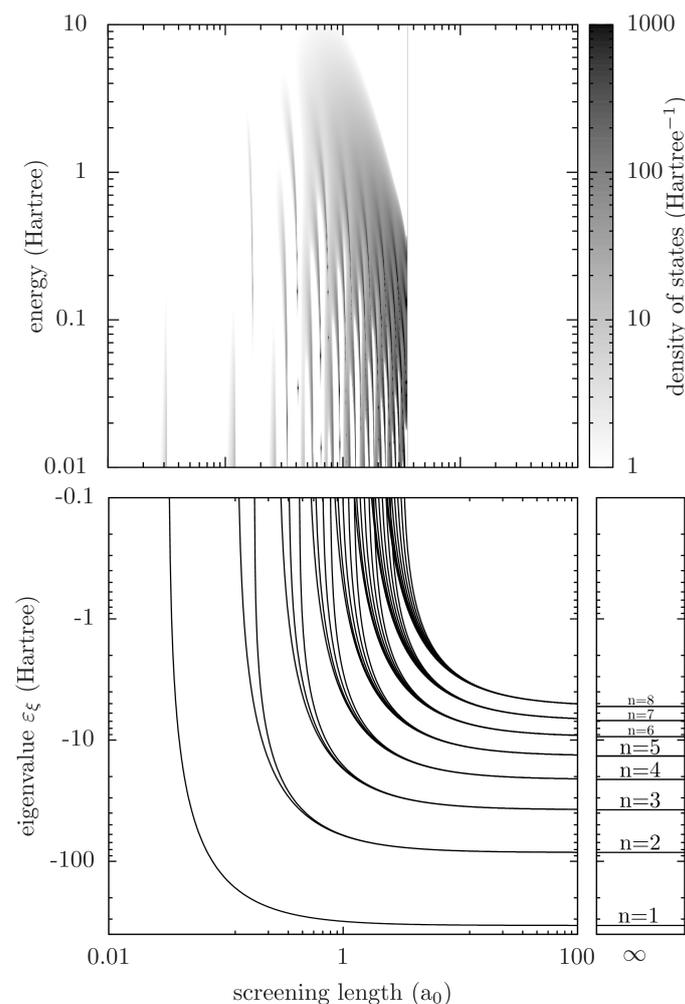

Figure 7. Electron in a screened Coulomb potential with charge $Z = 26$. Eigenvalues as functions of the screening length, for principal quantum numbers up to $n = 8$, and ion contribution to the density of states $\Delta\varrho(\varepsilon)$ of Equation (92), showing the corresponding resonances.

In conclusion, even assuming that a continuum-lowering model is yielding the correct energy shift, a sharp suppression of the bound states does not correspond to what stems from a screened potential with a proper accounting for the continuum.

In practice, the continuum-lowering argument or the introduction of Planck–Larkin partition functions suffices to justify the suppression of weakly bound states, which have negligible populations and do not yield significant contribution of the corresponding resonances. This suppression enables the convergence of the Saha partition function. However, when it comes to suppressing populated many-electron states or orbitals, this method is no longer valid, and in fact the whole point-like-ion hypothesis used in the treatment of interactions breaks down.

A proper answer to the problem requires one to account for the interactions among particles of the plasma directly in the calculation of the ion electronic structure while properly accounting for the continuum. As far as possible, such a calculation should account for both the polarization of free electrons around the ions, and the interactions of ions with their neighbours. This is the purpose of models of pressure-ionized plasmas.

Figure 8 shows the effect of various ionization potential depression models, either disregarding or performing the suppression of bound orbitals. Looking at Figure 8a, one can see that without suppressing any orbital, the effect on the mean ionzation remains moderate, with the Debye–Hückel model yielding the largest effect. In the case considered, the Stewart–Pyatt formula leads to results that are close to those of the ion-sphere model. Looking at Figure 8b, one can see that when performing the associated suppression of bound orbitals, the impact on the mean ionzation is much more pronounced. In fact, most of the effect of accounting for non-ideality corrections is in the modification of the partition function.
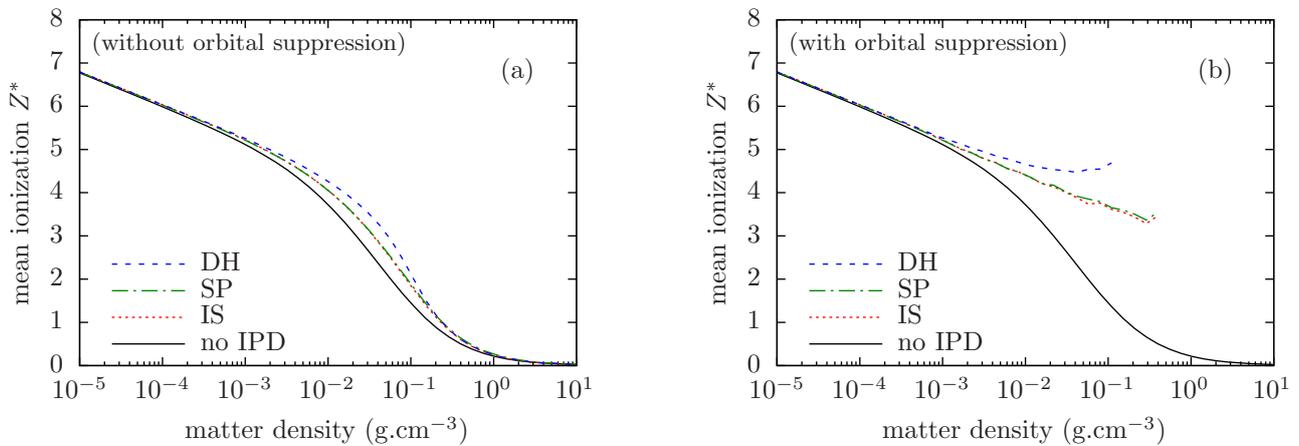

Figure 8. Mean ionization Z^* of a silicon plasma at 20 eV temperature, as a function of matter density. Comparison between average-atom model of isolated ion without any continuum lowering (no IPD, principal quantum number limited to $n = 8$), with Debye–Hückel continuum lowering (DH), with ion-sphere continuum lowering (IS), and with Stewart–Pyatt continuum lowering (SP). Comparisons are shown both without suppression of bound orbitals (**a**) and with suppression (**b**). In the latter case, the curves stop where suppression of a subshell having more than 10% of the electrons occurs (regime of significant pressure ionization).

4. Atomic Models of Pressure-Ionized Plasmas

Whenever the interactions of the ions with the surrounding ions and free electrons have an impact on the electronic structure, we will speak of "pressure-ionized" plasma. In such a case, the picture of a plasma of point-like ions and free electrons is not valid. It is then required to properly account for the surrounding particles in the modeling of the internal electronic structure of each ion. In the following, we will focus on the average-atom description of the plasma since it offers a simpler framework for such modeling. However, most of the presented models can be extended to a detailed description of the plasma.

The modeling of dense, pressure-ionized plasmas has historically been addressed using self-consistent-field models of the ion electronic structure, including all electrons (bound and continuum) and accounting for the surrounding ions through the notion of a Wigner–Seitz cavity. These models focus on the electronic structure around a bare nucleus and depart from the formalism of correlations in the plasma. Being models of the ion electronic structure, all these models necessarily rely, to some extent, on quantum mechanics for the electrons and thus avoid the Coulomb catastrophe.

Depending on the model, the WS cavity is seen either as a neutral spherical cell in which the ion is enclosed (ion-in-cell picture) or as a statistical cavity within which surrounding ions do not enter and beyond which they are uniformly distributed (ion-in-jellium picture).

A common feature of these models of pressure-ionized plasmas is that the resulting atomic potential has finite range, and thus naturally leads to a finite number of bound states.

4.1. Thomas–Fermi Ion-in-Cell Model

The Thomas–Fermi (TF) model is a semiclassical mean-field model of the ion electronic structure, accounting for all electrons and for the surrounding ions through the notion of an ion cell (see Figure 9). Application of the TF model at finite temperature to dense plasmas was first proposed in [80]. A numerical method for solving the TF set of equations was given in [81]. The equations of the TF model are:

$$\nabla^2 v_{\mathrm{el}}(r) = -4\pi e^2 n(r) \tag{97}$$

$$\lim_{r \to 0} v_{\mathrm{el}}(r) = -\frac{Ze^2}{r} \tag{98}$$

$$v_{\mathrm{el}}(R_{\mathrm{WS}}) = 0 \tag{99}$$

$$\int_{\mathrm{WS}} d^3 r \{ n(r) \} = Z \tag{100}$$

$$n(r) = \frac{4}{\sqrt{\pi} \Lambda_e^3} I_{1/2} \left(\beta \left(\mu_e^{\mathrm{F}}(n_e) - v_{\mathrm{el}}(r) \right) \right) \tag{101}$$

where the WS denotes that the integral is performed only within the WS sphere.
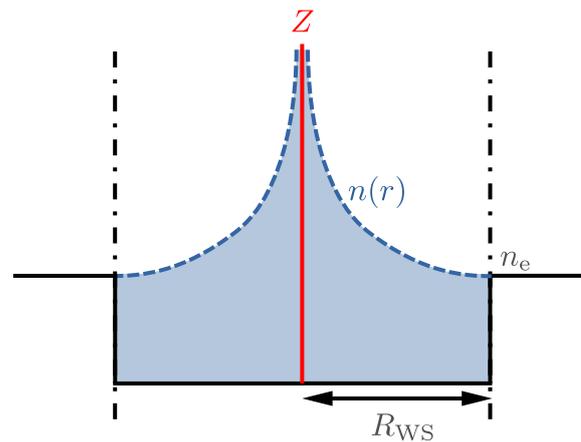

Figure 9. Schematic picture of the Thomas–Fermi model.

Equation (97) is the Poisson equation. Equations (98) and (99) are the boundary conditions at the origin and at the WS radius, respectively. The latter sets the reference of the energies. Equation (100) is the condition of neutrality of the ion sphere. Equation (101) corresponds to the local-ideal-Fermi-gas hypothesis. Equation (97), together with Equation (101), imply a mean-field approximation.

An oft-used extension of the TF model consists of adding a local exchange or an exchange-correlation contribution to the electrostatic potential. This is called the Thomas–

Fermi–Dirac model, referring to [82] in which a local exchange term was derived. In this case, Equation (101) is replaced by:

$$n(r) = \frac{4}{\sqrt{\pi}\Lambda_{\mathrm{e}}^3} I_{1/2}\left(\beta\left(\mu_{\mathrm{e}}^{\mathrm{F}}(n_{\mathrm{e}}) - v_{\mathrm{el}}(r) - \mu_{\mathrm{xc}}(n(r))\right)\right) \tag{102}$$

with $\mu_{\mathrm{xc}} = \partial f_{\mathrm{xc}}(n)/\partial n$ being the chemical potential associated with f_{xc}, an approximate exchange-correlation contribution to the free-energy per unit volume of a uniform electron gas.

Besides its heuristic setup, one may also derive the Thomas–Fermi–Dirac model from a variational principle. One approximates the free energy per ion as the free energy of an ion cell, filled with an electron gas, locally considered as an ideal Fermi gas of density $n(r)$.

$$\dot{F}\{\underline{n}; n_{\mathrm{i}}, T\} = \int_{\mathrm{WS}} d^3r\left\{f_{\mathrm{e}}^{\mathrm{F}}(n(r), T) + f_{\mathrm{xc}}(n(r), T)\right\} + \int_{\mathrm{WS}} d^3r\left\{-\frac{Zn(r)\mathrm{e}^2}{r} + \frac{\mathrm{e}^2}{2}\int_{\mathrm{WS}} d^3r'\left\{\frac{n(r)n(r)}{|\mathbf{r} - \mathbf{r}'|}\right\}\right\} \tag{103}$$

It is worth noting that this free energy does not include terms related to the ion motion or interactions. This is among the shortfalls of such kind of model, which only focuses on the electronic structure of a central ion. In a first approximation, an ion ideal-gas free energy contribution can be trivially added. However, a proper accounting for the ion–ion interactions in such a model is a far more difficult subject, on which we will elaborate later.

One performs the minimization of the free energy per ion while requiring the neutrality of the ion cell

$$\dot{F}_{\mathrm{eq}}(n_{\mathrm{i}}, T) = \underset{\underline{n}}{\mathrm{Min}}\ \dot{F}\{\underline{n}; n_{\mathrm{i}}, T\}\ \text{ s. t. } Z = \int_{\mathrm{WS}} d^3r\{n(r)\} \tag{104}$$

The result of this constrained minimization is equivalent to Equations (97)–(100) and (102).

Starting from the equilibrium free energy, one can rigorously write the thermodynamic quantities using the appropriate derivatives. One notably finds, for the pressure:

$$P_{\mathrm{thermo}}(n_{\mathrm{i}}, T) = -f_{\mathrm{e}}^{\mathrm{F}}(n_{\mathrm{e}}, T) - f_{\mathrm{xc}}(n_{\mathrm{e}}, T) + n_{\mathrm{e}}\mu_{\mathrm{e}}^{\mathrm{F}}(n_{\mathrm{e}}, T) + n_{\mathrm{e}}\mu_{\mathrm{xc}}(n_{\mathrm{e}}, T) \tag{105}$$

It can also be shown that the model fulfills the virial theorem [80].

In the TF model, the electron density is a local function of the potential. In fact, the hypothesis of locally having an ideal Fermi gas may be recovered from a local-density approximation of the quantum kinetic free energy of independent particles [83]. Since the electrostatic potential is zero at the WS radius, the density at the WS radius is equal to that obtained from the chemical potential:

$$Z^* = \frac{n_{\mathrm{e}}(R_{\mathrm{WS}})}{n_{\mathrm{i}}} = \frac{n_{\mathrm{e}}}{n_{\mathrm{i}}} \tag{106}$$

Due to its semiclassical character, the TF model does not yield a shell structure in the sense of quantum mechanics. Consequently, there are no ionization plateaus, as in the mean ionization of the quantum isolated ion. As an illustration, Figure 10a displays the TF mean ionization as a function of temperature for carbon at 10^{-4} g·cm^{-3}, compared to that of a quantum isolated ion.

On the other hand, in the TF model, pressure ionization is obtained through a squeezing of the ion cell when density is increased. As an example, Figure 10b shows the TF mean ionization as a function of matter density for carbon at a temperature of 20 eV.

In addition to being used in equation-of-state calculations, the TF model was also used for the calculation of radiative properties. Such calculations were performed either resorting to a heuristic use of the TF potential in orbital calculations [84] or from rigorous approaches to the dynamic semiclassical model [85–87]. In the latter case, the unphysical behavior of the TF electron density in the vicinity of the nucleus has strong consequences on the photoabsorption cross-section at high frequencies [86]. Moreover, the lack of shell

structure implies the absence of line emission and absorption in the spectra. For the reasons given above, the need for a quantum extension of the TF model was quickly recognized.
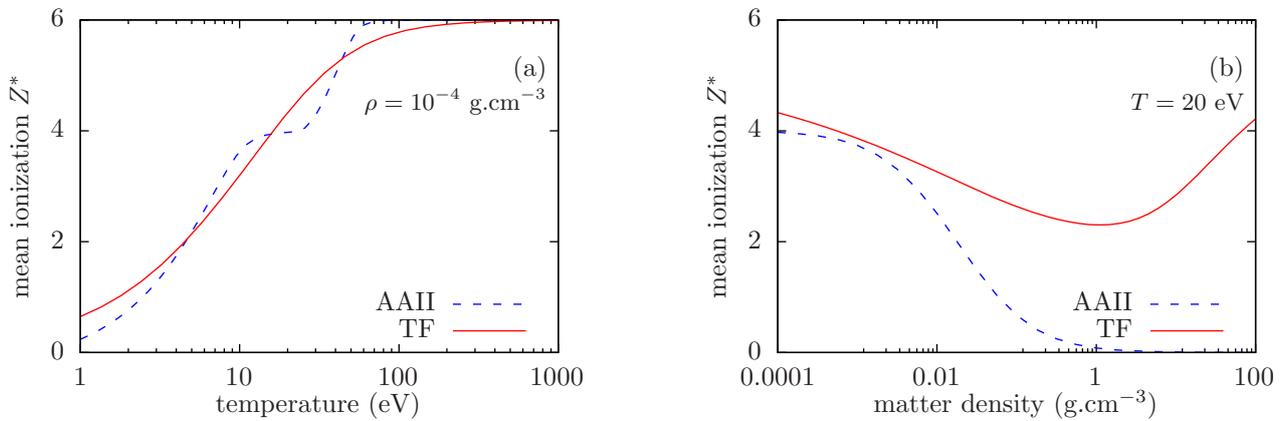

Figure 10. Mean ionization Z^* of a C plasma along the 10^{-4}-g·cm^{-3}-isochore (**a**), and along the 20-eV-isotherm (**b**). Comparison between the Thomas–Fermi model (TF) and the average-atom model of isolated ion (AAII).

Finally, let us remark that in the Thomas Fermi model, the equations are restricted to the WS cell. This renders the model versatile in the sense that it is rather insensitive to the modeling of the medium outside the WS sphere. On the one hand, one may interpret the ion sphere as an element of a highly ordered pile of neutral spheres. In [88], the TF ion cell is used in this way, as an approximation of the polyhedral WS cell of a metal lattice. On the other hand, one may interpret the ion cell as a statistical cavity surrounded by a homogeneous neutral plasma (jellium), as suggested later by Liberman in the context of his INFERNO model [89]. The coexistence of these two possible interpretations relates to the similar ambiguity of the physical picture underlying the ion-sphere model. This duality of interpretation left an imprint on the models proposed later as quantum extensions to the TF model.

4.2. Quantum Ion-in-Cell Models

Among the first quantum extensions to the TF model was the model of Rozsnyai [90]. This model is based on the solid-state picture of the ion cell. The bound electrons are described by resorting to energy bands, whose boundaries are obtained from the Wigner–Seitz cellular method (zeros of the wave function and of its derivative, see [91,92] or the monograph [93]). Positive-energy spectrum (with respect to the effective potential at infinity) is approximated using the TF approach, with a restriction on the energy integration in order to only cover the classically allowed range. The treatment of continuum electrons is therefore not consistent with that of bound electrons. In particular, the contributions of resonances or energy bands in the continuum are disregarded. However, because of the treatment of bound electrons through energy bands, the pressure ionization of a bound state occurs gradually and does not result in a proper discontinuity of observables.

A common variant of this model resorts to wave functions calculated with boundary conditions applied at infinity. In this case, the boundary condition is the exponential decay of the wave function, or, in practice, the matching onto localized zero-field solutions at the WS radius (third kind modified spherical Bessel function). This kind of model is, for instance, used in [27]. In this model, due to the semiclassical treatment of the continuum and the discrete nature of bound states, pressure ionization of a bound state results in a discontinuity of observables.

In practice, the equations of the latter model are the same as in the TF model, except that the electron density is partially calculated from quantum mechanics. Namely, one retains Equations (97)–(100), whereas the electron density is given by:

$$n(r) = \sum_{\zeta \text{ bound}} p_F(\mu, T, \varepsilon_\zeta) |\varphi_\zeta(\mathbf{r})|^2 + \frac{4}{\sqrt{\pi}\Lambda_e^3} I_{1/2}^{\text{inc.}} \left(\beta \left(\mu_e^F(n_e) - v_{el}(r) - \mu_{xc}(n(r)) \right); -\beta \left(v_{el}(r) + \mu_{xc}(n(r)) \right) \right) \tag{107}$$

where the sum only runs over the discrete part of the spectrum, and where $I_{1/2}^{\text{inc.}}$ is the incomplete Fermi integral defined as follows:

$$I_{1/2}^{\text{inc.}}(y; z) = \int_z^\infty dx \left\{ \frac{x^{1/2}}{e^{x-y} + 1} \right\} \tag{108}$$

Another slightly different variant of this model approximates the positive-energy spectrum using the non-degenerate limit of the 1-electron distribution instead of the Fermi–Dirac distribution [94][1]. Let us also mention that some models also use bands for both the negative and positive parts of the energy spectrum [95], with applications to matter in which an ion lattice may subsist.

The first fully quantum model of the ion cell in a plasma was Liberman's model named "INFERNO" [89,96,97]. Contrary to Rozsnyai, Liberman proposes the physical picture of an ion cell surrounded by a finite-temperature jellium, as sketched in Figure 11. A jellium is a homogeneous electron gas, neutralized by a homogeneous ion background.
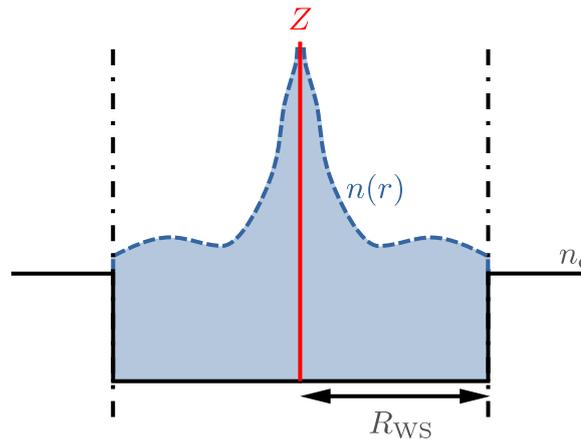
Figure 11. Schematic picture of Liberman's INFERNO model. The electron density is represented with a discontinuity at the WS radius, consistently with the interpretation proposed by Liberman of a homogeneous jellium surrounding the WS sphere.

The equations of the INFERNO model are the same as in the TF model, with an electron density fully calculated from quantum mechanics. One thus keeps Equations (97)–(100), with an electron density given by:

$$n(r) = \sum_{\zeta} p_F(\mu, T, \varepsilon_\zeta) |\varphi_\zeta(\mathbf{r})|^2 \tag{109}$$

where the sum runs over both the discrete and the continuum part of the spectrum. For the continuum, the sum is to be understood as an integral over the momentum. Contrary to the Rozsnyai model and its variants, the INFERNO model accounts for the resonances in the continuum.

Figure 12 shows the density of states obtained from the INFERNO model for silicon at 5 eV temperature and matter densities of 1.1 and 1.2 10^{-2} g·cm^{-3}. At these conditions, one can observe resonances related to the delocalizations of the 5p and 4f subshells. In particular, between 1.1 and 1.2 10^{-2} g·cm^{-3}, the 5p subshell is pressure-ionized, yielding a sharp resonance in the continuous spectrum. In order to illustrate the lack of resonances in Rozsnyai-like models, we also display the density of states obtained when using

Equation (107) for the electron density, at similar plasma conditions. The discrete spectrum from the Rozsnyai-like model is not shown, to avoid obfuscation of the figure.

Consistently, with the picture of an ion cell surrounded by a neutral jellium, the boundary condition applied to the wave functions φ_ζ at the WS radius is just the matching onto the zero-potential solution (a linear combination of Bessel functions, defining a phase shift). Like in the TF model, the medium surrounding the ion cell does not interact with the content of the ion cell. Consequently, the model can be formulated using equations restricted to the WS cell, with the jellium surrounding the WS sphere playing no direct role in the model.

The quantum electron density of Equation (109) is a nonlocal functional of the self-consistent potential. As a consequence, even if the potential is zero at the WS radius, the electron density $n(R_{WS})$ in general differs from the electron density obtained from the chemical potential n_e. The latter corresponds to the asymptotic value $\lim_{r\to\infty} n(r)$.
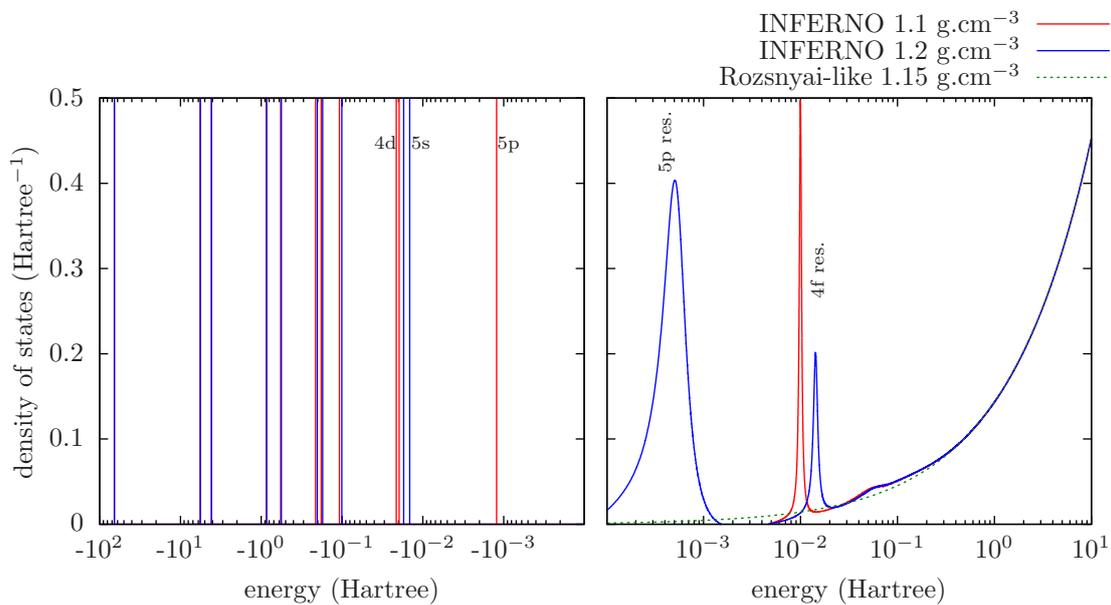
Figure 12. Density of states obtained from the INFERNO model in the case of silicon at 5 eV temperature and matter densities of 1.1 and 1.2 10^{-2} g·cm^{-3}. In the negative energy ranges, the Dirac distributions are represented by vertical lines. For the sake of comparison, the density of states stemming from the Rozsnyai-like model of Equation (107), at 5 eV temperature and 1.15 10^{-2} g·cm^{-3}, is also shown, only in the positive energy range.

This yields an ambiguity in the definition of the mean ionization Z^*, which is closely related to the ambiguity in the physical interpretation of the model. Either the electron density has a discontinuity at the WS radius or it is continuous, but electrons of the jellium have a chemical potential that is different from those of the ion cell.

Connected to this interpretation issue is the problem of defining the pressure in the model (electron pressure at the WS boundary versus electron pressure stemming from a jellium of density n_e). More generally, due to the lack of variational formulation for this model, any thermodynamic quantity is defined heuristically and may have more than one possible definition. Indeed, Liberman proposed two versions of his model (denoted A and T), differing in the region of integration for the free and internal energies [89,96,97]. Thermodynamic consistency among these quantities is in general not assured.

The sharp cut-off of the equations at the WS radius also implies that the virial theorem is not fulfilled. When trying to derive the virial theorem for the system, surface terms appear at the WS radius, which results in the impossibility of fulfilling the theorem (see, for instance [98]).

Nevertheless, Rozsnyai's and Liberman's models are among the most often used when dealing with pressure-ionized plasma, both in their respective average-atom versions (see, for instance, [99,100]) or in a modified version adapted to fixed configurations (see, for instance, [27]). To some degree of approximation, these models account for both the quantum shell structure of the ion and the pressure ionization phenomenon. Both also have relatively light computation costs, favored by the restriction of the equations to the WS cell. Of course, INFERNO involves a much higher computational cost than Rozsnyai's model, due to the quantum treatment of the continuum.

Moreover, a variant of Rozsnyai's model was used in [94] as the starting point to obtain an approximate, closed formula fitting the atomic potential. Such a fit for the atomic potential can be used to infer corrections to the isolated-ion energies, from perturbation theory [101,102]. Such an approach yields analytical formulae for the line shifts, which showed agreement with experimental measurements [103] of line shifts in He-like ions at electron densities of the order of 10^{23} cm^{-3} [104,105]. In prior studies, the simpler model of the ion-sphere had also been used, outside the context of point-like ion hypothesis, to calculate an analytical perturbing potential and infer line shifts [106].

4.3. Ion-in-Jellium Models

Models of an impurity (or a defect) in a jellium were developed during the 70's in the context of solid-state physics [107–109]. In these models, the perturbation generated by the impurity may extend spatially far from its origin. There is no restriction to a particular cell (see Figure 13a).
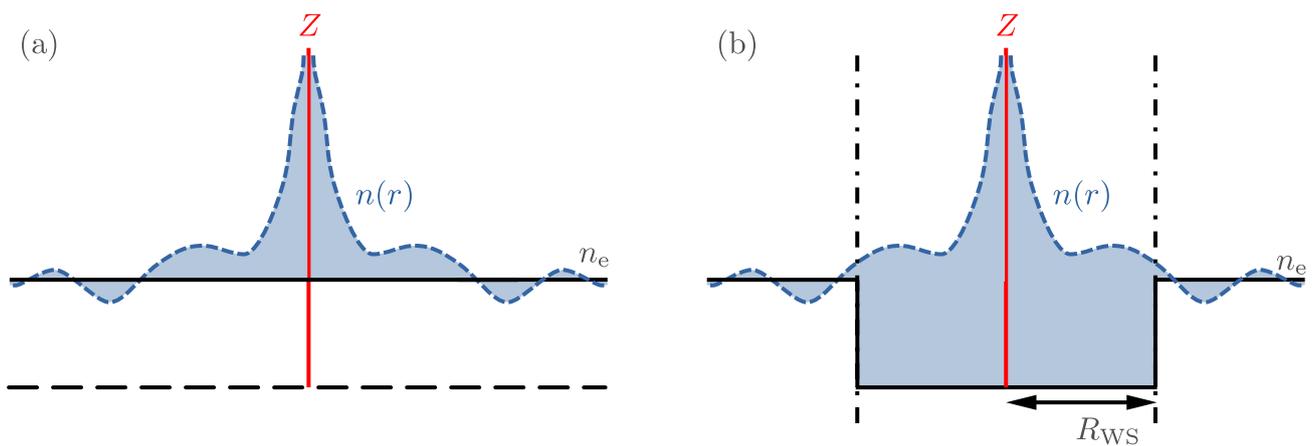

Figure 13. Schematic pictures of an impurity in a jellium (**a**), and of an ion-in-jellium model such as AJCI or VAAQP (**b**).

A first extension of the treatment of an impurity in a jellium to the modeling of an ion in a plasma was suggested by Perrot in the 90's, in his "Atome dans le Jellium de Charge Imposée" model (AJCI, atom in a jellium with fixed charge) [110]. In his model, Perrot introduces a WS statistical cavity in the jellium, much like the picture proposed by Liberman. However, he also considers an ion extending in the whole space, rather than enclosed within a cell (see Figure 13b). Consistently, the neutrality is assumed to hold in the whole space rather than in the ion cell. In this model, the uniform ion background of the jellium surrounding the cavity interacts with the electron density, which asymptotically tends to the jellium density. This leads to the charge density:

$$q_{\mathrm{e}}(n(r) - n_{\mathrm{i}} Z^* \theta(r - r_{\mathrm{WS}})) = q_{\mathrm{e}}(n(r) - n_{\mathrm{e}} \theta(r - r_{\mathrm{WS}})) \tag{110}$$

The AJCI model, like models of impurity in metals, resorts to a fixed jellium density n_{e}, given as an input to the model. It is also lacking a variational derivation. However, the

notion of an ion extending beyond the WS sphere, up to infinity, allows one in principle to solve the problem of surface terms in the virial theorem.

Starting from the founding ideas of the AJCI model, a model of a variational average-atom in a quantum plasma (VAAQP) was proposed and studied [111–114]. This showed that building an atom-in-jellium model within a variational framework enables one to set the jellium density from the thermodynamic equilibrium condition and to fulfill the virial theorem.

Formally, to treat the nuclei-electron plasma as a set of ions, we resort to a reasoning called a "cluster" decomposition. Let O be a quantity that may be calculated for any set of K nuclei, with spatial configuration $(\mathbf{R}_1...\mathbf{R}_K)$, including the empty set. We may then write (see [115] for more detail):

$$O(\mathbf{R}_1...\mathbf{R}_K) = O(\varnothing) + \sum_{j=1}^{K} \Delta O_1(\mathbf{R}_j) + \frac{1}{2} \sum_{j=1}^{K} \sum_{\substack{k=1 \\ k \neq j}}^{K} \Delta O_2(\mathbf{R}_j, \mathbf{R}_k) + ... \quad (111)$$

defining the ΔO_K terms recursively, so as to assure the equality for each value of K:

$$\Delta O_1(\mathbf{R}) = O(\mathbf{R}) - O(\varnothing) \quad (112)$$
$$\Delta O_2(\mathbf{R}_1, \mathbf{R}_2) = O(\mathbf{R}_1, \mathbf{R}_2) - \Delta O_1(\mathbf{R}_1) - \Delta O_1(\mathbf{R}_2) + O(\varnothing) \quad (113)$$
$$\vdots$$

The quantity O has a clustering property if the terms in Equation (111) exhibit a decreasing ordering, which makes Equation (111) a convergent expansion.

In the VAAQP model, we first assume that the electron density $n(\mathbf{R}_1...\mathbf{R}_{N_i}; \mathbf{r})$ for a system of N_i ion is correctly described by limiting the cluster expansion to the zeroth and first order only:

$$n(\mathbf{R}_1...\mathbf{R}_{N_i}; \mathbf{r}) = n_0(\mathbf{r}) + \sum_{j=1}^{N_i} \Delta n_1(\mathbf{R}_j; \mathbf{r}) = n_e + \sum_{j=1}^{N_i} q(|\mathbf{r} - \mathbf{R}_j|) \quad (114)$$

where the zeroth order term is identified as the homogeneous jellium density, and the first order term corresponds to the sum of spherically symmetric clouds of displaced electrons, corresponding each to an ion in a jellium. We also assume the first-order cluster expansion to hold for the free energy of the system. This leads us to write the free energy per ion as follows:

$$\dot{F}(n_i, T) = \dot{F}_0(n_e; n_i, T) + \Delta F_1\{n_e, \underline{q}; T\} \quad (115)$$

Here, $\dot{F}_0 = (f_e^F(n_e, T) + f_{xc}(n_e, T))/n_i$ is the free energy per ion of the uniform electron gas. We choose to treat ΔF_1 using a density-functional formalism [41–43] and decompose the ΔF_1 as suggested by Kohn and Sham [42]:

$$\Delta F_1\{n_e, \underline{q}; T\} = \Delta F_1^0\{n_e, \underline{q}; T\} + \Delta F_1^{el}\{n_e, \underline{q}; T\} + \Delta F_1^{xc}\{n_e, \underline{q}; T\} \quad (116)$$

ΔF_1^0 corresponds to the kinetic and entropic contribution to the free energy of a system of independent electrons subject to an external potential $v_{\text{trial}}\{n_e, \underline{q}; r\}$ that yields the electron density $n_e + q(r)$, with the contribution from a homogeneous system of density n_e subtracted.

$$\Delta F_1^0\{n_e, \underline{q}; T\} = \sum_{\xi} \int d^3r \left\{ p_F(\varepsilon_\xi; n_e, T) \left[(\varepsilon_\xi - v_{\text{trial}}(r) - Ts_F(\varepsilon_\xi; n_e, T)) |\varphi_\xi(\mathbf{r})|^2 - (\varepsilon_\xi - Ts_F(\varepsilon_\xi; n_e, T)) |\varphi_\xi^0(\mathbf{r})|^2 \right] \right\} \quad (117)$$

where the sum runs over both the discrete and continuum part of the spectrum and where the $\{\varphi_\xi^0\}$ correspond to the plane waves and only contribute in the continuum part. ΔF_1^{xc} corresponds to the exchange and correlation contribution to the free energy, with the contribution from the homogeneous system subtracted, taken in the local density approximation:

$$\Delta F_1^{\text{xc}}\{n_{\text{e}}, \underline{q}; T\} = \int d^3r \{ f_{\text{xc}}(n_{\text{e}} + q(r), T) - f_{\text{xc}}(n_{\text{e}}, T) \} \tag{118}$$

ΔF_1^{el} is the direct interaction term, in which we introduce the hypothesis of the WS cavity. We model the surrounding ions by a charge density $q_{\text{e}} n_{\text{e}} \theta(r - R_{\text{WS}})$, like in the AJCI model. This leads to:

$$\Delta F_1^{\text{el}} = \int d^3r \left\{ -\frac{Z(n_{\text{e}} + q(r) - n_{\text{e}}\theta(r - R_{\text{WS}}))e^2}{r} \right.$$
$$\left. +\frac{e^2}{2} \int d^3r' \left\{ \frac{(n_{\text{e}} + q(r) - n_{\text{e}}\theta(r - R_{\text{WS}}))(n_{\text{e}} + q(r) - n_{\text{e}}\theta(r' - R_{\text{WS}}))}{|\mathbf{r} - \mathbf{r}'|} \right\} \right\} \tag{119}$$

Accordingly, the condition of neutrality in the whole space can be written as:

$$Z = \int d^3r \{ n_{\text{e}} + q(r) - n_{\text{e}}\theta(r - R_{\text{WS}}) \} \tag{120}$$

Finally, the VAAQP model is based on the minimization of the free energy with respect to the displaced-electron density $q(r)$ and jellium density n_{e}, while requiring the neutrality condition:

$$\dot{F}_{\text{eq}}(N_{\text{i}}, V, T) = \underset{n_{\text{e}}, \underline{q}}{\text{Min}} \, \dot{F}\left\{ n_{\text{e}}, \underline{q}; n_{\text{i}}, T \right\} \text{ s.t. } \int d^3r \{ n_{\text{e}} + q(r) - n_{\text{e}}\theta(r - R_{\text{WS}}) \} = Z \tag{121}$$

This constrained minimization yields the following equations:

$$v_{\text{trial}}(r) = v_{\text{el}}(r) + \mu_{\text{xc}}(n_{\text{e}} + q(r)) - \mu_{\text{xc}}(n_{\text{e}}) \tag{122}$$

$$v_{\text{el}}(r) = -\frac{Ze^2}{r} + e^2 \int d^3r' \left\{ \frac{n_{\text{e}} + q(r) - n_{\text{e}}\theta(r' - R_{\text{WS}})}{|\mathbf{r} - \mathbf{r}'|} \right\} \tag{123}$$

$$\int d^3r \{ v_{\text{el}}(r)\theta(r - R_{\text{WS}}) \} = 0 \tag{124}$$

Equation (124) stems from the minimization condition with respect to the jellium density n_{e} and allows its value to be set. Thus, in the VAAQP model, the density of the uniform background is uniquely defined; it corresponds to the asymptotic electron density of each ion and is *set by the thermodynamic equilibrium condition*.

From the equilibrium free energy per ion, it is possible to rigorously obtain the other thermodynamic quantities, by calculating the appropriate derivatives. For the pressure, the following formula is obtained:

$$P_{\text{thermo}} = -f_{\text{e}}^{\text{F}}(n_{\text{e}}, T) - f_{\text{xc}}(n_{\text{e}}, T) + n_{\text{e}}\mu_{\text{e}}^{\text{F}}(n_{\text{e}}, T) + n_{\text{e}}\mu_{\text{xc}}(n_{\text{e}}, T) + n_{\text{e}}v_{\text{el}}(R_{\text{WS}}) \tag{125}$$

The first four terms correspond to the pressure of an ideal Fermi gas of density n_{e}. The last term is related to the WS cavity. Moreover, it can be shown that the virial pressure leads to the same formula as Equation (125), meaning that the *virial theorem is fulfilled* in the VAAQP model.

In the contributions to the free energy expression of Equation (115), the ions are disregarded. For that reason, the thermodynamic quantities from the VAAQP model may be viewed as electron contributions, which may be supplemented by ion contributions. Adding an ion ideal-gas contribution to the model is straightforward. However, adding

the results of a model of interacting ions is more problematic because part of the ion–ion interactions is necessarily included in the VAAQP model through the WS-cavity hypothesis.

Like INFERNO, the VAAQP model allows for the description of the ion shell structure, while the WS cavity assumed in the model enables the description of pressure ionization. Treating the perturbation of the density in the whole space, the model also accounts for the Friedel oscillations (see, for instance, [93]) of the displaced-electron density. The physical relevance of these oscillations in the case of ions in a plasma is rather unclear. However, accounting for these is essential to ensure the fulfilment of the virial theorem.

In the VAAQP model, the potential range is not strictly limited to the WS radius but has a strong decay, due to the total screening of the nucleus in the whole space. In practice, the variational equation Equation (124) most often constrains the atomic potential to take small values at the WS radius, of the order of the amplitude of Friedel oscillations. For that reason, the VAAQP model yields results that mostly agree with those of the INFERNO model, except in the low-temperature/high-density regime.

Figure 14 shows an example comparison of results from the isolated-ion, INFERNO, and VAAQP models in the case of silicon at 5-eV temperature. Both the mean ionization and the 1-electron energies are displayed. As is seen from theses figures, the energy correction, and consequently the mean ionization, are rather well estimated using the Stewart–Pyatt approach with the suppression of bound orbitals [45], up to cases of significant pressure ionization (here, around 0.1 g·cm^{-3}). The INFERNO and VAAQP models agree well in this regime. In the region of strong pressure ionization, the results from VAAQP depart significantly from those of INFERNO. Accordingly, the thermodynamic consistency of the INFERNO results is problematic in this region. However, differences in the 1-electron energies are less pronounced (see Figure 14b).
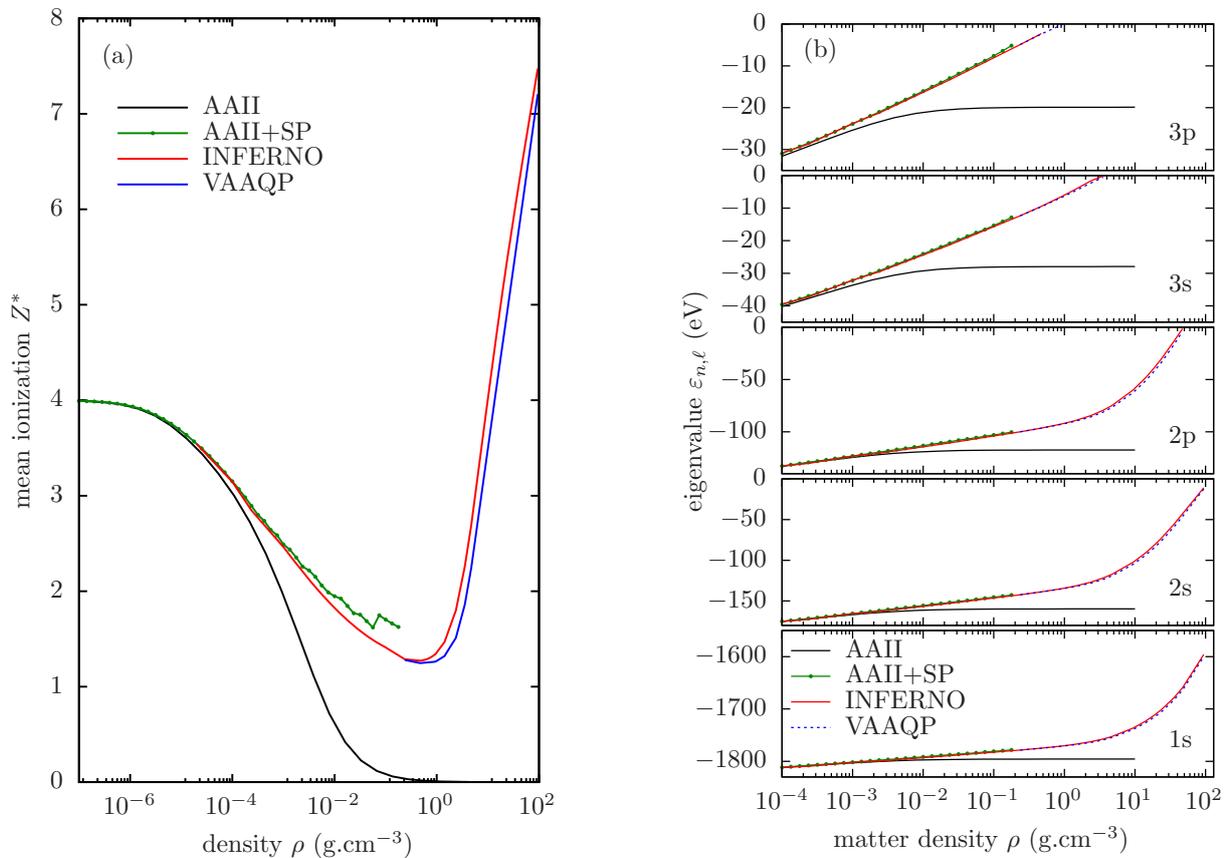

Figure 14. Mean ionization Z^* (**a**), and 1-electron eigenvalues (**b**) as a function of matter density, for silicon at 5-eV temperature. Comparisons between INFERNO, VAAQP, average-atom model of isolated ion (AAII), and AAII with Stewart–Pyatt correction and suppression of orbitals.

The VAAQP model was first applied to equation-of-state calculations [113,114,116] but was also used in the calculation of radiative properties [58,117].

Finally, let us point out that atom-in-jellium models seem a better starting point for improving the modeling of ion–ion correlations than ion–cell models since they account for the ion surroundings in the whole space.

4.4. Going beyond the Cavity Hypothesis, the Difficulty of Dense-Plasma Atomic Modeling

All models of pressure-ionized plasma that are described in the previous paragraphs focus on the description of the electronic structure of a particular ion, postulating that the surrounding ions will either restrict its spatial extension to a WS cell or will interact with it as a spread-out uniform medium, not entering the WS sphere. In these models, a key function is the inhomogeneous density $n(r)$ of the electron cloud associated with the ion. Of course such spatial inhomogeneity of the electron density around a nucleus is in fact referring to correlations among the positions of nuclei and electrons.

For an M-component classical fluid of particles interacting through pair potentials, obtaining the $M(M+1)/2$ pair distribution functions gives access to all statistical averages (see, for instance, [49]). The link relating the pair distribution functions to densities of fictitious systems with a particular particle placed at the origin is the Percus picture [47]. With such a link, one can use models of 1-particle densities to address pair distribution functions.

However, to correctly describe the electronic structure of an ion, one has to resort to quantum mechanics. It turns out that Percus' method is not applicable in the quantum-mechanical context. This may be seen as a consequence of the impossibility of separating the kinetic part of the partition function from its configurational (or interaction) part. For this reason, a practical approach to the correlation functions in quantum mechanics remains a long-standing, open problem (see, for instance, [118]).

In order to circumvent this problem, an idea is to keep the framework of classical statistical mechanics and include approximate accounting for the quantum behavior in the interaction potentials [119], or resorting to an effective temperature [120,121]. Approaches of this kind eventually led to the classical-mapping approach to quantum systems [122,123].

Another kind of approach aims to extend Percus' trick (see, for instance, [124]). Among the goals of such an effort is the quantum generalization of the hypernetted chain model, which may be derived in the classical framework using the Percus picture and the classical DFT (see, for instance, [125]). As was pointed out by Chihara [126], if one assumes that nuclei behave as classical particles, it is possible to partially apply the Percus trick. This requires one to supplement the model with assumptions about some of the correlation functions. This approach led to the "quantum hypernetted chain" (QHNC) model.

However, the DFT-based reasoning for deriving the HNC equations resorts to a functional Taylor expansion around a reference homogeneous medium at a given density. Even if this derivation leads to the HNC equations, it does not give access to the HNC free energy of the homogeneous system (see, for instance, [127] and [51] appendix). This is an issue for the modeling of the thermodynamic equilibrium of a plasma, which includes the determination of the free-electron density. For that reason, the QHNC approach was first used in the modeling of electrons in metals [128], considering given free-electron densities. The QHNC was also applied to the modeling of dense plasmas [129–132], in order to account for the ion–ion correlations. However, in this case it requires an additional assumption to set the density of free electrons.

4.5. VAMPIRES Model

A way towards an improved modeling of pressure-ionized plasma is to couple an atomic model of plasma to a classical model of fluid through its interaction potentials, without resorting to the point-like-ion hypothesis to split the problem.

In such a model, one should account for the impact of the ion–fluid structure on the electronic structure of ions but also for the effect of the electronic structure on the interaction

potentials in the ion fluid. The interaction potentials are then to be determined self-consistently with the electronic structure. Ideally, they should be seen as thermodynamic averages, obtained from the minimization of the total free energy.

For these reasons, an essential building block for such a model is a generalized free-energy functional related to a statistical model of a simple fluid, for an arbitrary interaction potential. A free-energy functional of the interaction potential has been available since the early 1960s for the HNC model [133,134]. The equivalent for the Debye–Hückel model was developed more recently [51,135,136].

Moreover, such free energy functionals can be formulated as minima of the related generalized free energy functionals of the pair distribution function. This offers an elegant way of deriving the integral equations of the corresponding fluid model, through a minimization with respect to the pair distribution function.

A preliminary work on a model accounting for both the bound electrons of an ion and the ion fluid structure was described in [137]. In this model, continuum electrons are excluded from the ion electronic structure, as in an isolated-ion model, and participate in a species of a classical fluid. This classical fluid may be treated either through the Debye–Hückel model (thus avoiding the Coulomb collapse) or by neglecting the polarization of the electrons as in an OCP. Applicability of this model has obvious limitations, due to its crude treatment of continuum electrons. However, this model formally introduces the screening of the effective potential in the electronic structure. In the DH case, when bound electrons are localized in a small region compared to the Debye length, this model yields the point-like DH correction of Equation (65).

The variational atomic model of plasma with ion radial correlations and electronic structure (VAMPIRES) [138] is both an atom-in-jellium model of the ion electronic structure and a statistical model of ion fluid. In this model, the continuum electrons are treated quantum-mechanically, as a part of the electronic structure partially shared among ions. This model stems from the minimization of an approximate free energy, and it was shown to be fulfilling the virial theorem.

Let us consider the free energy of N_i nuclei of atomic number Z and $N_i Z$ electrons, in a large volume V and at a fixed temperature T. The nuclei are approximated by indistinguishable classical particles, which allows us to write (see [139,140], and [138] for the present generalized form):

$$F_{eq}(N_i, V, T)$$
$$= \operatorname*{Min}_{\underline{w}} \iint_V \frac{d^3R_1...d^3P_{N_i}}{N_i! h^{3N_i}} \left\{ w(\mathbf{R}_1...\mathbf{P}_{N_i}) \left(\sum_{j=1}^{N_i} \frac{\mathbf{P}_j^2}{2m_i} + F_{eq}^e(\mathbf{R}_1...\mathbf{R}_{N_i}; N_i, V, T) + \frac{1}{\beta} \log\left(w(\mathbf{R}_1...\mathbf{P}_{N_i}) \right) \right) \right\}$$
$$\text{s. t.} \iint_V \frac{d^3R_1...d^3P_{N_i}}{N_i! h^{3N_i}} \left\{ w(\mathbf{R}_1...\mathbf{P}_{N_i}) \right\} = 1 \tag{126}$$

where $w(\mathbf{R}_1...\mathbf{P}_{N_i})$ denotes the probability distribution of the nuclei classical many-body states $(\mathbf{R}_1...\mathbf{P}_{N_i})$, and where F_{eq}^e is the equilibrium free energy of a system of electron with a fixed configuration $(\mathbf{R}_1...\mathbf{R}_{N_i})$ of the nuclei, plus the nucleus–nucleus interaction energy. The constraint simply enforces the correct normalization of the probability.

Electrons are modeled quantum-mechanically, using a finite-temperature density-functional formalism [41–43]. That is, we obtain F_{eq}^e from the following minimization:

$$F_{eq}^e(\mathbf{R}_1...\mathbf{R}_{N_i}; N_i, V, T) = \operatorname*{Min}_{\underline{n}} \left[F^0\{\underline{n}; V, T\} + W_{direct}\{\underline{n}; \mathbf{R}_1...\mathbf{R}_{N_i}; N_i\} + F^{xc}\{\underline{n}; V, T\} \right]$$
$$\text{s. t.} \int_V d^3r \{n(\mathbf{r})\} = Z N_i \tag{127}$$

$n(\mathbf{r})$ is the electron density; F^0 denotes the kinetic-entropic contribution to the free energy of a non-interacting electrons gas of density $n(\mathbf{r})$; and W_{direct} denotes the total direct-interaction energy, which includes the nucleus–nucleus contribution. F^{xc} is the contribution

of exchange and correlations. The constraint corresponds to the neutrality condition of the nuclei-electron system.

Like in the VAAQP model, we assume that the equilibrium electron density $n(\mathbf{R}_1...\mathbf{R}_{N_i};\mathbf{r})$ for a system of N_i nuclei is correctly described using a first-order cluster expansion (see Equation (114)). This leads us to the following Ansatz for the electron density:

$$n(\mathbf{R}_1...\mathbf{R}_{N_i};\mathbf{r}) \approx n_e + \sum_{j=1}^{N_i} q(|\mathbf{r} - \mathbf{R}_j|) \tag{128}$$

The system is seen as a set of ions, that is: nuclei, each with its spherical cloud of displaced electrons, sharing a common uniform background of free electrons. The minimization with respect to the electron density $n(r)$ is thus performed within a particular class of functions and consists of minimization with respect to the two parameters of the Ansatz, namely, n_e and the function $q(r)$.

The neutrality condition of Equation (127) can be rewritten using Equation (128), as:

$$\frac{n_e}{n_i} + \int_V d^3r \{q(\mathbf{r})\} = Z \tag{129}$$

Using Equation (128), W_{direct} can be written as:

$$W_{\text{direct}} = \frac{1}{2} \sum_{i=1}^{N_i} \sum_{\substack{j=1 \\ j \neq i}}^{N_i} v_{\text{ii}}\left\{\underline{q}; |\mathbf{R}_i - \mathbf{R}_j|\right\} + N_i\, W_{\text{intra}}\left\{\underline{q}; V\right\} + N_i\, W_{\text{bg}}\left\{\underline{q}, n_e; V\right\} \tag{130}$$

with the definitions:

$$v_{\text{ii}}\left\{\underline{q}; R, V\right\} = \frac{Z^2 e^2}{R} - 2Ze^2 \int_V d^3r\left\{\frac{q(r)}{|\mathbf{r}-\mathbf{R}|}\right\} + e^2 \int_V d^3r d^3r'\left\{\frac{q(r)q(r')}{|\mathbf{r}-\mathbf{r}'+\mathbf{R}|}\right\}$$

$$W_{\text{intra}}\left\{\underline{q}; V\right\} = -Ze^2 \int_V d^3r\left\{\frac{q(r)}{r}\right\} + \frac{e^2}{2} \int_V d^3r d^3r'\left\{\frac{q(r)q(r')}{|\mathbf{r}-\mathbf{r}'|}\right\}$$

$$W_{\text{bg}}\left\{\underline{q}, n_e; V\right\} = n_e e^2 \int_V d^3r d^3r'\left\{\frac{q(r)}{|\mathbf{r}-\mathbf{r}'|}\right\} + e^2\left(\frac{n_e^2}{2n_i} - n_e Z\right) \int_V d^3r\left\{\frac{1}{r}\right\} \tag{131}$$

v_{ii} plays the role of an ion–ion interaction potential, W_{intra} corresponds to an intra-ion interaction energy, and W_{bg} gathers all terms related to interactions with the electron homogeneous background. Contrary to what was done in VAAQP, the electrostatic interaction term pertaining to an ion is not the object of a specific hypothesis like Equation (119). In the VAMPIRES model, the interaction terms just follows from the cluster expansion of the electron density and the statistical treatment of the ion fluid.

Electron terms F^0 and F^{xc} are approximated using a first-order cluster expansion, as in VAAQP:

$$F^\bullet\left\{\underline{n}(\mathbf{r}) = n_e + \sum_{i=1}^{N_i} q(|\mathbf{r}-\mathbf{R}_i|); V, T\right\} = F^\bullet\{\underline{n}(\mathbf{r}) = n_e; V, T\} + \sum_{i=1}^{N_i} \Delta F_1^\bullet\left\{\underline{q}, n_e, \mathbf{R}_i; V, T\right\} \tag{132}$$

$$\Delta F_1^\bullet\left\{\underline{q}, n_e, \mathbf{R}; V, T\right\} = F^\bullet\{\underline{n}(\mathbf{r}) = n_e + q(|\mathbf{r}-\mathbf{R}|); V, T\} - F^\bullet\{\underline{n}(\mathbf{r}) = n_e; V, T\} = \Delta F_1^\bullet\left\{\underline{q}, n_e; V, T\right\} \tag{133}$$

where the $\bullet$ symbol is to be replaced by either the ^{0} or the ^{xc} label. $\Delta F_1^0\left\{\underline{q}, n_e; V, T\right\}$ is the kinetic and entropic contribution to the free energy of non-interacting electrons in a trial potential $v_{\text{trial}}\left\{\underline{q}, n_e; r; T\right\}$, which yields the electron density $n(r) = n_e + q(r)$, minus the contribution of the homogeneous background (see Equation (117)). $\Delta F_1^{xc}\left\{\underline{q}, n_e; V, T\right\}$ is

the exchange-correlation contribution to the free energy of a system of electrons having density $n(r) = n_e + q(r)$, minus the contribution of the homogeneous background (see Equation (118)).

At this point, the minimization of Equation (126) becomes

$$
\begin{aligned}
F_{eq}(N_i, V, T) = \underset{q, n_e}{\text{Min}} \Big[&F^0\{n_e; V, T\} + F^{xc}\{n_e; V, T\} \\
&+ N_i \Big(\Delta F_1^0\{\underline{q}, n_e; V, T\} + \Delta F_1^{xc}\{\underline{q}, n_e; V, T\} + W_{intra}\{\underline{q}, V\} + W_{bg}(\underline{q}, n_e; V) \Big) \\
&+ F_{eq}^i\{\underline{v}(R) = v_{ii}\{\underline{q}; R, V\}; N_i, V, T\} \Big]
\end{aligned}
$$

$$
\text{s. t. } \frac{n_e}{n_i} + \int_V d^3r\{q(r)\} = Z \tag{134}
$$

where $F_{eq}^i\{\underline{v}; N_i, V, T\}$ gathers the nuclei kinetic energy, entropy, and ion–ion interaction terms, forming the free energy of a one-component classical fluid of ions, interacting through the potential v_{ii}:

$$
F_{eq}^i\{\underline{v}; N_i, V, T\} = \underset{\underline{w}}{\text{Min}} \int_V \frac{d^3R_1 ... d^3P_{N_i}}{N_i! h^{3N_i}} \left\{ w(\mathbf{R}_1 ... \mathbf{P}_{N_i}) \left(\sum_{j=1}^{N_i} \frac{P_j^2}{2m_i} + \frac{1}{2} \sum_{i=1}^{N_i} \sum_{\substack{j=1 \\ j \neq i}}^{N_i} v(|\mathbf{R}_i - \mathbf{R}_j|) + \frac{1}{\beta} \log(w(\mathbf{R}_1 ... \mathbf{P}_{N_i})) \right) \right\}
$$

$$
\text{s. t. } \int_V \frac{d^3R_1 ... d^3P_{N_i}}{N_i! h^{3N_i}} \{w(\mathbf{R}_1 ... \mathbf{P}_{N_i})\} = 1 \tag{135}
$$

$$
\equiv \underset{\underline{w}}{\text{Min}} F^i\{\underline{w}, \underline{v}; N_i, V, T\} \text{ s. t. } \int_V \frac{d^3R_1 ... d^3P_{N_i}}{N_i! h^{3N_i}} \{w(\mathbf{R}_1 ... \mathbf{P}_{N_i})\} = 1 \tag{136}
$$

In the thermodynamic limit, the free energy per ion $\dot{F}_i = F_i / N_i$ of such a system has a logarithmic divergence because v_{ii} has a Coulomb tail. However, as in a usual OCP model, this divergence is cancelled by an opposite-sign divergence in W_{bg}. We therefore group these terms together, which renormalizes the free energy. We use either the HNC or the DH model to approximate the resulting divergence-free ion-fluid free energy per ion, as a functional of the interaction potential $v(r)$.

$$
\dot{F}_{eq}^i + W_{bg} \approx \dot{F}_{id, i}(n_i, T) + \dot{F}_{ex, eq}^{approx}\{\underline{v}; n_i, T\} \tag{137}
$$

$\dot{F}_{ex, eq}^{approx}$ is either the HNC or the DH excess free-energy per ion. Such approximate equilibrium free energy may be written as the minimum of a generalized free-energy functional of the radial correlation function $h(r) = g(r) - 1$:

$$
\dot{F}_{ex, eq}^{approx}\{\underline{v}; n_i, T\} = \underset{\underline{h}}{\text{Min}} \dot{F}_{ex}^{approx}\{\underline{v}, \underline{h}; n_i, T\} \tag{138}
$$

with the minimum occuring for $h(r)$ fulfilling the equations of the approximate model, either HNC or DH. In the DH case, we have [51]:

$$
\dot{F}_{ex}^{DH} = \frac{n_i}{2\beta} \int d^3r\{h(r)\beta v(r)\} + \frac{1}{2\beta n_i} \int \frac{d^3k}{(2\pi)^3}\{n_i h_k - \log(1 + n_i h_k)\} \tag{139}
$$

whereas in the case of HNC, we have [133,134]:

$$
\dot{F}_{ex}^{HNC} = \dot{F}_{ex}^{DH} + \frac{n_i}{2\beta} \int d^3r \left\{ (h(r) + 1) \log(h(r) + 1) - h(r) - \frac{h(r)^2}{2} \right\} \tag{140}
$$

Finally, the VAMPIRES model is based on the minimization of the following approximate free energy per ion $\dot{F}\{\underline{h}, \underline{q}, n_e\}$, with the neutrality constraint:

$$\dot{F}\{\underline{h}, \underline{q}, n_\mathrm{e}; n_\mathrm{i}, T\} = \dot{F}_{\mathrm{id,i}}(n_\mathrm{i}, T) + \dot{F}_{\mathrm{ex}}^{\mathrm{i\,approx}}\left\{\underline{h}, \underline{v}(R) = v_{\mathrm{ii}}\left\{\underline{q}, R\right\}; n_\mathrm{i}, T\right\}$$

$$+ \frac{f_\mathrm{e}^\mathrm{F}(n_\mathrm{e}; T)}{n_\mathrm{i}} + \frac{f_{\mathrm{xc}}(n_\mathrm{e}; T)}{n_\mathrm{i}} + \Delta F_1^0\left\{\underline{q}, n_\mathrm{e}; T\right\} + \Delta F_1^{\mathrm{xc}}\left\{\underline{q}, n_\mathrm{e}; T\right\} + W_{\mathrm{intra}}\left\{\underline{q}\right\} \tag{141}$$

$$\dot{F}_{\mathrm{eq}}(n_\mathrm{i}, T) = \underset{\underline{h}, \underline{q}, n_\mathrm{e}}{\mathrm{Min}}\, \dot{F}\{\underline{h}, \underline{q}, n_\mathrm{e}; n_\mathrm{i}, T\} \ \ \text{s. t. } \frac{n_\mathrm{e}}{n_\mathrm{i}} + \int d^3r\{q(r)\} = Z \tag{142}$$

The minimization with respect to $h(r)$ leads to the fluid integral equations, that is, the Ornstein–Zernike relation with the closure relation corresponding to the chosen approximate model:

$$h(r) = c(r) + n_\mathrm{i} \int d^3r' \left\{ c(|\mathbf{r}' - \mathbf{r}|) h(r') \right\} \tag{143}$$

$$c(r) = -\beta v_{\mathrm{ii}}(r) - \log(h(r) + 1) + h(r) \qquad \text{(HNC)} \tag{144}$$

$$c(r) = -\beta v_{\mathrm{ii}}(r) \qquad \text{(DH)} \tag{145}$$

The minimization with respect to $q(r)$ includes that on n_e, which is expressed as a functional $n_\mathrm{e}\{\underline{q}; n_\mathrm{i}\}$ using the neutrality constraint. It yields:

$$0 = -v_{\mathrm{trial}}\left\{\underline{q}, n_\mathrm{e}; r; T\right\} + \mu_{\mathrm{xc}}(n_\mathrm{e} + q(r), T) - \mu_{\mathrm{xc}}(n_\mathrm{e}, T) + v_{\mathrm{el}}\left\{\underline{h}, \underline{q}; r\right\}$$

$$- n_\mathrm{i} \int d^3r' \left\{ -v_{\mathrm{trial}}\left\{\underline{q}, n_\mathrm{e}; r'; T\right\} + \mu_{\mathrm{xc}}(n_\mathrm{e} + q(r'), T) - \mu_{\mathrm{xc}}(n_\mathrm{e}, T) \right\} \tag{146}$$

where we have defined:

$$v_{\mathrm{el}}\left\{\underline{h}, \underline{q}; r\right\} \equiv v_{\mathrm{intra}}\left\{\underline{q}; r\right\} + n_\mathrm{i} \int d^3r' \left\{ h(r') v_{\mathrm{intra}}\left\{\underline{q}; |\mathbf{r}' - \mathbf{r}|\right\} \right\} \tag{147}$$

$$v_{\mathrm{intra}}\left\{\underline{q}; r\right\} = \frac{-Z\mathrm{e}^2}{r} + \mathrm{e}^2 \int d^3r' \left\{ \frac{q(r')}{|\mathbf{r} - \mathbf{r}'|} \right\} \tag{148}$$

In order to solve Equation (146), we define the distribution $\tilde{v}_{\mathrm{el}}$ such that:

$$v_{\mathrm{el}}(r) = \tilde{v}_{\mathrm{el}}\{\underline{v}_{\mathrm{el}}, r\} - n_\mathrm{i} \int d^3r' \left\{ \tilde{v}_{\mathrm{el}}\{\underline{v}_{\mathrm{el}}, r'\} \right\} \tag{149}$$

We thus obtain from Equation (146) the following electron self-consistent equation:

$$v_{\mathrm{trial}}\left\{\underline{q}, n_\mathrm{e}; r; T\right\} = \tilde{v}_{\mathrm{el}}(r) + \mu_{\mathrm{xc}}(n_\mathrm{e} + q(r), T) - \mu_{\mathrm{xc}}(n_\mathrm{e}, T) \tag{150}$$

where $\tilde{v}_{\mathrm{el}}(r)$ is a shorthand notation for $\tilde{v}_{\mathrm{el}}\left\{\underline{v}_{\mathrm{el}}\left\{\underline{h}, \underline{q}\right\}, r\right\}$. From Equation (149), $\tilde{v}_{\mathrm{el}}$ may be expressed in the Fourier space as:

$$\tilde{v}_{\mathrm{el},k} = \begin{cases} v_{\mathrm{el},k} = -\frac{4\pi \mathrm{e}^2}{k^2}(Z - q_k)(1 + n_\mathrm{i} h_k) & \text{if } \mathbf{k} \neq 0 \\ 0 & \text{if } \mathbf{k} = 0 \end{cases} \tag{151}$$

The difference between $\tilde{v}_{\mathrm{el}}$ and v_{el} only impacts on integrals of product of $\tilde{v}_{\mathrm{el}}$ with a function that is not regular at $\mathbf{k} = 0$ in the Fourier space. For instance, we have:

$$\int d^3r\{\tilde{v}_{\mathrm{el}}(r)\} = 0 \neq \int d^3r\{v_{\mathrm{el}}(r)\} = -\frac{\beta n_\mathrm{e}}{n_\mathrm{i}} \tag{152}$$

where the last equality may be shown from the equations of the model.

Thermodynamic quantities are rigorously derived from the equilibrium free energy $\dot{F}_{\mathrm{eq}}$. Especially, the pressure is given by the following expression:

$$P_{\text{thermo}}(n_i, T) = n_i k_B T + n_i^2 \frac{\partial A^{\text{i approx}}}{\partial n_i}\bigg|_{\text{eq}} + n_e\big(\mu(n_e, T) + \mu_{\text{xc}}(n_e, T)\big) - f_0(n_e, T) - f_{\text{xc}}(n_e, T) \qquad (153)$$

In this formula, the first two terms correspond to the pressure of the ion fluid (ideal-gas and excess contributions), while the next four terms correspond to the pressure of the uniform electron gas, as in the VAAQP model. This means that displaced electrons only contribute to the pressure through the ion-fluid excess term. From the expression of the virial pressure, it can also be shown that the virial theorem is fulfilled in the VAMPIRES model.

Figure 15 presents results from the VAMPIRES model for lithium at 10 eV temperature. First, one sees from Figure 15e, which displays the mean ionzation as a function of density, that the accounting for ion–ion correlations in the model yields the qualitative behavior of pressure ionization.
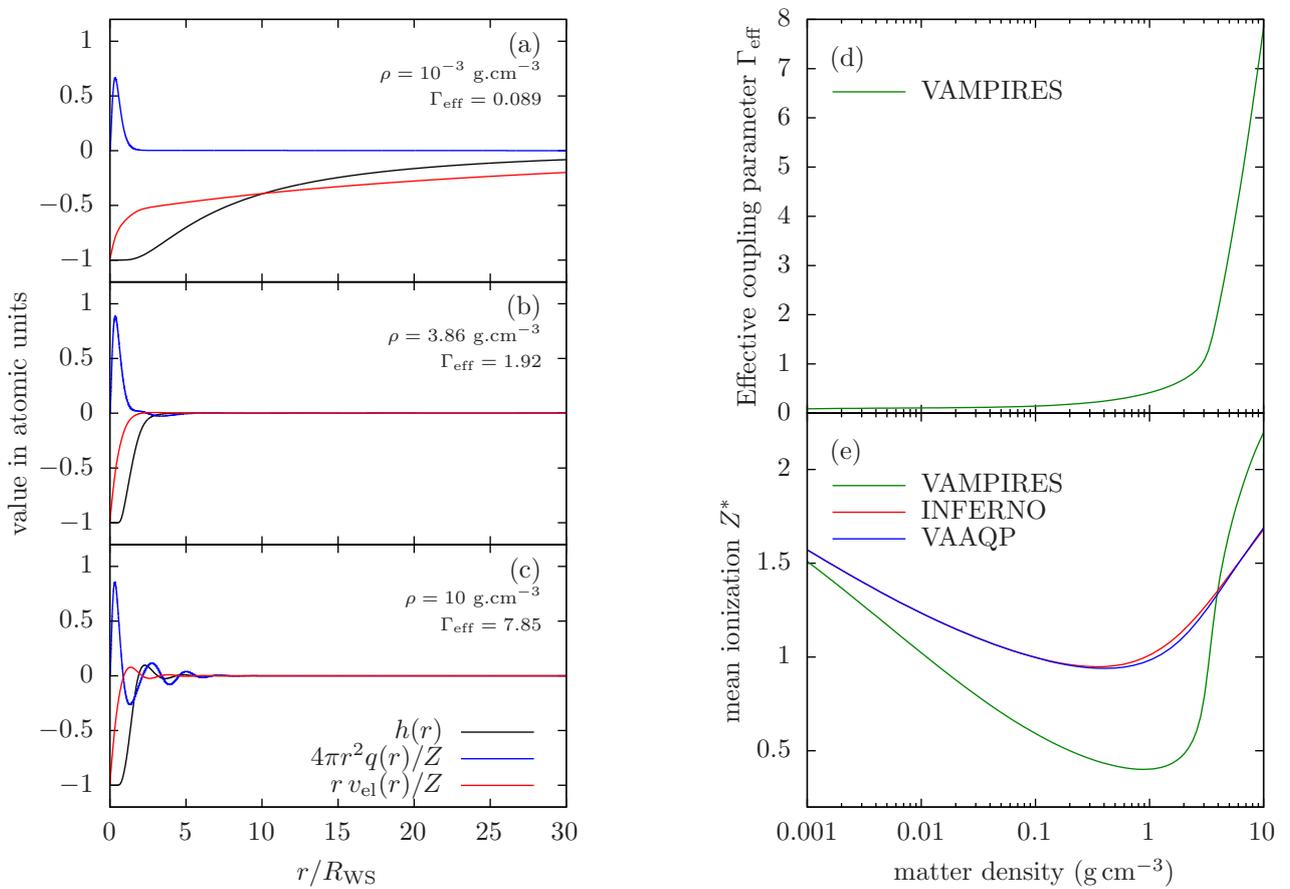
Figure 15. Results from the VAMPIRES model for lithium at 10 eV temperature. Pair correlation function $h(r)$, electron density $4\pi q(r)/Z$, and electrostatic potential $r\,v_{\text{el}}(r)/Z$, for various matter densities (**a**–**c**). Mean ionization Z^* (**e**) and effective coupling parameter Γ_{eff} (**d**) as functions of the matter density.

In order to quantify ion–ion coupling in this model, the usual coupling parameter $\Gamma = \beta Z^{*2} e^2 / R_{\text{WS}}$ is not relevant. The ion–ion potential is not purely Coulombic, and ion charge Z^* corresponds to an asymptotic limit, which, in general, is not relevant to the WS radius. Consequently, we use an effective coupling parameter $\Gamma_{\text{eff}} = -\beta \tilde{U}_{\text{ex}}^{\text{approx}}$, which really corresponds to the ratio of the ion-fluid interaction energy to the thermal energy.

Figure 15a–c present the ion–ion pair correlation function $h(r)$, electron-cloud density $q(r)$, and ion effective electrostatic potential $v_{\text{el}}(r)$, for three values of matter densities corresponding to weak, moderate, and strong coupling, respectively. In each case, close to

the central nucleus, one sees a sharp peak in the electron linear density, which corresponds to the bound electronic structure of the ion.

For a weakly coupled plasma (case of Figure 15a), one can see that the range of the potential v_{el} felt by the electrons extends way beyond the WS sphere. v_{el} variations may be decomposed into two regions. Close to the nucleus, the steep variation is related to the "internal" screening by the bound electronic structure. Far from the nucleus, the longer-range decay is related to both a tail of weakly displaced electrons and the DH-like decay of the ion–ion correlation function.

Moreover, one can see in Figure 15e that the mean ionization in these cases is lower than in INFERNO or VAAQP. However, in VAMPIRES, some of the electrons that do not participate in the background density n_e, which defines Z^*, may in fact be weakly displaced and play a role similar to the background electrons in an observable quantity. Especially, these electrons may interact significantly with the surrounding ions.

For a moderately coupled plasma (in the case of Figure 15b), the ion–ion pair correlation function has the shape of a cavity, resembling the WS cavity assumed in VAAQP. In such situations, results from the VAMPIRES model are indeed close to those of VAAQP and of INFERNO. One may check in the figure that the range of v_{el} is close to R_{WS}.

For a strongly coupled plasma (case of Figure 15c), the ion–ion pair correlation function exhibits oscillations beyond the WS radius, which is typical of liquid-like behavior. According to the model equation Equation (147), the correlation peaks of $h(r)$ draw some electrons. They are also "dressed" with the ion electron cloud density. This generates repulsive features between the central nucleus and the first correlation peak and between the correlations peaks because of the potential overlap of electron clouds. Consistently, electrons are displaced away from these regions of potential overlap. As a consequence, v_{el} has a zero inside the WS sphere, and its effective range is thus shorter than R_{WS}.

In this model, it seems that the pressure ionization phenomenon goes along with the switching to the liquid-like regime. This is illustrated in Figure 15d,e. The increase in the mean ionization is connected to a sharp increase in the coupling parameter. Across the pressure ionization edge, the plasma switches from a moderate-coupling to a strong-coupling regime, with the related feedback on the range of v_{el}. In addition to decreasing the value of R_{WS}, the range of v_{el} switches from longer than R_{WS} to shorter than R_{WS}. This explains why pressure ionization leads to a steeper increase in the mean ionization in this model than in VAAQP or INFERNO.

In the VAMPIRES model, the pressure-ionization phenomenon, as well as the switching from the Debye–Huckel-scale to the WS-scale decay, stems from a first-principle accounting for the structure of the ion fluid. At the same time, at each thermodynamic condition, the ionization state of the plasma is obtained from the condition of thermodynamic equilibrium.

One of the known modeling issues for such a model is that the electrons of an ion feel the surrounding ions through their average distribution, given by the pair correlation function. Among the possible outcomes of such a modeling effort could be that this static picture breaks down at some thermodynamic conditions.

Work on the VAMPIRES model is still in progress, and applicational studies are still to be performed. Therefore, the following sections will only focus on applications of cavity-based models, which may, however, give relevant information.

5. Radiative Processes and Photoabsorption in Dense Plasmas

From the electrodynamics of continuous media, we can relate the photoabsorption cross-section per ion σ_{abs} to the plasma dielectric function ϵ_ω as follows [141]:

$$\sigma_{\text{abs}}(\omega) = \frac{\omega \text{Re}(n_\omega^{\text{ref}})}{n_{\text{i}}\epsilon_0 c} \text{Im}(\epsilon_\omega) \tag{154}$$

$$\text{Re}(n_\omega^{\text{ref}}) = \left(\frac{\text{Re}(\epsilon_\omega) + |\epsilon_\omega|}{2\epsilon_0} \right)^{1/2} \tag{155}$$

where n_ω^{ref} corresponds to the refraction index of the plasma.

One then decomposes the dielectric function of the plasma into contributions from the various ions. Of course, such a decomposition depends on the considered atomic model. In the case of an ideal plasma of isolated ions, the response of the plasma is directly the sum of the responses of each isolated ion. In the case of an ion-cell model, one sees the response of the plasma as the sum of the responses of each ion cell. For an atom-in-jellium model such as VAAQP, the cluster expansion [115], which is used for the free energy, is extended to the plasma susceptibility [142–144].

In the dipole approximation, valid for wavelengths large compared to the typical atomic radius, we may write, limiting ourselves to the average-atom framework:

$$\text{Im}(\epsilon_\omega) = 4\pi\epsilon_0 \frac{n_{\text{i}}e^2}{\hbar} \text{Im} \int d^3r d^3r' \left\{ zz' \mathcal{D}_\omega^{\text{R}}(\mathbf{r}, \mathbf{r}') \right\} \tag{156}$$

where $\mathcal{D}_\omega^R$ is the atomic retarded susceptibility of the average atom, which can be written, at finite temperature, as (see, for instance, [145]):

$$\mathcal{D}_\omega^{\text{R}}(\mathbf{r}, \mathbf{r}') = -\frac{i}{\hbar} \int_{-\infty}^{+\infty} d\tau \left\{ \text{Tr} \left(\hat{\varrho} \left[\hat{n}_{\mathbf{r}}^H(\tau), \hat{n}_{\mathbf{r}'}^H(0) \right] \right) \theta(\tau) e^{i\omega\tau} \right\} \tag{157}$$

In the framework of the time-dependent density-functional theory [146–150], one can properly relate the density susceptibility to the response of the electron density to a frequency-dependent external potential:

$$\delta n_\omega(\mathbf{r}) = \int d^3r' \left\{ \mathcal{D}_\omega^{\text{R}}(\mathbf{r}, \mathbf{r}') \delta v_{\text{ext},\omega}(\mathbf{r}') \right\} \tag{158}$$

where $\delta v_{\text{ext},\omega}(\mathbf{r}')$ is the frequency-dependent perturbation of the potential, and $\delta n_\omega(\mathbf{r})$ is the resulting perturbation in the frequency-dependent density.

5.1. Independent Particle Approximation and the Effect of Screening

The simplest approximate approach to the retarded susceptibility is to use the retarded susceptibility of a system of independent particles. The latter susceptibility is obtained directly from the dynamic perturbation theory, which yields:

$$\mathcal{D}_\omega^{\text{R}}(\mathbf{r}, \mathbf{r}') \approx \mathcal{D}_\omega^{\text{R},0}(\mathbf{r}, \mathbf{r}') = \sum_{\xi, \zeta} \left(p_{\text{F}}(\mu, T, \varepsilon_\xi) - p_{\text{F}}(\mu, T, \varepsilon_\zeta) \right) \frac{\varphi_\xi^*(\mathbf{r}) \varphi_\xi(\mathbf{r}') \varphi_\zeta(\mathbf{r}) \varphi_\zeta^*(\mathbf{r}')}{\varepsilon_\zeta - \varepsilon_\xi - \hbar\omega} \tag{159}$$

where ξ, ζ label Kohn–Sham orbitals, and where the sums run over both the discrete and the continuum part of the 1-electron spectrum.

This approach notably disregards collective phenomena such as plasma oscillations, which stem from the feedback of the electrons on the potential (potential induced by the density perturbation).

In the average-atom approach, the independent-particle approximation leads to the average-atom Kubo–Greenwood formula:

$$\text{Im}(\epsilon_\omega) = 4\pi\epsilon_0 n_{\text{i}}e^2 \frac{\pi}{3} \sum_{\xi, \zeta} \left(p_{\text{F}}(\mu, T, \varepsilon_\xi) - p_{\text{F}}(\mu, T, \varepsilon_\zeta) \right) \left| \langle \varphi_\xi | \mathbf{R} | \varphi_\zeta \rangle \right|^2 \delta(\hbar\omega - \hbar\omega_{\zeta,\xi}) \tag{160}$$

where $\hbar\omega_{\zeta,\xi} = \varepsilon_\zeta - \varepsilon_\xi$. Within this approximation, the photoabsorption can be decomposed into bound–bound, bound–continuum, and continuum–continuum contributions. Although we use the average-atom context here as an example for the discussion, a similar treatment can be performed in the case of a more detailed model yielding the contributions of the various excited states to the plasma dielectric function.

The oscillator strengths are the numbers defined as follows:

$$f_{\xi,\zeta} = \frac{2}{3}\frac{m_{\rm e}}{\hbar^2}\hbar\omega_{\zeta,\xi}|\langle\varphi_\xi|\mathbf{R}|\varphi_\zeta\rangle|^2 \tag{161}$$

when ξ, ζ belong to the discrete part of the spectrum. In the case where either ξ or ζ belongs to the continuum, this expression is to be understood as a density of oscillator strength, also called a differential oscillator strength.

Furthermore, in the case of both ξ and ζ belonging to the continuum, the dipole matrix elements are conditionally convergent integrals. In practice, in the independent-particle approximation, one can use the Ehrenfest theorem in order to recast the dipole matrix elements into their acceleration form [151]:

$$\left|\langle\varphi_\xi|\mathbf{R}|\varphi_\zeta\rangle\right| = \frac{1}{m_{\rm e}\omega_{\zeta,\xi}^2}\left|\int d^3r\left\{\langle\varphi_\xi|\mathbf{r}\rangle\nabla_{\mathbf{r}}v_{\rm eff}(r)\langle\mathbf{r}|\varphi_\zeta\rangle\right\}\right| \tag{162}$$

where $v_{\rm eff}(r)$ is the effective potential associated with the orbitals $\{\varphi_\xi\}$. The role of dipole matrix elements involving two continuum orbitals is rather specific to plasma physics because it implies non-zero populations for the continuum orbitals.

An example of the continuum–continuum contribution to the opacity of a plasma is given in Figure 16, corresponding to silicon at 2.36 g·cm^{-3} matter density and 5 eV temperature. In the presented calculation, the double sum, or more precisely the double integral, of Equation (160) was performed using continuum wave functions obtained from the VAAQP model. Approximate methods allowing one to avoid the double summation exist (see, for instance, [152]). One can see in this figure that, at high frequency, one recovers the Kramers classical result [153,154] involving the bare-nucleus charge, and not an effective ion charge. This is expected since the atomic response at high frequencies essentially involves the electrons located in the vicinity of the nucleus.
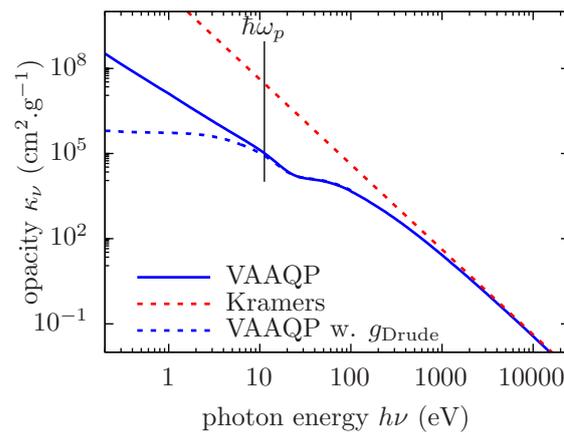
Figure 16. Continuum–continuum contribution to the opacity of a silicon plasma at 5 eV temperature and 2.36 g·cm^{-3} matter denisty. Calculation using orbitals from the VAAQP model, and comparison with the Kramers formula and the opacity corrected using the $g_{\rm Drude}$ function of Equation (167).

When the effective potential defining the orbitals is screened, the oscillator strengths have a behavior that is qualitatively different from those of an isolated ion. The underlying reasons are closely related to the limitation of the number of bound states.

For a potential having a Coulomb-tail (pure Coulomb potential or potential stemming from an isolated-ion model), the continuity of the cross section across the ionization threshold may easily be expressed through the matching of the two quantities:

$$f_{\xi,\zeta} \frac{1}{d\varepsilon_\xi/dn_\xi}\bigg|_{\varepsilon_\xi \to 0-} = f_{\xi,\zeta} \frac{n_\xi^3}{Z^{*2}}\bigg|_{\varepsilon_\xi \to 0-} = \frac{df_{\ell_\xi,\zeta}(\varepsilon)}{d\varepsilon}\bigg|_{\varepsilon \to 0+} \tag{163}$$

where n_ξ, ℓ_ξ are the principal and orbital quantum numbers of orbital ξ, respectively, and where $(d\varepsilon_\xi/dn_\xi)^{-1}$ gives the density of states of the quasi-continuum of infinitely close discrete states in the $n \to \infty$ limit, for a Coulomb-tail potential.

For Coulomb-tail potential, we have a finite value of the differential oscillator strength at the threshold. With screening, the behavior of radial wave functions at infinity is changed: the radial wave functions tend to Bessel functions instead of Coulomb functions in the case of Coulomb potential. Due to the related change in the normalization coefficient, the differential oscillator strength smoothly goes to zero [155]. This change in the behavior of oscillator strengths becomes more pronounced as density is increased since the potential is screened over shorter distances.

Figure 17 shows an illustration of this oscillator-strength drop near the photo-ionization threshold in the case of silicon at 5-eV temperature and matter densities of 10^{-3} and 10^{-2} g·cm^{-3}. In this figures, oscillator strengths are multiplied by the $(d\varepsilon_\xi/dn_\xi)^{-1}$ term of Equation (163), in order to emphasize the continuity with differential oscillator strengths. The results from the VAAQP model (or INFERNO, with both models being in agreement) are compared to those of an isolated ion with an average configuration fixed to the VAAQP average configuration, as well as to results from a Coulomb potential with a charge fixed to the VAAQP mean ionization. For both the Coulomb potential and the isolated-ion, in principle, the set of bound states is infinite, as well as the series of oscillator strengths. At the low density of 10^{-3} g·cm^{-3}, one can see that despite the qualitatively different behavior of oscillator strengths near the photo-ionization threshold, a quantitative agreement is obtained between the VAAQP model and the isolated-ion. On the contrary, at the higher density of 10^{-2} g·cm^{-3}, the change of behavior has a larger quantitative impact.
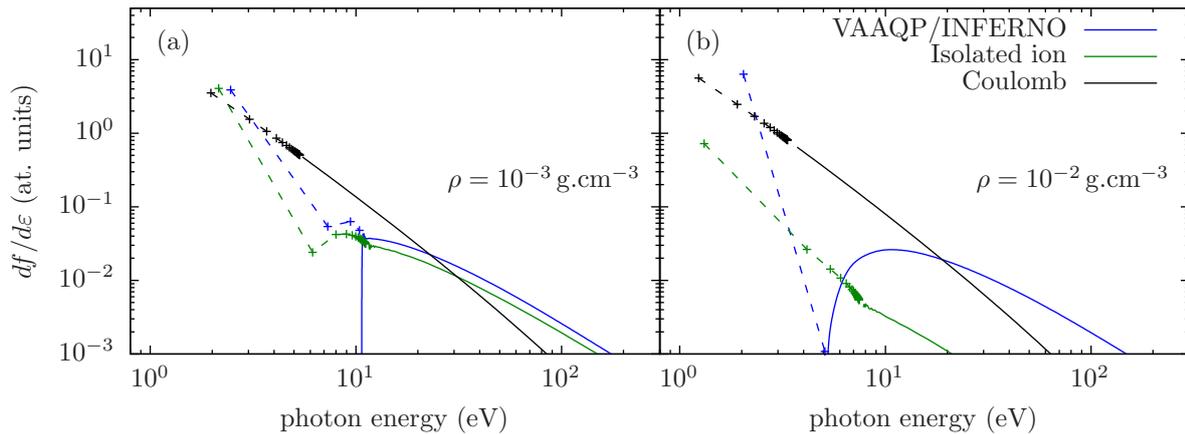

Figure 17. Differential oscillator strengths for the $4s - p$ (continuous solid lines) and oscillator strengths for the discrete $4s - np$ transitions (crosses connected by dashed lines, with values being multiplied by the $(d\varepsilon_\xi/dn_\xi)^{-1}$ term of Equation (163)), for a silicon plasma at 5-eV temperature and matter densities of 10^{-3} (**a**) and 10^{-2} g·cm^{-3} (**b**). Comparison between results from VAAQP/INFERNO (in blue, same results at these conditions), from an isolated ion having the average configuration taken from VAAQP/INFERNO (in green) and from a Coulomb potential with charge Z^* taken from VAAQP/INFERNO (in black).

Using a model such as INFERNO or VAAQP, one accounts for both the decrease in the oscillator strength and the appearance of a resonance when a bound state disappears. Using an isolated ion with continuum lowering in order to suppress subshells does not account for either of these phenomena. Figure 18 shows the oscillator strengths at two matter densities between which the 5p subshell gets pressure-ionized. One can easily see how the discrete oscillator strength is replaced by an equivalent contribution from a resonance in the differential oscillator strength. Thus, the corresponding bound–bound channel does not disappear but is replaced by a contribution to the bound–continuum channels. For the sake of comparison, the energy of the photoionization threshold obtained from the average-atom of an isolated ion with Stewart–Pyatt IPD is also shown. The location of the threshold is in good agreement with VAAQP in this case of relatively low density, but the cross-section of an isolated-ion model would be different. Moreover, obtaining a fully continuous variation of the opacity with density requires correct and consistent accounting for the resonances in the bound–continuum and continuum–continuum contributions to the opacity.
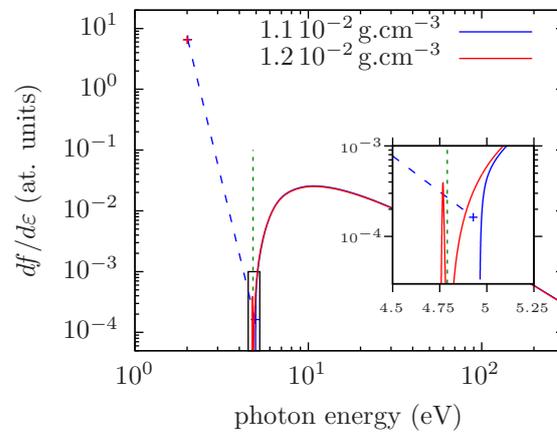
Figure 18. Differential oscillator strengths for the 4s-p (continuous solid lines) and oscillator strengths for the 4s-np transitions (crosses connected by dashed lines, values multiplied by the $(d\varepsilon_\xi/dn_\xi)^{-1}$ term of Equation (163)), for a silicon plasma at 5-eV temperature and matter densities of $1.1\,10^{-2}$ and $1.2\,10^{-2}$ g·cm^{-3}. Results are taken from VAAQP/INFERNO (same results at these conditions). Between the two matter densities considered, the 5p subshell disappears and is replaced by the corresponding resonance in the *p* continuous spectrum. The vertical dotted line in green indicates the position of the 4s photo-ionization threshold obtained from the Stewart–Pyatt formula [45].

5.2. Fluctuations around the Average Atomic State and the Need for Detailed Modeling

Whereas the average microstate of a whole macroscopic plasma may virtually sample many atomic excited states, the average-atom approach is based on the average *atomic* state of the plasma.

In terms of detailed atomic modeling, spectral quantities such as the opacity or emissivity may reveal the contributions of the various species that have significant populations because different atomic states usually contribute at distinct frequencies. Even when the various spectral features are unresolved due to physical broadening, the statistical distribution among the various species yields a statistical broadening of the unresolved feature.

For that reason, detailed modeling of plasma is somehow mandatory in order to calculate realistic estimates of spectral quantities. The physical pictures underlying average-atom models can often be extended to more detailed modeling. For instance, the models [27,156] rely on various extensions of the ion-cell model to detailed configuration or superconfiguration accounting.

The variational approach leading to the VAAQP model can be formally generalized to configurations or superconfigurations [112]. This approach was notably used to build

an approximate DCA model resorting only to results from the VAAQP model (VAAQP-DCA, [58]).

From an average-atom standpoint, the populations of the various levels may be obtained from the analysis of fluctuations around the average atomic state [157]. Starting from an approximate detailed model that resorts to the average-atom energies and orbitals, models of fluctuations can be used to perform a statistical approach. An example of such an approach is the Gaussian approximation [25], which was applied to the VAAQP-DCA model in [58]. In this context, the independent particle approximation [158–160] to the fluctuations of orbital populations leads to an overestimation of the statistical broadening, whereas correlated fluctuations [25] yield more realistic estimates.

As an illustration of the need for detailed modeling, Figure 19b displays the ion charge state distributions for silicon at 60 eV temperature and 45 mg·cm^{-3} matter density resulting from two detailed models: the DCA model from [58] and the STA model of [27]. In Figure 19a the corresponding transimission spectra is shown, compared to the measured spectrum from [161] (areal density of 80μg·cm^{-2}). The measure was in fact performed on a plasma of SiO$_2$. However, the ionization competition between oxygen and silicon in the mixture was studied using an isolated-ion detailed model with Stewart–Pyatt continuum lowering [162]. Its effect on the populations of silicon was shown to be rather weak. In Figure 19a, one can easily identify the contributions from the various charge states. One may note a slight shift in the positions of some spectral features obtained from the DCA model of [58]. This is due to the lack of orbital relaxation in this approach, whereas it is accounted for in the STA model of [27]. Let us, however, mention that it is possible to account for orbital relaxation even when starting from an average-atom description, by using the static linear response [163,164].
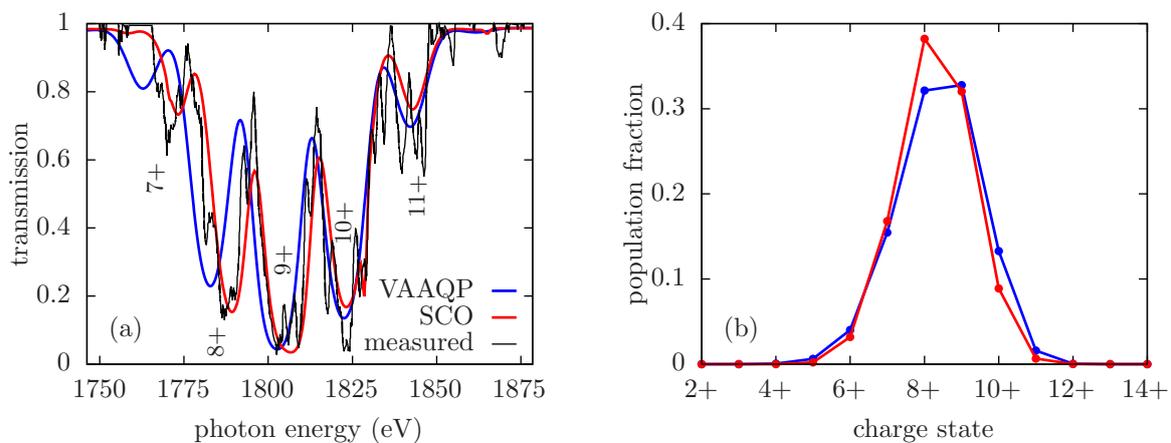
Figure 19. Transmission of a silicon plasma from [161], at areal density of 80 μg·cm^{-2}. Estimated plasma conditions are 60 eV temperature and 45 mg·cm^{-3} matter density. Comparison between results from a DCA approach based on the VAAQP model [58], from the SCO approach [27], and measured transmission spectrum from [161]. In the calculations, an arbitrary line width of 4 eV was added to the statistical width to mimic the physical broadening and instrumental resolution.

Even resorting to known models, the detailed modeling of plasma still remains an implementation challenge. For elements of moderate or high atomic numbers, especially at high temperatures, the number of excited states that contribute to radiative properties may be enormous. Statistical approaches are available to reduce the number of species, leading to various levels of detail in the spectra. However, one often has to make a tradeoff between the level of detail and the completeness of the approach. Detailed modeling is also used in the collisional-radiative modeling of non-equilibrium plasmas [7]. In this context, the number of states or statistical objects that may be accounted for is limited by the rank of the subsequent collisional-radiative matrix. The issue of choosing a relevant tradeoff is even more important in this context (see, especially, chapter 1 of [7]).

In the specific case of pressure ionization, the removal of some orbitals from the discrete 1-electron spectrum results in the removal of any configuration having non-zero population of these orbitals. This ultimately leads to a truncation of the charge state distribution, pushing it towards higher charge states.

Figure 20 shows the charge state distributions obtained for iron at 40 eV temperature, at various matter densities. The case of 15.6 g·cm^{-3} (2-fold compression) illustrates the pressure ionization of the 3d subshell, whereas the case of 78 g·cm^{-3} (10-fold compression) illustrates the pressure ionization of the 3p subshell. In these cases, the results of both the reconstructed DCA model of [58] and an approximate, statistical treatment of the model through the Gaussian approximation are displayed. One can see how the charge state distribution of the DCA model is pushed towards higher ionization stages as available configurations for the lowest ionization stages are removed. On the other hand, the Gaussian approximation of fluctuations does not account properly for this cut-off but still yields the same qualitative trend of a narrow peak on the average charge state.
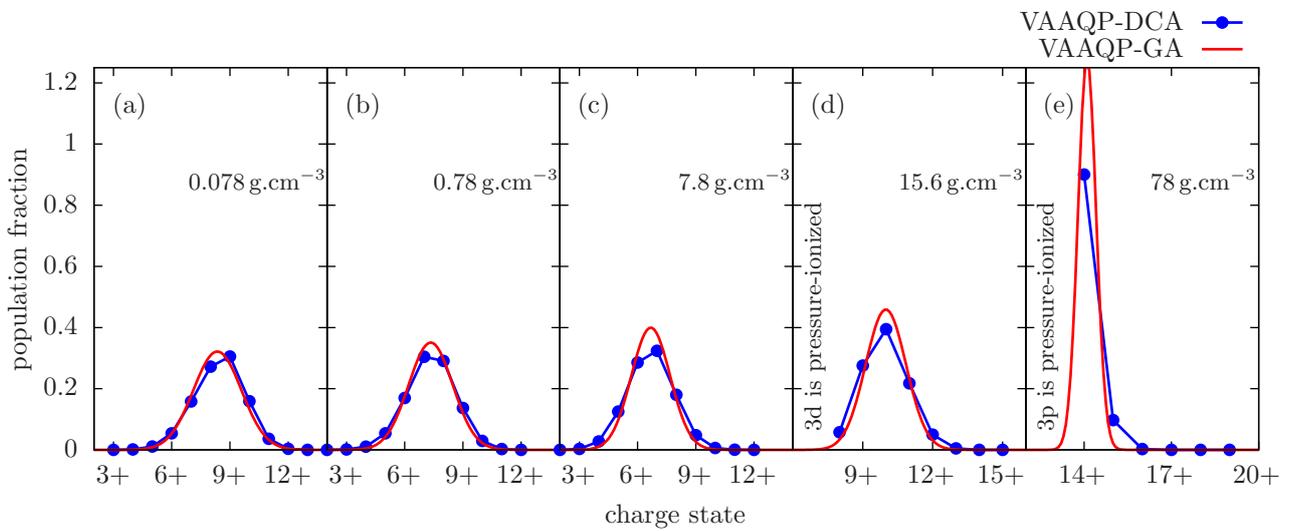
Figure 20. Charge state distributions of an iron plasma at 40-eV temperature, for various matter densities ranging from 1/100th (**a**) to 10 times (**e**) solid density. Comparison between a DCA approach reconstructed from the VAAQP model (VAAQP-DCA) [58] and an approximate treatment of this model using the Gaussian approximation [25,58] (VAAQP-GA).

5.3. Collective Phenomena

One may expect collective phenomena to play a significant role when the frequency of the perturbing potential is lower or of the order of the plasma frequency ω_{P}.

$$\omega_{\mathrm{P}} = \sqrt{\frac{4\pi n_{\mathrm{e}} e^2}{m_{\mathrm{e}}}} \tag{164}$$

Close to the plasma frequency, the perturbing field is resonant with the natural frequency of the free-electron gas, and its feedback may have a large impact on the plasma response. At frequencies much lower than the plasma frequency, the static collective behavior of the plasma, *i.e.* the screening, prevents the electromagnetic field from propagating in the plasma. The plasma behaves as a conductor, and its conductivity is limited by the collisions of the electrons on the ions. Indeed, below the plasma frequency, speaking in terms of dynamic conductivity would be more relevant than in terms of opacity. As is clear from Equation (164), collective effects have an impact on a frequency range that extends farther as density is increased. They thus have a specific importance for dense plasmas.

The continuum–continuum opacity obtained from the independent-particle approximation exhibits an unphysical divergence at zero frequency. On the other hand, the Drude

model, which accounts for collisions, yields a finite value of the direct-current conductivity, as well as of the corresponding opacity.

In [152], a very simple, heuristic approach is proposed in order to recover the Drude-like collective behavior at low frequency (very similar approaches are also described in [165–167]).

From the Boltzmann equation in the relaxation-time approximation, one may derive Ziman's static conductivity [168]:

$$\gamma_{\text{Ziman}} = \frac{-2n_e q_e^2}{(2\pi)^3 m_e^2} \frac{1}{3} \int d^3 k \left\{ \frac{k^2}{\omega_{\text{col}}(k)} \left. \frac{\partial f_0(\varepsilon)}{\partial \varepsilon} \right|_{\varepsilon_k} \right\} \tag{165}$$

where f_0 is the free-electron energy distribution, and ω_{col} is the collision frequency.

In the quantum-mechanical framework, the collision frequency $\omega_{\text{col}}(k)$ of electrons corresponds to the net rate of elastic scattering out of the momentum **k**. We may estimate the latter by summing the electron–ion elastic-scattering cross section, which may be estimated in the limit of weak scattering [10]. One obtains:

$$\omega_{\text{col}}(k) = \frac{4\pi n_i}{m_e k} \sum_\ell (\ell + 1) \sin^2(\Delta_{k,\ell+1} - \Delta_{k,\ell}) \tag{166}$$

The heuristical method of correction [152] for the opacity is as follows. One first writes the continuum–continuum photoabsorption cross-section in the low-frequency limit in terms of the scattering cross-section (the method is given in [169,170]). Then, by analogy with Ziman's formula Equation (165) and by resorting to the collision frequency of Equation (166), one identifies the correcting factor that allows one to recover Ziman's result.

$$g_{\text{Drude}}(k, \omega) = \frac{\omega^2}{\omega^2 + \omega_{\text{col}}^2(k)} \tag{167}$$

This factor introduces a Drude-like behavior in the low-frequency part of the spectral opacity. Figure 16 shows the effect of the correcting function g_{Drude} in the case of silicon at 5 eV temperature and 2.36 g·cm^{-3} matter density. As may be seen from the figure, this correction has a strong impact below the plasma frequency.

At low frequencies, the complex refraction index may also have a significant imaginary part. The assumption $n_\omega^{\text{ref}} = 1$, often used in the dielectric regime ($\omega >> \omega_P$), is no longer valid, and a more realistic estimate is required. In [152], a simple estimate obtained from the Drude formula is used. However, since $\text{Im}(\epsilon_\omega)$ is known, one can also use the Kramers–Kronig relations to obtain $\text{Re}(\epsilon_\omega)$:

$$\text{Re}(\epsilon_\omega) = \epsilon_0 + \frac{1}{\pi} \mathcal{PP} \int_{-\infty}^{+\infty} d\omega' \left\{ \frac{\text{Im}(\epsilon_\omega)}{\omega' - \omega} \right\} \tag{168}$$

Then, one uses Equations (155) and (154) to obtain the opacity.

Figure 21 displays the results of the present approach [117], using the heuristic coefficient g_{Drude} and the refraction index obtained from the Kramers–Kronig relation, for the case of silicon at solid density and 2.5 eV temperature, using the VAAQP and INFERNO models. Rather good agreement is found with measurements performed on cold solid silicon [171]. In fact, with cold solid silicon being a metal, it is not so surprising that plasma models can give a reasonable description of it.

The method of [152,165–167] enables a smooth transition to the static collective behavior of the plasma, accounting for electron–ion collisions, but does not account for the dynamic screening by electron, which notably yields the collective plasma oscillations. In an approach based on an effective system of independent particles, a description of the collective behavior is accounted for through the self-consistency of the effective potential.

Whereas the static atomic potential is calculated self-consistently, the frequency-dependent perturbation of the potential is not, when using the independent-particle linear response.
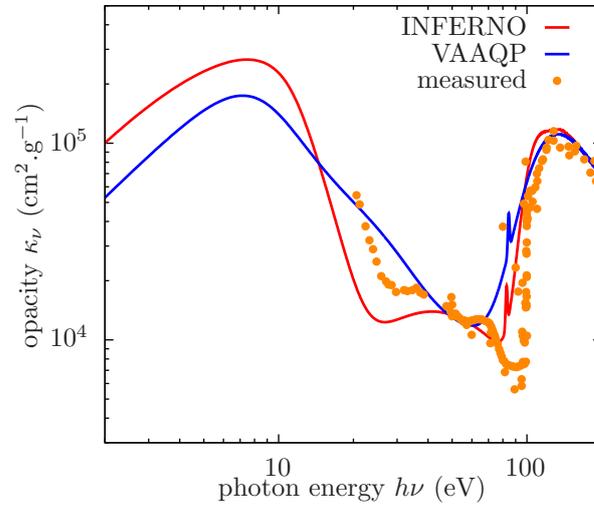

Figure 21. Opacity of cold silicon at solid density (2.36 g·cm^{-3}) in the visible-to-XUV range, typical of the L and M edges. Comparison between results from INFERNO and VAAQP at a temperature of 2.5 eV, using the heuristic accounting for collective effects, and measurements of the opacity of cold silicon [171].

5.4. Self-Consistent Linear Response

Using a time-dependent density functional formalism [146–150] to calculate the linear response leads to a self-consistent scheme for the frequency-dependent density perturbation and induced potential:

$$\delta n_\omega(\mathbf{r}) = \int d^3 r' \left\{ \mathcal{D}_\omega^R(\mathbf{r}, \mathbf{r}') \delta v_{\text{ext},\omega}(\mathbf{r}') \right\} = \int d^3 r' \left\{ \mathcal{D}_{0,\omega}^R(\mathbf{r}, \mathbf{r}') \left(\delta v_{\text{ext},\omega}(\mathbf{r}') + \delta v_{\text{ind},\omega}(\mathbf{r}') \right) \right\} \tag{169}$$

$$\delta v_{\text{ind},\omega}(\mathbf{r}) = e^2 \int d^3 r' \left\{ \frac{\delta n_\omega(\mathbf{r}')}{|\mathbf{r} - \mathbf{r}'|} \right\} + \left. \frac{\partial \mu_{\text{xc}}(n)}{\partial n} \right|_{n(\mathbf{r})} \delta n_\omega(\mathbf{r}) \tag{170}$$

where we limit ourselves to the adiabatic local density approximation of the exchange-correlation term.

These equations are solved in [147] to obtain photoabsorption cross-sections of neutral rare gases, which do not involve continuum–continuum channels. However, in these calculations, the accounting for channel mixing between bound–bound and bound–continuum contributions has a significant impact on the photoabsorption cross-section, especially near the photo-ionization edge. Figure 22 displays the result of a self-consistent dynamic linear response calculation using the same model as [147], on one of their cases of application. The results are in close agreement both with those of [147] and with the measurement of [172] on liquid xenon and exhibit the significant impact of channel mixing.

In the case of a plasma, the contribution of continuum–continuum transitions causes difficulties since they involve non-localized wave functions. The cluster expansion, on which the VAAQP model is based, is an efficient method to substract the non-integrable contribution of the homogeneous medium. From the corresponding self-consistent linear-response formalism, a sum rule for the atomic dipole was derived in [173]:

$$\int d^3 r \{z \delta n_\omega(\mathbf{r})\} = \frac{1}{m_e \omega^2 \left(1 - \frac{\omega_P^2}{\omega^2} \right)} \left(- \int d^3 r \left\{ \delta n_\omega(\mathbf{r}) \frac{\partial v_{\text{trial}}(\mathbf{r})}{\partial z} \right\} + \int d^3 r \left\{ \delta v_{\text{ind},\omega}(\mathbf{r}) \frac{\partial n(\mathbf{r})}{\partial z} \right\} \right) \tag{171}$$

Formally, this relation plays the same role as the switching between the length and acceleration form of the dipole matrix element, but in the context of the self-consistent linear response. More precisely, the factor in front of the right-hand side stems from the contribution of the homogeneous medium and causes a singularity at the plasma frequency. This is due to the accounting for the induced field in the homogeneous plasma response, while disregarding collisions, which would saturate this resonant behavior. If one takes the factor in the $\omega >> \omega_P$ limit, then the first term on the right-hand side of Equation (171) may be recovered from Equation (162). The second term is purely due to the accounting for the induced potential, that is, for self-consistency in the dynamic behavior of the displaced-electron density. These effects potentially include the coupling with plasmons or the mixing among the various particle–hole channels.

The implementation of Equation (171) was achieved in the TF model [87,174]. The TF model is a relevant first-step because the VAAQP model is rigorously equivalent to the usual TF model when the electron density is taken in the TF approximation [98]. However, the TF model leads to unphysical results for the radiative properties, especially at high frequencies [86]. It is therefore of limited practical use.

In the quantum version of the VAAQP model, although progress was achieved in the understanding of the problem, the application of the self-consistent linear-response approach still leads to inconclusive results [175]. In particular, the direct check of Equation (171) from an implementation of the self-consistent linear response using standard methods described in [147,176] failed. The self-consistent linear response in the context of dense plasmas thus remains an open problem, at least from an implementation standpoint.
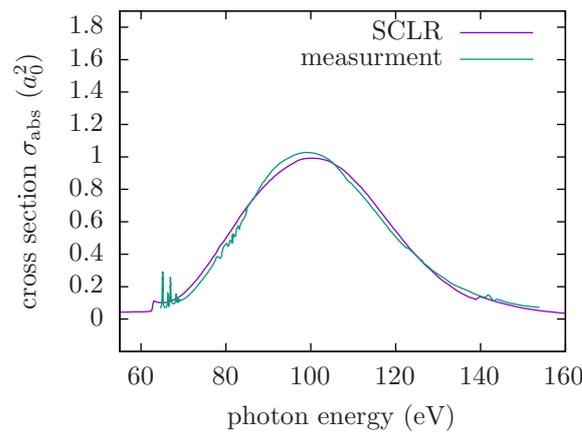
Figure 22. Photoabsorption cross section of neutral Xe in the XUV region typical of the N-edge. Comparison between the self-consistent linear response of the DFT atom, using Gunnarsson–Lundqvist exchange-correlation term (same model as in [147]), the independent-particle approximation, and measurements from [172].

6. Some Words on Collisional Processes

In the heuristic bridging to the Ziman formula (see Section 5.3), we obtained the collisional frequency considering the net rate of electron–ion elastic-scattering out of momentum **k**. In this context, we used the electron–ion elastic-scattering cross-section stemming from the limit of weak collisions. The latter only depends on the wave functions through the phase shifts (see, for instance, [10]):

$$\sigma_{\text{scatter}}(\varepsilon_k) = a_0^2 \frac{4\pi}{k^2} \sum_{\ell} (2\ell + 1) \sin^2(\Delta_{k,\ell}) \tag{172}$$

The elastic scattering of electrons by ions may be categorized as an elementary collisional atomic process, even if it does not change the ion electronic state. Figure 23a displays the total electron–ion elastic-scattering cross section for a silicon plasma at a temperature of 5

eV, for various values of the matter density. Below matter density of 1 g·cm^{-3}, the results from the INFERNO and VAAQP models agree well.

The distorted-wave approximation (see, for instance, [10]) is widely used for the calculation of cross sections of collisional processes for isolated ions [177,178]. A straightforward approach to collisional ionization in dense plasmas consists of extending heuristically this method to models of pressure-ionized plasmas. For example, one may calculate the collisional-excitation cross section by generalizing the configuration-averaged collision strength [178] to the orbitals and fractional occupation numbers given by an average-atom model such as INFERNO or VAAQP.

As an illustration, in Figure 23b we display the 2p→3s collisional-excitation cross section, obtained using the distorted-wave approach using the INFERNO and VAAQP models, respectively. The chosen case is a silicon plasma at 5 eV temperature, for matter densities of 10^{-3}, 10^{-1}, and 2.36 g·cm^{-3}. At high energies, the Born behavior (plane-wave incoming and outgoing electrons) is recovered. At matter density of 10^{-3} g·cm^{-3}, the 7d bound orbital is delocalized, but still contributes a sharp resonance in the continuum. At matter density of 10^{-1} g·cm^{-3}, the same occurs for the 3d bound orbital.
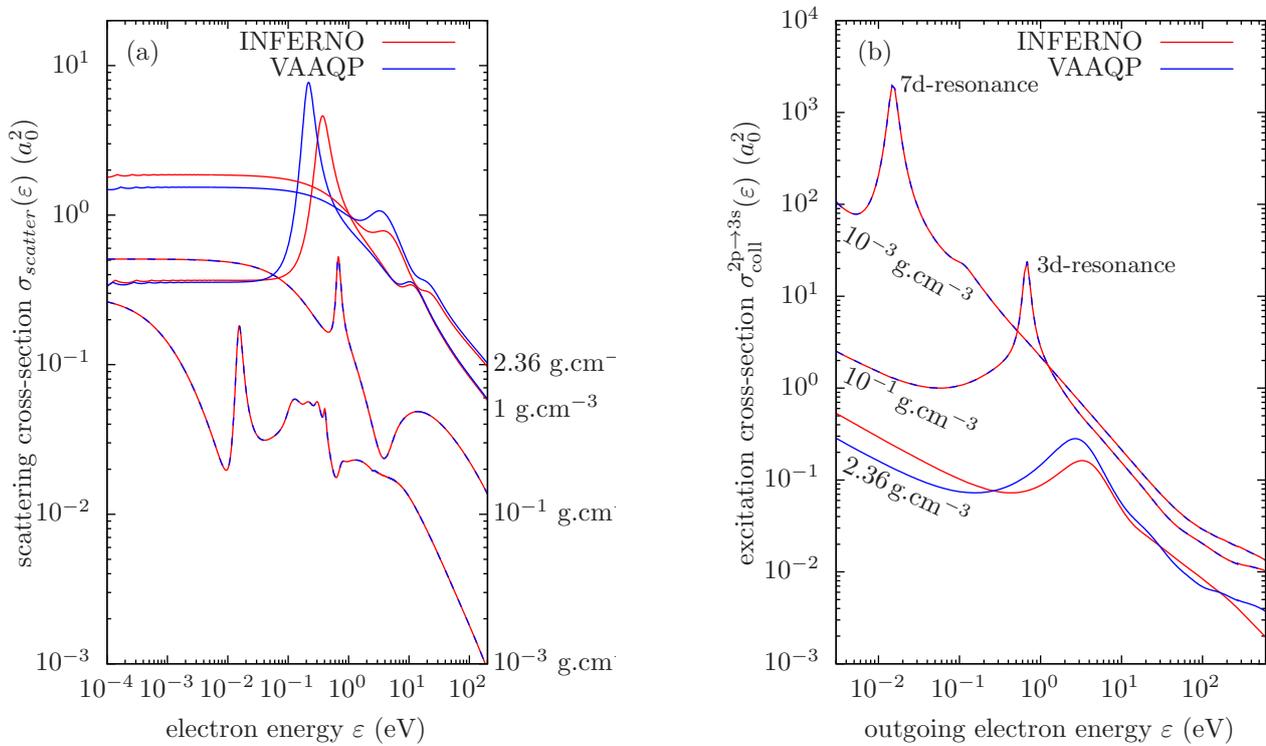
Figure 23. Total electron–ion elastic-scattering cross section (**a**) and 2p→3s collisional-excitation cross section (**b**) for a silicon plasma at a temperature of 5 eV, for various values of the matter density. Comparison between results from the INFERNO and VAAQP models, which are in close agreement up to matter density of 0.1 g·cm^{-3}.

As a direct consequence of these resonances, we obtain sharp, quasi-discrete features in the corresponding cross-sections. These near-threshold sharp features may be seen as the remnants of the correponding dielectronic recombination channels, namely, 2p→3s,7d, and 2p→3s,3d.

One thus can see how, prior to effectively removing them, screening of the potential may redispatch the collisional channels. Part of the dielectronic recombination channels then becomes collisional excitation.

However, the application of the usual distorted-wave method to dense plasma may be questionable in the context of dense plasmas. For instance, the effect of transient spatial

localization of electrons was pointed as a potentially relevant effect, lacking in the usual distorted-wave approach [179].

More generally, one may question the usual approach to the collisional process in the context of dense-plasma models. In fact, collisional processes are introduced as a perturbative accounting for continuum electrons, supplementing an ion Hamiltonian that disregards them (see, for instance, [10]). Yet, models of pressure-ionized plasma account for the continuum electron as part of the ion electronic structure. In this framework, one should probably adapt, re-interpret, or redefine the whole approach to collisional processes. To the best of the author's knowledge, such a rigorous approach to collisional processes in pressure-ionized plasma is an open question.

Finally, let us mention that measures of a collisional-ionization cross-section in a dense plasma were recently performed and showed significant impact of density effects [180].

7. Conclusions

Atomic models of dense plasmas in themselves are still an active field of research, facing open questions as regards their theoretical foundations. The main shortfalls of models based on the notion of continuum lowering are rather well identified. However, models used in order to go beyond the continuum lowering picture are still mostly based on the picture of a Wigner–Seitz cavity. This picture may be seen as a practical, heuristic way of introducing the pressure ionization in the models but seems poorly motivated, especially for weakly and strongly coupled plasmas.

Progress is still ongoing towards achieving a better modeling of pressure ionization, closer to the first principles. That means obtaining pressure ionization directly as a consequence of the plasma structure. Recent research efforts were carried out in this direction with the models based on the QHNC approach and the VAMPIRES model. These models may be viewed as steps in the understanding of the problem but, for sure, they do not exhaust the theoretical challenge of the consistent modeling of nucleus–electron plasmas.

It is to be expected that defining a relevant notion of ion may not be possible in all plasma conditions. Defining the validity domain of atomic physics of plasma, if not of a particular model, remains among the most challenging issues.

Finding a satisfactory model of ions in dense plasmas is the essential first step towards applying many methods and notions from atomic physics. This notably includes the calculation of radiative properties or atomic processes typically involved in collisional-radiative modeling.

As regards radiative properties, most approaches are based on the independent-particle approximation. In these methods, the high number of excited states in high-temperature, mid-to-high-Z plasmas may still constitute an implementation challenge, requiring a tradeoff between completeness and level of detail.

A self-consistent linear-response was successfully applied as regards bound electrons and their related contribution to radiative properties since the 1980s [147,181,182]. However, despite a significant theoretical effort [87,173,175], the consistent treatment of the continuum electron remains an issue in the quantum framework. Yet, this would constitute an important step towards a first-principles approach to the collective effects on radiative properties. Heuristic approaches to collective effects are known [152,165–167]. However, all of them are in fact very similar, and a better-founded approach would be of great interest.

Addressing collisional processes is especially required for the collisional-radiative modeling of dense plasmas. Work is in progress to study the collisional processes in the framework of fully quantum models of screening in dense plasmas. From a direct application of the distorted-wave approach, it appears that screening of the potential can result in a different distribution of transitions among excitation, ionization, and dielectronic channels. However, the theoretical justification for applying the distorted-wave approach to models that account for continuum electrons deserves deeper investigation.

Some dense-plasma models, such as INFERNO, have now been studied and used for many years, but experimental checks of their validity are scarce and do not really allow

one to discriminate among the various models. Equation-of-state measurements often have large experimental uncertainties and rarely access the temperature of the plasma. On the other hand, measurements of radiative properties are most often performed on diluted plasma (see, for instance, [183–187]), addressing regimes in which differences among models are not pronounced. Direct-current conductivity measurements [188,189] or X-ray Thomson scattering may address relevant regimes but usually requires one to take a further step in the modeling in order to interpret the measurements [190,191].

Efforts to improve atomic models of dense plasmas are timely, in view of the growing concern for understanding the warm-dense matter, with applications to stellar astrophysics and planetology in mind. These efforts are also in sync with the recent advances in experiments on warm and hot dense plasmas, enabled by the advent of new facilities and experimental platforms. One may cite, for instance, the recent convergent-spherical shockwave experiments at NIF [192,193], which give access to equation-of-state and X-ray Thomson scattering data at Gbar pressures; the opacity measurements of compressed plasma at OMEGA [194]; the measurement of spectral emission of dense, near-equilibrium plasma using buried layers at ORION [103,195]; or the experiments on the photoionization of metals using tunable X-ray free-electron laser at LCLS [196]. These recent improvements in experimental techniques may allow one to better investigate the models' limitations.

Notes

1   In [94], this model is called "finite-temperature ion-sphere model", whereas what we call in the present article "ion-sphere model" is called "uniform electron gas model".

References

1.   Dyson, F.J.; Lenard, A. Stability of Matter. I. *J. Math. Phys.* **1967**, *8*, 423–434. [CrossRef]
2.   Dyson, F.J.; Lenard, A. Stability of Matter. II. *J. Math. Phys.* **1968**, *9*, 698–711.
3.   Lebowitz, J.L.; Lieb, E.H. Existence of Thermodynamics for Real Matter with Coulomb Forces. *Phys. Rev. Lett.* **1969**, *22*, 631–634. [CrossRef]
4.   Lieb, E.H.; Lebowitz, J.L. The constitution of matter: Existence of thermodynamics for systems composed of electrons and nuclei. *Adv. Math.* **1972**, *9*, 316–398. [CrossRef]
5.   Lieb, E.H. The stability of matter. *Rev. Mod. Phys.* **1976**, *48*, 553–569. [CrossRef]
6.   Mihalas, D. *Stellar Atmospheres*; W H Freeman & Co.: New York, NY, USA, 1978.
7.   Ralchenko, Y. *Modern Methods in Collisional-Radiative Modeling of Plasmas*; Springer: Berlin/Heidelberg, Germany, 2016.

8. Baranger, M. Simplified Quantum-Mechanical Theory of Pressure Broadening. *Phys. Rev.* **1958**, *111*, 481–493. [CrossRef]
9. Stambulchik, E.; Maron, Y. Stark effect of high-n hydrogen-like transitions: Quasi-contiguous approximation. *J. Phys. B At. Mol. Opt. Phys.* **2008**, *41*, 095703. [CrossRef]
10. Sobel'man, I.I.; Vainshtein, L.A.; Yukov, E.A. *Excitation of Atoms and Broadening of Spectral Lines*; Springer: Berlin/Heidelberg, Germany, 1995.
11. Boercker, D.B.; Iglesias, C.A.; Dufty, J.W. Radiative and transport properties of ions in strongly coupled plasmas. *Phys. Rev. A* **1987**, *36*, 2254–2264. [CrossRef] [PubMed]
12. Talin, B.; Calisti, A.; Godbert, L.; Stamm, R.; Lee, R.W.; Klein, L. Frequency-fluctuation model for line-shape calculations in plasma spectroscopy. *Phys. Rev. A* **1995**, *51*, 1918–1928. [CrossRef] [PubMed]
13. Gomez, T.A.; Nagayama, T.; Cho, P.B.; Kilcrease, D.P.; Fontes, C.J.; Zammit, M.C. Introduction to spectral line shape theory. *J. Phys. B At. Mol. Opt. Phys.* **2022**, *55*, 034002. [CrossRef]
14. Racah, G. Theory of Complex Spectra. I. *Phys. Rev.* **1942**, *61*, 186–197. [CrossRef]
15. Racah, G. Theory of Complex Spectra. II. *Phys. Rev.* **1942**, *62*, 438–462. [CrossRef]
16. Racah, G. Theory of Complex Spectra. III. *Phys. Rev.* **1943**, *63*, 367–382. [CrossRef]
17. Judd, B.R. *Second Quantization and Atomic Spectroscopy*; The Johns Hopkins University Press: Baltimore, MD, USA, 1967.
18. Yutsis, A.P.; Levinson, I.B.; Vanagas, V.V. *Mathematical Apparatus of the Theory of Angular Momentum*; Israel Program for Scientific Translations Ltd.: Jerusalem, Israel, 1962.
19. Bar-Shalom, A.; Klapisch, M. NJGRAF—An efficient program for calculation of general recoupling coefficients by graphical analysis, compatible with NJSYM. *Comput. Phys. Commun.* **1988**, *50*, 375–393. [CrossRef]
20. Gaigalas, G.; Fritzsche, S.; Grant, I.P. Program to calculate pure angular momentum coefficients in jj-coupling. *Comput. Phys. Commun.* **2001**, *139*, 263–278. [CrossRef]
21. Moszkowski, S.A. On the Energy Distribution of Terms and Line Arrays in Atomic Spectra. *Prog. Theor. Phys.* **1962**, *28*, 1–23. [CrossRef]
22. Bauche-Arnoult, C.; Bauche, J.; Klapisch, M. Variance of the distributions of energy levels and of the transition arrays in atomic spectra. *Phys. Rev. A* **1979**, *20*, 2424–2439. [CrossRef]
23. Bauche-Arnoult, C.; Bauche, J.; Klapisch, M. Variance of the distributions of energy levels and of the transition arrays in atomic spectra. II. Configurations with more than two open subshells. *Phys. Rev. A* **1982**, *25*, 2641–2646. [CrossRef]
24. Bauche-Arnoult, C.; Bauche, J.; Klapisch, M. Variance of the distributions of energy levels and of the transition arrays in atomic spectra. III. Case of spin-orbit-split arrays. *Phys. Rev. A* **1985**, *31*, 2248–2259. [CrossRef] [PubMed]
25. Perrot, F. Correlated fluctuations of electron populations in high temperature plasmas. *Phys. A* **1988**, *150*, 357–370. [CrossRef]
26. Bar-Shalom, A.; Oreg, J.; Goldstein, W.H.; Shvarts, D.; Zigler, A. Super-transition-arrays: A model for the spectral analysis of hot, dense plasma. *Phys. Rev. A* **1989**, *40*, 3183–3193. [CrossRef] [PubMed]
27. Blenski, T.; Grimaldi, A.; Perrot, F. A superconfiguration code based on the local density approximation. *J. Quant. Spectrosc. Radiat. Transf.* **2000**, *65*, 91–100. [CrossRef]
28. Mazevet, S.; Abdallah, J. Mixed UTA and detailed line treatment for mid-Z opacity and spectral calculations. *J. Phys. B At. Mol. Opt. Phys.* **2006**, *39*, 3419. [CrossRef]
29. Iglesias, C.A.; Sonnad, V. Partially resolved transition array model for atomic spectra. *High Energy Density Phys.* **2012**, *8*, 154–160. [CrossRef]
30. Saha, M.N. Ionization in the solar chromosphere. *Philos. Mag.* **1920**, *40*, 472–488. [CrossRef]
31. Saha, M.N. On a Physical Theory of Stellar Spectra. *Proc. R. Soc. Lond. Ser. A* **1921**, *99*, 135–153. [CrossRef]
32. Slater, J.C. A Simplification of the Hartree–Fock Method. *Phys. Rev.* **1951**, *81*, 385–390. [CrossRef]
33. Talman, J.D.; Shadwick, W.F. Optimized effective atomic central potential. *Phys. Rev. A* **1976**, *14*, 36–40. [CrossRef]
34. Klapisch, M. A program for atomic wavefunction computations by the parametric potential method. *Comput. Phys. Commun.* **1971**, *2*, 239–260. [CrossRef]
35. Slater, J.C. The Self Consistent Field and the Structure of Atoms. *Phys. Rev.* **1928**, *32*, 339–348. [CrossRef]
36. Cowan, R.D. *The Theory of Atomic Structure and Spectra*; University of California Press: Berkeley, CA, USA, 1981.
37. Froese-Fischer, C. *The Hartree–Fock Method for Atoms: A Numerical Approach*; John Wiley & Sons Inc.: Hoboken, NJ, USA, 1977.
38. Grant, I.P. *Relativistic Quantum Theory of Atoms and Molecules: Theory and Computation*; Springer: Berlin/Heidelberg, Germany, 2006.
39. Slater, J.C. The Theory of Complex Spectra. *Phys. Rev.* **1929**, *34*, 1293–1322. [CrossRef]
40. Chandrasekhar, S. Stochastic Problems in Physics and Astronomy. *Rev. Mod. Phys.* **1943**, *15*, 1–89. [CrossRef]
41. Hohenberg, P.; Kohn, W. Inhomogeneous Electron Gas. *Phys. Rev.* **1964**, *136*, B864–B871. [CrossRef]
42. Kohn, W.; Sham, L.J. Self-consistent equations including exchange and correlation effects. *Phys. Rev.* **1965**, *140*, A1133–A1138. [CrossRef]
43. Mermin, N.D. Thermal properties of the inhomogeneous electron gas. *Phys. Rev.* **1965**, *137*, A1441–A1443. [CrossRef]
44. Slater, J.C. The virial and molecular structure. *J. Chem. Phys.* **1933**, *1*, 687. [CrossRef]
45. Stewart, J.C.; Pyatt, K.D. Lowering of ionization potentials in plasmas. *Astrophys. J.* **1966**, *144*, 1203–1211. [CrossRef]
46. Griem, H.R. High-Density Corrections in Plasma Spectroscopy. *Phys. Rev.* **1962**, *128*, 997–1003. [CrossRef]
47. Percus, J.K. Chapter the pair distribution function in classical statistical mechanics. In *The Equilibrium Theory of Classical Fluids*; W. A. Benjamin, Inc.: New York, NY, USA, 1964; pp. II-33–II-170.

48. Debye, P.; Hückel, E. Zur Theorie des Elektrolyte. I. Gefrierpunktserniedrigung und verwandte Erscheinungen. *Phys. Z.* **1923**, *24*, 185–206.
49. Landau, L.D.; Lifshitz, E.M. *Statistical Physics*; Pergamon Press: Oxford, UK, 1959.
50. Kirkwood, J.G. Statistical Mechanics of Fluid Mixtures. *J. Chem. Phys.* **1935**, *3*, 300–313. [CrossRef]
51. Piron, R.; Blenski, T. Simpler free-energy functional of the Debye–Hückel model of fluids and the non-uniqueness of free-energy functionals in the theory of fluids. *Phys. Rev. E* **2019**, *99*, 052134. [CrossRef] [PubMed]
52. Brush, S.G.; Sahlin, H.L.; Teller, E. Monte Carlo Study of a One-Component Plasma. I. *J. Chem. Phys.* **1966**, *45*, 2102–2118. [CrossRef]
53. Hansen, J. Statistical Mechanics of Dense Ionized Matter. I. Equilibrium Properties of the Classical One-Component Plasma. *Phys. Rev. A* **1973**, *8*, 3096–3109. [CrossRef]
54. Springer, J.F.; Pokrant, M.A.; Stevens, F.A. Integral equation solutions for the classical electron gas. *J. Chem. Phys.* **1973**, *58*, 4863–4867. [CrossRef]
55. Ng, K.C. Hypernetted chain solutions for the classical one-compoenent plasma up to $\Gamma = 7000$. *J. Chem. Phys.* **1974**, *61*, 2680–2689. [CrossRef]
56. Carley, D.D. Computations of Radial Distribution Functions for a Classical Electron Gas. *Phys. Rev.* **1963**, *131*, 1406–1409. [CrossRef]
57. Carley, D.D. Radial Distributions of Ions for a Primitive Model of an Electrolyte Solution. *J. Chem. Phys.* **1967**, *46*, 3783–3788. [CrossRef]
58. Piron, R.; Blenski, T. Variational average-atom in quantum plasmas (VAAQP)—Application to radiative properties. *High Energy Density Phys.* **2013**, *9*, 702–713. [CrossRef]
59. Morita, T. Theory of Classical Fluids: Hyper-Netted Chain Approximation, I. *Prog. Theor. Phys.* **1958**, *20*, 920–938. [CrossRef]
60. Morita, T. Theory of Classical Fluids: Hyper-Netted Chain Approximation, II. *Prog. Theor. Phys.* **1959**, *21*, 361–382. [CrossRef]
61. Van Horn, H. Crystallization of a classical, one-component Coulomb plasma. *Phys. Lett. A* **1969**, *28*, 706–707. [CrossRef]
62. Hansen, J. Crystallization of the classical one-component plasma. *Phys. Lett. A* **1972**, *41*, 213–214. [CrossRef]
63. Slattery, W.L.; Doolen, G.D.; DeWitt, H.E. *N* dependence in the classical one-component plasma Monte Carlo calculations. *Phys. Rev. A* **1982**, *26*, 2255–2258. [CrossRef]
64. Levinson, N. On the Uniqueness of the Potential in a Schrödinger Equation for a Given Asymptotic Phase. *Danske Vidensk. Selsk. K. Mat.-Fys. Medd.* **1949**, *25*, 9.
65. Jauch, J.M. On the Relation Between Scatteriing Phase and Bound States. *Helv. Phys. Acta* **1957**, *30*, 143–156.
66. Ma, Z.Q. The Levinson theorem. *J. Phys. A Math. Gen.* **2006**, *39*, R625–R659. [CrossRef]
67. Abramowitz, M.; Stegun, I.A. *Handbook of Mathematical Functions with Formulas, Graphs, and Mathematical Tables.djvu*; Dover Publication, Inc.: New York, NY, USA, 1965.
68. Kittel, C. *Quantum Theory of Solids*; Wiley: Hoboken, NJ, USA, 1991.
69. Bargmann, V. On the number of bound states in a central field of force. *Proc. Nat. Acad. Sci. USA* **1952**, *38*, 961–966. [CrossRef]
70. Beth, E.; Uhlenbeck, G.E. The quantum theory of the non-ideal gas. II. Behaviour at low temperatures. *Physica* **1937**, *4*, 915–924. [CrossRef]
71. Larkin, A.I. Thermodynamic functions of a low-temperature plasma. *JETP* **1960**, *38*, 1896–1898.
72. Ebeling, W. Equation of State and Saha Equation of Partially Ionized Plasmas. *Physica* **1968**, *38*, 378–388. [CrossRef]
73. Ebeling, W. Statistical Derivation of the Mass-Action Law for Interacting Gases ans Plasmas. *Physica* **1974**, *73*, 573–584. [CrossRef]
74. Ebeling, W.; Kraeft, W.D.; Kremp, D.; Röpke, G. Energy Levels in Hydrogen Plasmas and the Planck–Larkin Partition Function—A Comment. *Astrophys. J.* **1985**, *290*, 24–27. [CrossRef]
75. Rogers, F.J. On the Compensation of Bound and Scattering State Contributions to the Partition Functtlon. *Phys. Lett.* **1977**, *61A*, 358–360. [CrossRef]
76. Rogers, F.J. Occupation Numbers for Reacting Plasmas: The Role of the Planck–Larkin Partition Function. *Astrophys. J.* **1986**, *310*, 723. [CrossRef]
77. Herzfeld, K.F. Über die Wahrscheinlichkeit der Quantenzustände. *Ann. der Phys.* **1916**, *51*, 261. [CrossRef]
78. Urey, H.C. The Distribution of Electrons in the Various Orbits of the Hydrogen Atom. *Astrophys. J.* **1924**, *59*, 1. [CrossRef]
79. Fermi, E. Über die Wahrscheinlichkeit der Quantenzustände. *Z. Phys.* **1924**, *26*, 54–56. [CrossRef]
80. Feynman, R.P.; Metropolis, N.; Teller, E. Equation of State of Elements Based on the Generalized Fermi-Thomas Theory. *Phys. Rev.* **1949**, *75*, 1561–1573. [CrossRef]
81. Latter, R. Temperature Behavior of the Thomas-Fermi Statistical Model for Atoms. *Phys. Rev.* **1955**, *99*, 1854–1870. [CrossRef]
82. Dirac, P.A.M. Note on exchange phenomena in the Thomas atom. *Proc. Camb. Phil. Soc.* **1930**, *26*, 376–385. [CrossRef]
83. Kirzhnits, D.A. Quantum corrections to the Thomas–Fermi equation. *JETP* **1957**, *5*, 64.
84. Latter, R. Atomic Energy Levels for the Thomas–Fermi and Thomas–Fermi–Dirac Potential. *Phys. Rev.* **1955**, *99*, 510–519. [CrossRef]
85. Ball, J.A.; Wheeler, J.A.; Firemen, E.L. Photoabsorption and Charge Oscillation of the Thomas–Fermi Atom. *Rev. Mod. Phys.* **1973**, *45*, 333. [CrossRef]
86. Ishikawa, K.; Felderhof, B.U. High-frequency photoabsorption by an ion immersed in a plasma as calculated from Bloch's hydrodynamic model. *Phys. A* **1998**, *253*, 541–554. [CrossRef]

87. Caizergues, C.; Blenski, T.; Piron, R. Linear response of a variational average atom in plasma: Semi-classical model. *High Energy Density Phys.* **2014**, *12*, 12–20. [CrossRef]

88. Slater, J.C.; Krutter, H.M. The Thomas-Fermi Method for Metals. *Phys. Rev.* **1935**, *47*, 559–568. [CrossRef]

89. Liberman, D.A. Self-consistent field model for condensed matter. *Phys. Rev. B* **1979**, *20*, 4981–4989. [CrossRef]

90. Rozsnyai, B.F. Relativistic Hartree–Fock-Slater Calculations for Arbitrary Temperature and Matter Density. *Phys. Rev. A* **1972**, *5*, 1137–1149. [CrossRef]

91. Wigner, E.; Seitz, F. On the Constitution of Metallic Sodium. *Phys. Rev.* **1933**, *43*, 804–810. [CrossRef]

92. Wigner, E.; Seitz, F. On the Constitution of Metallic Sodium. II. *Phys. Rev.* **1934**, *46*, 509–524. [CrossRef]

93. Ashcroft, N.W.; Mermin, N.D. *Solid State Physics*; Harcourt College Publishers: San Diego, CA, USA, 1976.

94. Rosmej, F.; Bennadji, K.; Lisitsa, V.S. Effect of dense plasmas on exchange-energy shifts in highly charged ions: An alternative approach for arbitrary pertubation potentials. *Phys. Rev. A* **2011**, *84*, 032512. [CrossRef]

95. Massacrier, G.; Böhme, M.; Vorberger, J.; Soubiran, F.; Militzer, B. Reconciling ionization energies and band gaps of warm dense matter derived with ab initio simulations and average atom models. *Phys. Rev. Res.* **2021**, *3*, 023026. [CrossRef]

96. Liberman, D.A. Inferno: A better model of atoms in dense plasmas. *J. Quant. Spectrosc. Radiat. Transf.* **1982**, *27*, 335. [CrossRef]

97. Bennett, B.I.; Liberman, D.A. *Inferno*; Technical Report LA-10309-M; Los Alamos National Laboratory: Santa Fe, NM, USA, 1985.

98. Piron, R. Variational Average-Atom in Quantum Plasmas (VAAQP). Ph.D. Thesis, École Polytechnique, Palaiseau, France, 2009. Available online: https://theses.hal.science/tel-00446558/ (accessed on 4 April 2024). (In French)

99. Wilson, B.; Sonnad, V.; Sterne, P.; Isaacs, W. PURGATORIO—A new implementation of the INFERNO algorithm. *J. Quant. Spectrosc. Radiat. Transf.* **2006**, *99*, 658–679. [CrossRef]

100. Pénicaud, M. An average atom code for warm matter: Application to aluminum and uranium. *J. Phys. Condens. Matter* **2009**, *21*, 095409. [CrossRef] [PubMed]

101. Li, X.; Rosmej, F. Quantum-number-dependent energy level shifts of ionsin dense plasmas: A generalized analytical approach. *Eur. Phys. Lett.* **2012**, *99*, 33001. [CrossRef]

102. Iglesias, C. On spectral line shifts from analytic fits to the ion-sphere model potential. *High Energy Density Phys.* **2019**, *30*, 41–44. [CrossRef]

103. Beiersdorfer, P.; Brown, G.; McKelvey, A.; Shepherd, R.; Hoarty, D.J.; Brown, C.R.D.; Hill, M.P.; Hobbs, L.M.R.; James, S.F.; Morton, J.; et al. High-resolution measurments of Cl^{15+} line shifts in hot, solid-density plasmas. *Phys. Rev. A* **2019**, *100*, 012511. [CrossRef]

104. Li, X.; Rosmej, F. Analytical approach to level delocalization and line shifts in finite temperature dense plasmas. *Phys. Lett. A* **2020**, *384*, 126478. [CrossRef]

105. Zeng, J.; Ye, C.; Li, Y.; Yuan, J. Ionization potential depression in dense iron plasmas near solid density. *Results Phys.* **2022**, *40*, 105836. [CrossRef]

106. Massacrier, G.; Dubau, J. A theoretical approach to N-electron ionic structure under dense plasma conditions: I. Blue and red shift. *J. Phys. B At. Mol. Opt. Phys.* **1990**, *23*, 2459S–2469S. [CrossRef]

107. Arponen, J.; Hautojärvi, P.; Nieminen, R.; Pajanne, E. Charge density and positron annihilation at lattice defects in aluminium. *J. Phys. F Met. Phys.* **1973**, *3*, 2092–2108. [CrossRef]

108. Manninen, M.; Nieminen, R.; Hautojärvi, P.; Arponen, J. Electrons and positrons in metal vacancies. *Phys. Rev. B* **1975**, *12*, 4012–4022. [CrossRef]

109. Jena, P.; Singwi, K.S. Electronic structure of hydrogen in simple metals. *Phys. Rev. B* **1978**, *17*, 3518–3524. [CrossRef]

110. Perrot, F. (CEA, DAM, DIF, F-91297 Arpajon, France) Private Communication. 1998.

111. Blenski, T.; Cichocki, B. Variational approach to the average-atom-in-jellium and superconfigurations-in-jellium models with all electrons treated quantum-mechanically. *High Energy Density Phys.* **2007**, *3*, 34–47. [CrossRef]

112. Blenski, T.; Cichocki, B. Variational theory of average-atom and superconfigurations in quantum plasmas. *Phys. Rev. E* **2007**, *75*, 056402. [CrossRef] [PubMed]

113. Piron, R.; Blenski, T. Variational-average-atom-in-quantum-plasmas (VAAQP) code and virial theorem: Equation-of-state and shock-Hugoniot calculations for warm dense Al, Fe, Cu, and Pb. *Phys. Rev. E* **2011**, *83*, 026403. [CrossRef]

114. Piron, R.; Blenski, T. Variational average-atom in quantum plasmas (VAAQP)—Recent progress, virial theorem and applications to the equation-of-state of warm dense Be. *High Energy Density Phys.* **2011**, *7*, 346–352. [CrossRef]

115. Felderhof, B.U.; Ford, G.W.; Cohen, E.G.D. Cluster Expansion for the Dielectric Constant of a Polarizable Suspension. *J. Stat. Phys.* **1982**, *28*, 135–164. [CrossRef]

116. Piron, R.; Blenski, T.; Cichocki, B. Variational Average-Atom in Quantum Plasmas (VAAQP)—A check of thermodynamic consistency. *High Energy Density Phys.* **2009**, *5*, 258–262. [CrossRef]

117. Piron, R.; Blenski, T. Average-atom model calculations of dense-plasma opacities: Review and potential applications to white-dwarf stars. *Contrib. Plasma Phys.* **2018**, *58*, 30–41. [CrossRef]

118. Percus, J.K. At the boundary between reduced density-matrix and density-functional theories. *J. Chem. Phys.* **2005**, *122*, 234103. [CrossRef]

119. Lado, F. Effective Potential Description of the Quantum Ideal Gases. *J. Chem. Phys.* **1967**, *47*, 5369–5375. [CrossRef]

120. Dharma-wardana, M.W.C.; Perrot, F. Simple Classical Mapping of the Spin-Polarized Quantum Electron Gas: Distribution Functions and Local-Field Corrections. *Phys. Rev. Lett.* **2000**, *84*, 959–962. [CrossRef] [PubMed]

121. Perrot, F.; Blenski, T. Electronic structure and statistical mechanics of ionic configurations in hot plasmas. *J. Phys. IV Fr.* **2000**, *10*, Pr5-473–Pr5-479. [CrossRef]

122. Dufty, J.; Dutta, S. Classical representation of a quantum system at equilibrium: Theory. *Phys. Rev. E* **2013**, *87*, 032101. [CrossRef]

123. Dutta, S.; Dufty, J. Classical representation of a quantum system at equilibrium: Applications. *Phys. Rev. E* **2013**, *87*, 032102. [CrossRef]

124. Chihara, J. Derivation of Quantal Hyper-Netted Chain Equation from the Kohn–Sham Theory. *Prog. Theor. Phys.* **1978**, *59*, 76–86. [CrossRef]

125. Hansen, J.P.; MacDonald, I.R. *Theory of Simple Liquids*; Academic Press: Cambridge, MA, USA, 1976.

126. Chihara, J. Unified description of metallic and neutral liquids and plasmas. *J. Phys. Condens. Matter* **1991**, *3*, 8715. [CrossRef]

127. Dewitt, H.E.; Rogers, F.J. Helmholtz free energy of electron screened plasmas in the hypernetted-chain (HNC) approximation. *Phys. Lett. A* **1988**, *132*, 273–275. [CrossRef]

128. Anta, J.A.; Louis, A.A. Probing ion–ion and electron–ion correlations in liquid metals within the quantum hypernetted chain approximation. *Phys. Rev. B* **2000**, *61*, 11400–11410. [CrossRef]

129. Starrett, C.E.; Saumon, D. Fully variational average atom model with ion–ion correlations. *Phys. Rev. E* **2012**, *85*, 026403. [CrossRef]

130. Starrett, C.E.; Saumon, D. Electronic and ionic structures of warm and hot dense matter. *Phys. Rev. E* **2013**, *87*, 013104. [CrossRef]

131. Starrett, C.; Saumon, D. A simple method for determining the ionic structure of warm dense matter. *High Energy Density Phys.* **2014**, *10*, 35–42. [CrossRef]

132. Chihara, J. Average Atom Model based on Quantum Hyper-Netted Chain Method. *High Energy Density Phys.* **2016**, *19*, 38–47. [CrossRef]

133. Morita, T.; Hiroike, K. A New Approach to the Theory of Classical Fluids. I. *Prog. Theor. Phys.* **1960**, *23*, 1003–1027. [CrossRef]

134. Lado, F. Perturbation Correction for the Free Energy and Structure of Simple Fluids. *Phys. Rev. A* **1973**, *8*, 2548–2552. [CrossRef]

135. Piron, R.; Blenski, T. Free-energy functional of the Debye–Hückel model of simple fluids. *Phys. Rev. E* **2016**, *94*, 062128. [CrossRef] [PubMed]

136. Blenski, T.; Piron, R. Free-energy functional of the Debye–Hückel model of two-component plasmas. *High Energy Density Phys.* **2017**, *24*, 28–32. [CrossRef]

137. Piron, R.; Blenski, T. Variational average-atom model of electron–ion plasma with correlations and quantum bound electrons. *arXiv* **2019**, arXiv:1904.13289.

138. Blenski, T.; Piron, R. Variational atomic model of plasma accounting for ion radial correlations and electronic structure of ions. *Phys. Rev. E* **2023**, *107*, 035209. [CrossRef] [PubMed]

139. Kirkwood, J.G. Quantum Statistics of Almost Classical Assemblies. *Phys. Rev.* **1933**, *44*, 31–37. [CrossRef]

140. Zwanzig, R.W. Transition from Quantum to "Classical" Partition Function. *Phys. Rev.* **1957**, *106*, 13–15. [CrossRef]

141. Landau, L.D.; Lifshitz, E.M. *Electrodynamics of Continuous Media*; Pergamon Press: Oxford, UK, 1960.

142. Błeński, T.; Cichocki, B. Linear response of partially ionized, dense plasmas. *Laser Part. Beams* **1992**, *10*, 299–309. [CrossRef]

143. Blenski, T.; Cichocki, B. Polarizability of partially ionized, dense plasmas (application to photo-absorption calculations). *J. Quant. Spectrosc. Radiat. Transf.* **1994**, *51*, 49–58. [CrossRef]

144. Felderhof, B.U.; Blenski, T.; Cichocki, B. Dielectric function of an electron–ion plasma in the optical and X-ray regime. *Phys. A* **1995**, *217*, 161–174. [CrossRef]

145. Fetter, A.L.; Walecka, J.D. *Quantum Theory of Many-Particle Systems*; Dover Publication, Inc.: Mineola, NY, USA, 2003.

146. Stott, M.J.; Zaremba, E. Linear-response theory within the density-functional formalism: Application to atomic polarizabilities. *Phys. Rev. A* **1980**, *21*, 12–23. [CrossRef]

147. Zangwill, A.; Soven, P. Density-functional approach to local-field effects in finite systems: Photoabsorption in the rare gases. *Phys. Rev. A* **1980**, *21*, 1561–1572. [CrossRef]

148. Runge, E.; Gross, E.K.U. Density-Functional Theory for Time-Dependent Systems. *Phys. Rev. Lett.* **1984**, *52*, 997–1000. [CrossRef]

149. Dhara, A.K.; Ghosh, S.K. Density-functional theory for time-dependent systems. *Phys. Rev. A* **1987**, *35*, 442–444. [CrossRef]

150. Ghosh, S.K.; Dhara, A.K. Density-functional theory of many-electron systems subjected to time-dependent electric and magnetic fields. *Phys. Rev. A* **1988**, *38*, 1149–1158. [CrossRef] [PubMed]

151. Bethe, H.A.; Salpeter, E.E. *Quantum Mechanics of One- and Two-Electron Atoms*; Springer: Berlin/Heidelberg, Germany, 1957.

152. Perrot, F. A new approximation for calculating free-free absorption in hot dense plasmas. *Laser Part. Beams* **1996**, *14*, 731–748. [CrossRef]

153. Kramers, H.A. On the theory of X-ray absorption and of the continuous X-ray spectrum. *Philos. Mag. Ser. 6* **1923**, *46*, 836–871. [CrossRef]

154. Zel'dovich, Y.B.; Raizer, Y.P. *Physics of Shock Waves and High-Temperature Hydrodynamic Phenomena*; Academic Press: Cambridge, MA, USA, 1968.

155. Shore, B.W. On the threshold behaviour of bound–bound and bound-free photoabsorption for the screened Coulomb potentials. *J. Phys. B* **2019**, *8*, 2023–2040. [CrossRef]

156. Perrot, F. Model for atomic species in a dense plasma: Description and applications. *Phys. Rev. A* **1987**, *35*, 1235–1244. [CrossRef] [PubMed]

157. Green, J.M. The statistical mechanics of the interdependent electrons in the screening constant model of the many-electron-atom. *J. Quant. Spectrosc. Radiat. Transf.* **1964**, *4*, 639–662. [CrossRef]

158. Shalitin, D.; Stein, J.; Ron, A. Level and line broadening for Thomas–Fermi atoms at finite temperature. *Phys. Rev. A* **1984**, *29*, 2789–2795. [CrossRef]

159. Stein, J.; Shalitin, D.; Ron, A. Average-atom models of line broadening in hot dense plasmas. *Phys. Rev. A* **1985**, *31*, 446–450. [CrossRef] [PubMed]

160. Blenski, T.; Cichocki, B. Density-functional approach to the absorption bands in a dense, partially ionized plasma. *Phys. Rev. A* **1990**, *41*, 6973–6981. [CrossRef] [PubMed]

161. Wei, H.G.; Shi, J.R.; Zhao, G.; Zhang, Y.; Dong, Q.L.; Li, Y.T.; Wang, S.J.; Zhang, J.; Liang, Z.; Zhang, J.Y.; et al. Opacity Studies of Silicon in Radiatively Heated Plasma. *Astrophys. J.* **2008**, *683*, 577–583. [CrossRef]

162. Li, Y.; Gao, C.; Tian, Q.; Zeng, J.; Yuan, J. Ionization competition effects on population distribution and radiative opacity of mixture plasmas. *Phys. Plasmas* **2015**, *22*, 113302. [CrossRef]

163. Liberman, D.A.; Albritton, J.R.; Wilson, B.G.; Alley, W.E. Self-consistent-field calculations of atoms and ions using a modified local-density approximation. *Phys. Rev. A* **1994**, *50*, 171–176. [CrossRef] [PubMed]

164. Hansen, S.B. Self-consistent and detailed opacities from a non-equilibrium average-atom model. *Phil. Trans. R. Soc. A* **2023**, *381*, 20220212. [CrossRef]

165. Johnson, W.R.; Guet, C.; Bertsch, G.F. Optical properties of plasmas based on an average-atom model. *J. Quant. Spectrosc. Radiat. Transf.* **2006**, *99*, 327–340. [CrossRef]

166. Kuchiev, M.Y.; Johnson, W.R. Low-frequency plasma conductivity in the average-atom approximation. *Phys. Rev. E* **2008**, *78*, 026401. [CrossRef] [PubMed]

167. Johnson, W. Low-frequency conductivity in the average-atom approximation. *High Energy Density Phys.* **2009**, *5*, 61–67. [CrossRef]

168. Ziman, J.M. A theory of the electrical properties of liquid metals. I: The monovalent metals. *Philos. Mag. J. Theor. Exp. Appl. Phys.* **1961**, *6*, 1013–1034. [CrossRef]

169. Somerville, W.B. The continuous absorption coefficient of the negative hydrogen molecular ion. *Astrophys. J.* **1964**, *139*, 192–197. [CrossRef]

170. Ashkin, M. Radiative Absorption Cross Section of an Electron in the Field of an Argon Atom. *Phys. Rev.* **1966**, *141*, 41–44. [CrossRef]

171. Henke, B.L.; Davis, J.C.; Gullikson, E.M.; Perera, R.C.C. *A Preliminary Report on X-ray Photoabsorption Coefficients and Atomic Scattering Factors for 92 Elements in the 10–10.000 eV Region*; Technical Report LBL–26259 UC–411; Lawrence Berkeley Laboratory: Berkeley, CA, USA, 1988.

172. Haensel, R.; Keitel, G.; Schreiber, P.; Kunz, C. Optical Absorption of Solid Krypton and Xenon in the Far Ultraviolet. *Phys. Rev.* **1969**, *188*, 1375–1380. [CrossRef]

173. Blenski, T. On the linear dynamic response of average atom in plasma. *J. Quant. Spectrosc. Radiat. Transf.* **2006**, *99*, 84–101. [CrossRef]

174. Blenski, T.; Piron, R.; Caizergues, C.; Cichocki, B. Models of atoms in plasmas based on common formalism for bound and free electrons. *High Energy Density Phys.* **2013**, *9*, 687–695. [CrossRef]

175. Caizergues, C.; Blenski, T.; Piron, R. Dynamic linear response of atoms in plasmas and photo-absorption cross-section in the dipole approximation. *High Energy Density Phys.* **2016**, *18*, 7–13. [CrossRef]

176. Mahan, G.D.; Subbaswamy, K.R. *Local Density Theory of Polarizability*; Springer: New York, NY, USA, 1990.

177. Sampson, D.H.; Zhang, H.L.; Fontes, C.J. A fully relativistic approach for calculating atomic data for highly charged ions. *Phys. Rep.* **2009**, *477*, 111–214. [CrossRef]

178. Peyrusse, O. Atomic configuration averages and non-local thermodynamical equilibrium plasma spectroscopy calculations. *J. Phys. B At. Mol. Opt. Phys.* **1999**, *32*, 683–700. [CrossRef]

179. Zeng, J.; Ye, C.; Liu, P.; Gao, C.; Li, Y.; Yuan, J. The Strong Enhancement of Electron-Impact Ionization Processes in Dense Plasma by Transient Spatial Localization. *Int. J. Mol. Sci.* **2022**, *23*, 6033. [CrossRef] [PubMed]

180. van den Berg, Q.Y.; Fernandez-Tello, E.V.; Burian, T.; Chalupský, J.; Chung, H.K.; Ciricosta, O.; Dakovski, G.L.; Hájková, V.; Hollebon, P.; Juha, L.; et al. Clocking Femtosecond Collisional Dynamics via Resonant X-ray Spectroscopy. *Phys. Rev. Lett.* **2018**, *120*, 055002. [CrossRef] [PubMed]

181. Zangwill, A.; Liberman, D. A nonrelativistic program for optical response in atoms using a time-dependent local density approximation. *Comput. Phys. Commun.* **1984**, *32*, 63–73. [CrossRef]

182. Doolen, G.; Liberman, D.A. Calculations of photoabsorption by atoms using a linear response method. *Phys. Scr.* **1987**, *36*, 77. [CrossRef]

183. Davidson, S.J.; Foster, J.M.; Smith, C.C.; Warburton, K.A.; Rose, S.J. Investigation of the opacity of hot, dense aluminum in the region of its K edge. *Appl. Phys. Lett.* **1988**, *52*, 847–849. [CrossRef]

184. Bruneau, J.; Chenais-Popovics, C.; Desenne, D.; Gauthier, J.C.; Geindre, J.P.; Klapisch, M.; Le Breton, J.P.; Louis-Jacquet, M.; Naccache, D.; Perrine, J.P. Time-resolved L-shell absorption spectroscopy: A direct measurement of density and temperature in a germanium laser-produced plasma. *Phys. Rev. Lett.* **1990**, *65*, 1435–1438. [CrossRef] [PubMed]

185. Da Silva, L.B.; MacGowan, B.J.; Kania, D.R.; Hammel, B.A.; Back, C.A.; Hsieh, E.; Doyas, R.; Iglesias, C.A.; Rogers, F.J.; Lee, R.W. Absorption measurements demonstrating the importance of Δn=0 transitions in the opacity of iron. *Phys. Rev. Lett.* **1992**, *69*, 438–441. [CrossRef] [PubMed]

186. Bailey, J.E.; Rochau, G.A.; Iglesias, C.A.; Abdallah, J.; MacFarlane, J.J.; Golovkin, I.; Wang, P.; Mancini, R.C.; Lake, P.W.; Moore, T.C.; et al. Iron-Plasma Transmission Measurements at Temperatures Above 150 eV. *Phys. Rev. Lett.* **2007**, *99*, 265002. [CrossRef] [PubMed]

187. Bailey, J.E.; Nagayama, T.; Loisel, G.P.; Rochau, G.A.; Blancard, C.; Colgan, J.; Cosse, P.; Faussurier, G.; Fontes, C.J.; Gilleron, F.; et al. A higher-than-predicted measurement of iron opacity at solar interior temperatures. *Nature* **2015**, *517*, 56–59. [CrossRef] [PubMed]

188. Renaudin, P.; Blancard, C.; Faussurier, G.; Noiret, P. Combined Pressure and Electrical-Resistivity Measurements of Warm Dense Aluminum and Titanium Plasmas. *Phys. Rev. Lett.* **2002**, *88*, 215001. [CrossRef] [PubMed]

189. Korobenko, V.N.; Rakhel, A.D. Electrical resistivity and equation of state measurements on hot expanded aluminum in the metal-nonmetal transition range. *Phys. Rev. B* **2007**, *75*, 064208. [CrossRef]

190. Gregori, G.; Glenzer, S.H.; Rogers, F.J.; Pollaine, S.M.; Landen, O.L.; Blancard, C.; Faussurier, G.; Renaudin, P.; Kuhlbrodt, S.; Redmer, R. Electronic structure measurements of dense plasmas. *Phys. Plasmas* **2004**, *11*, 2754–2762. [CrossRef]

191. Sperling, P.; Rosmej, S.; Bredow, R.; Fletcher, L.B.; Galtier, E.; Gamboa, E.J.; Lee, H.J.; Reinholz, H.; Röpke, G.; Zastrau, U.; et al. Electrical conductivity calculations in isochorically heated warm dense aluminum. *J. Phys. B At. Mol. Opt. Phys.* **2017**, *50*, 134002. [CrossRef]

192. Kraus, D.; Chapman, D.A.; Kritcher, A.L.; Baggott, R.A.; Bachmann, B.; Collins, G.W.; Glenzer, S.H.; Hawreliak, J.A.; Kalantar, D.H.; Landen, O.L.; et al. X-ray scattering measurements on imploding CH spheres at the National Ignition Facility. *Phys. Rev. E* **2016**, *94*, 011202. [CrossRef] [PubMed]

193. Swift, D.C.; Kritcher, A.L.; Hawreliak, J.A.; Lazicki, A.; MacPhee, A.; Bachmann, B.; Döppner, T.; Nilsen, J.; Collins, G.W.; Glenzer, S.; et al. Absolute Hugoniot measurements from a spherically convergent shock using X-ray radiography. *Rev. Sci. Instrum.* **2018**, *89*, 053505. [CrossRef]

194. Hu, S.X.; Bishel, D.T.; Chin, D.A.; Nilson, P.M.; Karasiev, V.V.; Golovkin, I.E.; Gu, M.; Hansen, S.B.; Mihaylov, D.I.; Shaffer, N.R.; et al. Probing atomic physics at ultrahigh pressure using laser-driven implosions. *Nat. Commun.* **2022**, *13*, 6780. [CrossRef] [PubMed]

195. Hoarty, D.J.; Allan, P.; James, S.F.; Brown, C.R.D.; Hobbs, L.M.R.; Hill, M.P.; Harris, J.W.O.; Morton, J.; Brookes, M.G.; Shepherd, R.; et al. Observations of the Effect of Ionization-Potential Depression in Hot Dense Plasma. *Phys. Rev. Lett.* **2013**, *110*, 265003. [CrossRef] [PubMed]

196. Ciricosta, O.; Vinko, S.M.; Chung, H.K.; Cho, B.I.; Brown, C.R.D.; Burian, T.; Chalupský, J.; Engelhorn, K.; Falcone, R.W.; Graves, C.; et al. Direct Measurements of the Ionization Potential Depression in a Dense Plasma. *Phys. Rev. Lett.* **2012**, *109*, 065002. [CrossRef] [PubMed]